UNIVERSITE DE LIMOGES

ECOLE DOCTORALE Science – Technologie – Santé

FACULTE DES SCIENCES ET TECHNIQUES

INSTITUT DE RECHERCHE XLIM

ACADEMIE DES SCIENCES DE LA RUSSIE

CENTRE DE RECHERCHE SUR LES FIBRES OPTIQUES

Année : 2008 **Thèse N° [ ]**

Thèse

pour obtenir le grade de

DOCTEUR DE L'UNIVERSITE DE LIMOGES

DISCIPLINE: ELECTRONIQUE DES HAUTES FREQUENCES ET OPTRONIQUES

SPECIALITE : PHOTONIQUE

présentée et soutenue le 24 novembre 2008 par : GAPONOV Dmitry

Optical properties of Microstructured Optical Fibers and fiber laser based on Large Mode Area Bragg Fiber

Propriétés optiques de fibres optiques microstructurées et laser à fibre de Bragg à grande aire modale

Thèse dirigée par Philippe ROY et Alexander S. BIRIUKOV

Rapporteurs

KULEVSKII Lev A.	**Professeur, Laboratoire de la Optique Nonlinéaire Diapason IR, Institut de physique générale Prokhorov de l'Académie des Sciences de la Russie (ASR), Moscou.**
USPENSKII Yurii A.	**Directeur de recherche, Théorique département, Institut de physique Lebedev de l'ASR, Moscou.**

Examinateurs

BIRIUKOV Alexander S.	**Professeur, Directeur de Secteur Théorique, Centre de Recherche sur les Fibres Optiques de l'ASR, Moscou.**
ROY Philippe	**Chargé de recherche, HDR, Xlim, Limoges.**
FEVRIER Sébastien	**Maître de conférence, Xlim, Limoges.**

Contents

Acknowledgements

An author is expressing a sincere gratitude to his scientific supervisor - professor, doctor of physic-mathematical sciences Alexander S. Biriukov for a proposed theme of theoretic researches, statement of actual problems in science at present and also for help in working at present work.

The author is appreciated his colleague Andey D. Pryamikov for daily fruitful discussions of closely connected scientific questions.

The author is giving thanks to Sergey L. Semenov for participation in assignment of a possibility of carrying out an experimental part of the work in XLIM laboratory of the University of Limoges in France.

For inestimable help while carrying out the experimental part of his work, valuable remarks and useful discussions of obtained results the author is deeply obliged to Michael E. Likhachev a senior research worker of Optical Fiber Technology Laboratory of FORC RAS.

The author is feeling a deep gratitude to his scientific supervisor in XLIM laboratory of University of Limoges, France, CNRS scientific researcher, Philippe Roy for useful discussions, all-out support and help.

The author is also giving a lot of thanks to scientific researcher of XLIM laboratory Sebastien Fevrier for participation in work and useful discussions while carrying out both theoretical and experimental investigations.

The author is expressing thankfulness to a head of the Optical Fiber Technology Laboratory of FORC RAS Mikhail M. Bubnov for interesting in and support of his work.

The author is grateful to Mikhail N. Sapozhnikov a scientific English editor of the journal “Quantum Electronics” for his high quality translations of some parts of the presented work.

The author is appreciating to director of FORC RAS an academician Eugeniy M. Dianov for support and constant interest and attention to this work.

Main designations

MOF – Microstructured Optical Fiber

TIR – Total Internal Reflection

RIP – Refractive Index Profile

HF - Holey Fiber

PBGF – Photonic Band Gap Fiber

BF – Bragg Fiber

ARROW - Anti Resonant Reflection Optical Waveguide

FP – Fabry-Perot resonator

LMA – Large Mode Area

NA – Numerical Aperture

n_{eff} - Effective refractive index

β – Phase propagation constant

c – Speed of light in vacuum

– Waveguide losses

D – Dispersion parameter

v_g - Group velocity

n_0 - Refractive index of a BF core

n_1 - Refractive index of high-index layer in BF

n_2 - Refractive index of low-index layer in BF

Δn_{BF} – Contrast of refractive indices between layers in BF

n_i - Refractive index of inclusion in HF

n - Refractive index of matrix in HF

d – diameter of inclusion in HF

Λ - pitch between centers of inclusions in HF

Publications

[1] A.S. Biriukov, D.V. Bogdanovich, **D.A. Gaponov**, A.D. Priamikov, "*Optical properties of bragg optical waveguides*", Quantum Electronics, 38, N7, pp.620-633 (2008)

[2] **D.A. Gaponov**, A.S. Biriukov, "*Optical properties of microstructure tellurite glass fibers*", Quantum Electronics, 36, N4, pp. 343-348 (2006)

[3] **D.A. Gaponov**, A.S. Biriukov, "*Effective method of optical properties analysis of microstructured optical fibers*", Foton-Express, N6, pp. 77-104 (2005)

[4] S. Février, **D. Gaponov**, P. Roy, M. E. Likhachev, S. L. Semjonov, M. M. Bubnov, E. M. Dianov, M. Y. Yashkov, V. F. Khopin, M. Y. Salganskii, and A. N. Guryanov, "*High-power photonic-bandgap fiber laser*," Opt. Lett. 33, pp. 989-991 (2008)

[5] **D.A. Gaponov**, A.S. Biriukov, *"Numerical modeling of process of light propagation in photonic crystal waveguides by means of cylindrical functions expansion method", scientific* session MEPhI-2005, Section L-1 (2005)

[6] A.S. Biriukov, D.V. Bogdanovich, **D.A. Gaponov**, A.D. Pryamikov, "*Optical fiber waveguide with a multilayered dielectrical cladding*" Preprint of FORC RAS, N14, p. 38 (Moscow, 2008)

[7] **D. Gaponov**, P. Roy, S. Février, M. E. Likhachev, S.L. Semjonov, M.M. Bubnov, E. M. Dianov, M.Yu.Yashkov, V. F. Khopin, M. Yu. Salganskii, A. N. Guryanov, "*High-Power Photonic Bandgap Fibre Laser*", ECOC'2007, Pds3.9 (2007)

[8] Philippe Roy, Laure Lavoute, Sébastien Février, Jean-Louis Auguste, Jean-Marc Blondy, **Dmitry Gaponov**, Mathieu Devautour, Aude Roy, Philippe Leproux, Laurent Bigot, Géraud Bouwmans, Vincent Pureur, "*Microstructured fibres and applications*", CLEO /Europe-IQEC 2007, Topic Area CJ (2007)

[9] Février Sébastien, **Gaponov Dmitry**, Lecaplain C., Martel G. , Roy Philippe , Hideur A, Likhachev Mikhail , Yashkov M.Y. , Salganskii M.Y., "*Photonic Bandgap Fibers for High-Power CW and Pulsed Applications*", IEEE/LEOS Winter Topical Meetings, TuD3.1 (2008)

[10] Février Sébastien, **Gaponov Dmitry**, Roy Philippe, Lecaplain C., Martel G. , Roy Philippe , Hideur A, Likhachev Mikhail , Yashkov M.Y. , Salganskii M.Y., "*Cladding-pumped ytterbium-doped photonic bandgap fibre laser*", Photonics Europe 2008, Paper 6990-21 (2008)

PREFACE

General characteristic

Present work has experimentally-theoretical character. The **theoretical part** of it is dealt with analysis of optical properties of basic types of microstructured waveguides based on most effective methods of numerical simulations. In the **experimental part** of the work a possibility of a practical application of active BF with large mode area (LMA) in creation of an effective and singlemode fiber laser is demonstrated.

Theme relevance

A rush development of a new field in a fiber optics "Microstructured Optical Fibers" (MOF) showed the big prospects in applying such structures in different fields of science and technology. Optical properties of MOF hardly depend on its geometry, but an analytical solution of electrodynamics tasks arising in each case generally seems not possible. That's why an important task here is implementation of methods for MOF computational modeling.

From the other hand, a structure of BF was not optimized to have minimal waveguide losses in no papers in detail. Besides, wasn't paid a proper attention to a question of which mode is fundamental in the hollow and all-solid BF and why. Insufficient, for our mind, optical properties of BF having cladding structure differing from quarter wave when a cladding period is appreciably greater than wavelength were investigated. From view of the aforesaid it seems actual a revision of BF analysis in general with an aim to generalize it to the wider range of possible cladding structures and to develop an optimization method for them.

An analysis of 2-D structures assumes larger costs of a computing time in contrast to Bragg structures. One of known from literature methods – a multipole method allows a computational time minimizing due to taking into account cylindrical geometry and symmetry of the task. With help of this method a possibility of an effective analysis of basic MOF types appears. That is demonstrating in this work by the example of optical properties investigation of tellurite holey fibers (tellurite HF). The

reason to use namely the tellurite glass as a material for holey fibers is determined by its higher refractive index and also its higher nonlinear properties in comparison to the silica glass.

Finally, one of the perspective trends in MOF utilization is a possibility of LMA MOF creation. Recently, it was shown that the arising problem of singlemodeness of the output irradiance with the simultaneous low bend sensitivity is possible to solve with helps of bragg waveguides. Then the actual and important task is the creation of fiber laser based on large mode area bragg fiber with the similar structure and to investigate of its potential and properties.

Main aims

The main aim of the theoretical part of the work is numerical modeling and the analysis of optical properties of main MOF types such as bragg fibers and 2-D structures on the example of tellurite HF. **The aim of the experimental part** of the work is the investigation of the active large mode area BF and creation the fiber laser based on it.

Main problems

Aims of the work were achieved by solving of following problems:

1. Realization of numerical methods for modeling BF and 2-D structures by the example of HF.

2. The theoretical analysis of ARROW (Anti Resonant Reflection Optical Waveguides) BF

3. The theoretical analysis of HF optical properties by the example of waveguides based on the tellurite glass.

4. The development of the method for optimization of geometric parameters of BF for obtaining waveguide structures with lowest waveguide losses.

5. The creation of the fiber laser based on large mode area BF

Scientific novelty

- the original method of finding of the BF cladding structure that has lowest optical loss for the given wavelength was proposed and realized

- the necessity of taking into account all complex resonators composing a multilayer cladding at the optical loss spectrum analysis of the ARROW BF was shown

- optical properties of holey fibers based on tellurite glass were investigated theoretically by means of the multipole method

- modal properties of the active BF with considerable contents of Yb ions in the core were investigated theoretically and experimentally

- the effective and singlemode generation in the fiber laser based on the cladding pumped active LMA BF was obtained for the first time

Practical significance

The optimization method suggested allows projecting both hollow and solid core BF with lowest optical loss.

The multipole method realized, with taking into account all inaccuracies that were made by the authors of this method in their original work[1], allows calculating optical properties of MOF (in particular, of photonic bandgap fibers with the hollow or solid core) quite quickly and precisely. Method capabilities are demonstrated by the example of the HF made of tellurite glass. The calculations results allow to properly selecting MOF geometrical parameters to obtain desired optical properties such us spectral position of the dispersion zero point, singlemodeness regions etc.

The fiber laser based on solid core active LMA BF and realized to the best of our knowledge for the first time was demonstrated a potential possibility and perspectives for using such LMA BF as active medium for compact high-power fiber lasers.

[1] T.P. White, B.T.Kuhlmey, R.C.McPhedran, *"Multipole method for microstructured optical fibers. I. Formulation"*, J.Opt.Soc.Am. B, 19, 10 (2002).

Defending regulations

- The method developed for the optimization of BF cladding that allows to design structures with lowest waveguide losses at the given wavelength,

- The analysis of optical properties of ARROW BF showing that it's necessary to take into account all complex cladding resonators instead of resonances of the only one, closest to the core, high-index layer,

- The analysis of optical properties of 2-D MOF on example of tellurite HF by means of the multipole method,

- The created fiber laser based on the cladding pumped active LMA BF and with the effective singlemode generation.

Work approval

The results of investigations developed in the present thesis were published in four papers, one pre-print, were reported on four international conferences: European Conference on Optical Communication ECOC-2007 (Germany, Berlin, 2007), The European Conference on Lasers and Electro-Optics and the International Quantum Electronics Conference CLEO-2007 (Germany, Munich, 2007), Institute of Electrical and Electronics Engineers / Laser & Electro-Optics Society Winter Topical Meetings IEEE/LEOS-2008 (Italy, Sorrento, 2008), Photonics Europe-2008 (France, Strasbourg), and also on FORC RAS seminars. The work "Fiber laser based on large mode area Bragg Fiber" being a part of the present thesis shared a 2-3 place on a competition between works of young scientists of FORC RAS.

Work structure

Thesis is consisting of an introduction, four chapters, a conclusion and a bibliography. The work is developed on 90 pages of a typewritten text, is consisted of 32 figures. The bibliography is consisted of 157 items.

Chapter I. Overview

This chapter is introduction into a field of fiber optics, connected with the microstructured optical waveguides (MOF). Brief survey of a history of appearance and MOF development are represented and the classification of their basic groups is conducted at first. Then physical principles, which lie in a basis of their waveguide properties for each MOF group are explained. Also the overview and classification of MOF types and subgroups are conducted and their unique properties differed from properties of step index fibers are examined with describing basic fields of its applications existed at present.

I.1 Introduction

I.1.1 History of the origin of new branch in fibre optics "Microstructured Optical Waveguides"

It's possible to say without overstatement that one of most important human achievements in twenties century became creation of optical fiber waveguides. After presenting glass fiber waveguide with optical losses about 20 dB/km in 1970 year by Corning Glass Works company [11] rapid development of fiber optics was initiated. Since then and up to now optical losses practically reached its fundamental level around 0.15 dB/km.

From 70th and up to 90th years of last century it was not pay proper attention for a possibility of creation waveguides with principally different waveguide mechanisms probably due to a great advance achieved. In particular, appeared works [12; 13] theoretically demonstrated the possibility of light guiding in, so called, Bragg fibers where main waveguide mechanism instead of total internal reflection was constructive interference occurring with reflection on periodically layered cladding structure.

Realization of the idea about creation of the medium in which bandgap would be exist in electromagnetic eigen photon states connected with works of Yablonovitch and John [14; 15] after a decade later. In these works they took mathematical apparatus of solid state physics for the solution of electrodynamic problems. Actually, it was demonstrated a possibility of "complete" bandgap existing in two or three

dimensions in periodically layered medium with dielectric permittivity modulation period compared with the light wavelength from the optical range. Few years after practical realization of such structures that have been called “photonic crystals” was initiated (see, for example, [16-18]). Besides, the recognition of the possible prospects of applying such structures as the waveguide cladding appeared approximately in the same time. Broad possibilities of designing of optical fibers with unique properties immediately arisen. Then these possibilities to govern many parameters of waveguides, for example, dispersion, mode field diameter, numerical aperture, single-mode behavior in considerably wider limits than those obtained with the aid of the standard step-index fibers, subsequently caused an appearance of the entire branch in fiber optics – “Microstructured optical fibers”. A quantity of scientific groups, which began to investigate waveguides with new possibilities, increased each year in an avalanche, and at the beginning of 21 century a large variety of practical MOF realizations already has been demonstrated. Let us further give classification and brief development of different MOF types which was formed up to the present time.

I.1.2 Brief overview of MOF development

1972, 1975 First description of bandgap arising for photons in periodically layered medium [19; 20]

Ideas of:

1976 bragg fiber [12],

1987 photonic crystal [14; 15],

1993 photonic bandgap fiber (PBGF) [21].

First fabrications of MOFs, demonstrations of their unique properties and creation of devices based on them:

1996 holey fiber [22],

1997 endlessly singlemode HF [23],

1998 large mode area HF [24],

1999 hollow core PBGF [25],

1999 hollow core BF [26],

1999 all-solid BF fabrication [27],

2000 birefringent HF [28].

2000 Supercontinuum generation in HF [29]

2000 Fiber laser based on HF [30]

2002 HF with ultra flattened dispersion [31]

2003 Large mode area fiber laser based on HF [32]

2004 All-solid PBGF [33]

2005 Hollow core PBGF with low optical loss [34]

2006 Large mode area BF [35]

2006 Kagome-type MOF [36]

2006 Q-switched fiber laser based on all-solid PBGF [37]

2007 Cladding pumped large mode area fiber laser based on all-solid BF [7]

I.1.3 Classification of MOF types

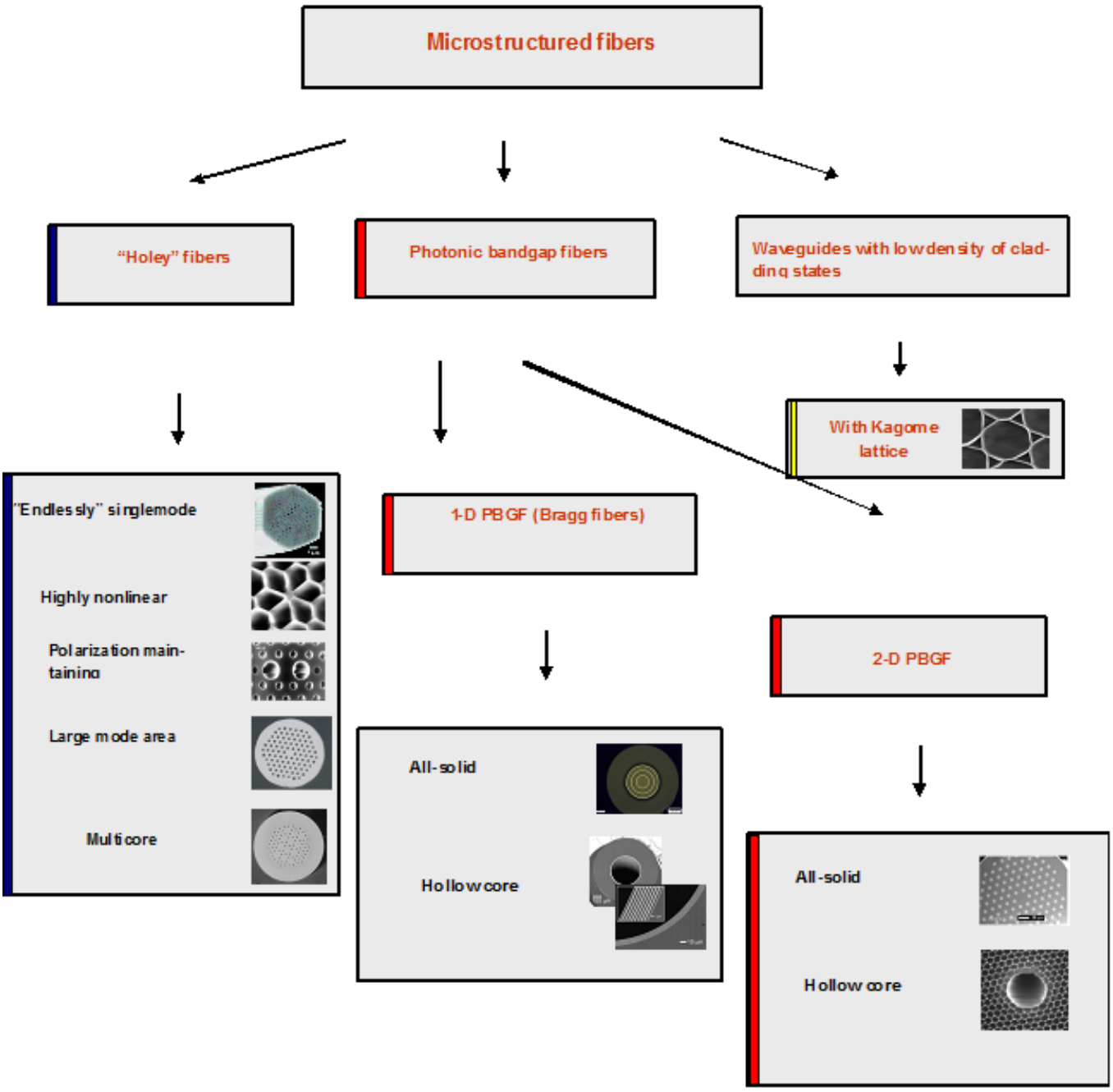

Fig. 1: *Classification of MOF types*

There are three basic MOF groups (Fig.1)

I. Holey fibers (HF) –

Waveguides with the solid glass core which refractive index are more than "average" refractive index of the cladding $n_{core} > \langle n_{cladd} \rangle$ due to a presence of air inclusions in the cladding. The main waveguide mechanism is frustrated total internal reflection.

II. Waveguides based on photonic band gap, or photonic bandgap fibers (PBGF) –

Waveguides with the core which refractive index are lower than "average" refractive index of the cladding $n_{core} < \langle n_{cladd} \rangle$ (hollow core fibers, in particular). The main waveguide mechanism here is defined by "bragg" reflections from the microstructured cladding, or, in other words, when there is a bangap in photon eigen frequencies. .

III. Waveguides with low density of cladding states –

Waveguides with hollow core, but waveguide mechanism is defined due to fact that core mode not interacted with cladding modes because of their low density. At the same time there is no bandgap in photon states and that distinguishes this waveguides from waveguides of group II.

Varieties of MOF from group I:

- *Endlessly singlemode HF*
- *Large mode area HF*
- *Highly nonlinear HF*
- *Polarisation maintaining HF*
- *Multicore fibers*

Group II divided in two subgroups:

- One dimensional PBGF, i.e. Bragg fibers:
    - *Hollow core BF*
    - *All-solid BF*
- Two dimensional PBGF:
    - *Hollow core 2-D PBGF*
    - *All-solid 2-D PBGF*

Finally, group III is consisted of MOF with cladding having *Kagome-type lattice.*

I.1.4 Holey fibers

A holey fiber has the glass core enclosed in the cladding made of the same glass with air holes lowering cladding "average" refractive index with respect to the core. That's why the main waveguide mechanism is almost the same as in step index fibers.

A quantity of core guiding modes of such fiber is determined only by the value of the ratio (d/Λ), whered –is a diameter of air inclusions and Λ - a distance between their axes (i.e. pitch). In this case a periodicity of air inclusions displacement is not obligatory [38], because the main factor here is "average" cladding refractive index value. Existing of air holes allows refractive an increasing of the refractive index contrast more than order of magnitude compared with standard glass step index fibers. This fact principally determines the new properties of HF distinguishing it from the usual optical waveguides.

Possibility of flexible manipulating of dispersion properties with helps of geometry parameters is unique. Such fibers can have anomalous dispersion in much shorter wavelength range [39; 40], its absolute value can be more than magnitude larger [41; 42] compared with step-index fibers. And the dispersion wavelength dependence, in principle, can be quite weak in the broad spectral range [43; 44].

Another one important property of HF is the fact that they be able to supporting only one mode in the very broad spectral range, which practically coincides with the

range of transparency of a quartz glass, so called “endlessly singlemode” waveguides [23].

Singlemode waveguide regime can be realized with large or small effective mode area. Large mode area HF can be used for high peak power transmission [24]. While in HF with the small mode field diameter role of nonlinear effects is notably increasing compared with standard waveguides and it can be useful, for example, in optical parametric amplifiers creation or in supercontinuum generation [29; 45-47].

Often HF has hexagonal symmetry of the holes displacement in the cladding. That’s why the fundamental mode is twofold degenerate and one needs to break symmetry for artificial birefringence inducing. This can be done either by replacing two opposite holes to the holes of the larger diameter [48], or by using elliptically shaped holes [49] instead of circular ones. In these cases birefringence can reaches values of in order of magnitude higher than in usual PANDA constructions. At the same time the temperature sensitivity can be more than ten times smaller [50], or even absent [51] making such HF very important for practice.

One more variety of HF are the multicore-fibers [52] with two or more singlemode cores, not concentrically located in the general case, in the common or double cladding. After core doping by active ions such multicore-waveguides can be used as fiber amplifiers or the powerful lasers with pumping into the cladding [53; 54]. After arranging cores on the sufficiently small distance, their interacting core guided modes are sensitive to the bends, which is successfully applying in the bending sensors [55].

I.1.5 Photonic bandgap fibers

Origin of the complete “stop band” in the spectrum of electron eigenstates in a crystal is caused by presence of a strict periodicity of the crystal lattice in all three directions. Propagation of the electron with energy, which falls into the “stop band”, is impossible in this structure. Physically this means that for a de Broglie wave, which corresponds to electron with this energy, the atomic lattice will work as “ideal” ref-

lector, i.e., all reflections from atomic layers will be summarized in phase – this is so-called “Bragg reflection”.

There proved to be possible [56] to realize structures similar to crystalline atomic lattices in the optical wavelength range also. In this case for photons the periodically structured dielectric medium with the lattice period compared with the wavelength of light is the analog of the periodic potential for electrons. Such structures were called “photon” crystals (PC). Introducing linear defect into this three-dimensional structure we obtain that irradiation with the frequency which falls into “photon stop band” can exist only in the limits of this defect, and the PC cladding is effective reflector for the irradiation. Thus, this structure can work as waveguide for irradiation with frequencies which fall in corresponding “photon stop bands”. Therefore such waveguide structures were called photonic bandgap fibers (PBGF).

Two subgroups of PBGF are distinguished with respect to cladding geometry.

I.1.5.1 Bragg fibers

Waveguides where cladding represented by well-known in optics multilayered dielectric mirror are related to the first subgroup. Here, photonic band gap is formed in the radial direction for the specific wavelength. In other words, such cladding is representing by itself 1-D photonic crystal. Its mirror properties are defined by Fresnel reflection from dielectric boundaries of the multilayer structure with alternating values of permittivity with following constructive interference of reflected waves. The reflection from multilayer dielectric mirrors formally resembling x-ray scattering phenomenon in crystals and is described by Bragg condition. That’s why waveguides with multilayered, periodical claddings and with a core made of optically less dense material (in particular, air) was called “bragg” [13]. Typically, as for all PBGF, the irradiation with frequencies only from specific spectral ranges can propagate in the core of waveguides with multilayer cladding structure. And contrary, there are existing only specific bragg waveguiding structures where light with the given wavelength can propagate with quite low losses. Hence, not for arbitrary widths (even if they are

compatible with the wavelength) of layers of the periodical cladding irradiation can be effectively localized in the core.

Nevertheless that theoretical investigation of such structures was initiated at the end of 1970 years its experimental realization has been accomplished only quite recently. For example BF with the hollow core was realized in work [26] and in [27] was realized BF with the solid core for the first time in both cases.

BFs with the hollow core are of interest mainly by their possibility to almost entirely eliminate influence of a material on waveguide properties of the fiber structure. Optical losses in hollow BF are still appreciable for the light wavelength from the telecommunications range. But such waveguides already has losses lower than material losses by an order of magnitude at the generation wavelength of CO_2 laser [57]. From the other hand a mode with lowest losses in hollow BF is nondegenerate TE_{01} mode that excludes an influence of polarization mode dispersion. Also in such waveguides it's possible to realize regimes where the dispersion reaches high absolute values [58] that can be applied for a dispersion control in different devices.

Also at present a great interest for researches offering BF with the solid core. For example in [35] the possibility of reducing a bent sensitivity (compared with step index and holey fibers) while keeping the mode field diameter unchanged was shown. In BF with the solid core also is possible to obtain large absolute dispersion values [59].

I.1.5.2 Two dimensional PBGF

The second subgroup of PBGF is consisted of waveguides with the core made of optically less dense material than "average" refractive index of the cladding formed by periodically arranged holes (or dielectric rods). Such arrangement of holes in cladding is forming the photonic bandgap in a transverse direction for the given wavelength. Such cladding represents the 2-D photonic crustal. The core here can be either hollow, or solid like in BF.

A) Hollow 2-D PBGF

In PBGF with the hollow core a localization of light is provided by bragg reflection from the microstructured cladding (from air holes in this case) with following constructive interference, like in BF. Loss mechanisms have many common properties with hollow BF. One mechanism of waveguide losses here is finite cladding structure of waveguide along radius and its decreasing to the some necessary level can be provided by addition of corresponding amount of layers with holes into the cladding structure.

For arising of another loss mechanism in PBGF corresponds the interaction of the "defect" core mode with "surface" modes [56] (pp. 73–76), [60] (pp. 210–215).

"Surface" modes are guided modes within bandgap localized in a glass material that surrounds the hollow core. Interaction of surface modes with the core mode leads to its dispersion curves anticrossing and, hence, to appearance of high loss regions [61].

However, it seems that taking into account all mechanisms described above isn't a sufficient condition for ensuring the low loss level in such structures. It is considered that a main contribution to optical losses in hollow PBGF brings a scattering on roughness that appears on air/glass boundaries due to frozen capillary waves which are thermally induced while a drawing process [34].

Thus, the loss level in hollow PBGF existing at presents not allowing of its utilization as a transmission medium in long haul telecommunications.

However, as in BF case, there are some fields where effective use of hollow PBGF already is possible. For example they can be used as waveguides that delivers high power of industry lasers (CO_2, Nd^{3+} solid-state) [62; 63], as optical sensors when core is filled by gas [63; 64]. Dispersion properties of PBGF allow them to use in optical amplifiers schemes, for chirped pulses recompression etc. [65]

B) All-solid 2-D PBGF

Such PBGF represents by itself the structure with the solid core and with the cladding composed by periodically arranged dielectric rods with higher refractive in-

dex. The physical mechanism of photonic bandgap creation here is well described by Anti Resonant Reflection Optical Waveguide (ARROW) model [66- 68]. High index rods effectively reflect light to the core if they are in antiresonance and contrary, allow light to leaks out from the core when they are in resonance. Photonic states of the individual rod considered as the separate step index waveguide are either its guided modes or leaky modes (analytical extension of guided modes below cut-off).

Leaky modes of separate rods interacting with each other create a "photonic band" which center is some specific mode of individual rod. The photonic bandgap lies in between two neighbor photonic bands.

Like all PBGF waveguides, all-solid PBGF have the same set of unique properties – dispersion, spectral, and modal. However they have one important advantage – whole silica construction with all consequences, such as simpler drawing process, splice, doping and bragg gratings writing that makes them more adapted for use in practice in fiber lasers and amplifiers than less mechanically stable holey structures. Also it was shown that all-solid 2-D PBGF can be less bend sensitive than step-index waveguides [69].

I.1.6 Waveguides with low density of cladding states.

To the third group of MOF we can relate waveguides where usual hexagonal-like cladding lattice is changed to Kagome type lattice. Kagome lattice represents structure made of intersections of three sets of parallel lines where triangles which are result of these intersections have common points only in apexes (Fig.1). Silica edges of such triangles have a width in order of a micron and interspaces are filled with air.

There are no band gaps in the cladding of such structure, but density of photonic states is so low, that the core mode doesn't interact with cladding modesthrefore providing its localization in the core [70].

A transmission spectrum can be considerably wider in this case than in hollow PBGF [36]. At the same time losses are quite low and high loss ranges here are defined only by resonances of silica "edges" [71]. In [72] perspectives of using of such structures as waveguides in middle infrared range was shown.

Chapter II. Analysis of optical properties of Bragg Fibers

In this Chapter the electrodynamic problem of propagation of light in a fibre with a cladding made of coaxial dielectric layers with alternating values of the refractive index is solved. A method is described for determining the structure of the multilayer cladding of a fibre having the minimal optical loss of the guided radiation for a particular mode. Differences in the optimization of hollow and solid core BF were described. Losses in a fibre with a cladding with quasi-periodic layer thicknesses are calculated and the dispersion properties of the fibre are analysed. The analysis is performed for the lowest TE and TM modes and for the lowest hybrid mode.

Main results of this Chapter are published in works [1; 6].

II.1 Introduction

It is accepted that the first theoretical study of a dielectric Bragg waveguide in the visible and IR spectral ranges was performed in [13]. Only the lowest of the TE modes was analysed and it was pointed out that BFs are potentially efficient mode filters and, therefore, they can operate in the single-mode regime even at large core diameters. At the same time, optical losses in BFs were not calculated and only the general scheme was proposed, which can be used in principle to calculate them. Later [73], concrete and rather pessimistic data about losses in BFs were reported. The authors of [73] explained large losses in hollow BFs (more than 10^6 dB/km) by the impossibility to provide the high efficiency of radiation coupling into a fiber. Because of the absence of data on the fiber structure, the wavelength of guided radiation, and the mode type, it is impossible to verify the results obtained in [73].

In [74], the optical properties of a hybrid mode (the HE_{11} mode, according to the author) of a BF made entirely of silica were calculated. The author of [74] concluded based on his calculations that it is this mode that should have the highest Q factor, and to achieve optical losses smaller than 0.1 dB/km, it is sufficient to have

eight layers in the cladding, which in this case had the refractive-index contrast in neighbouring layers equal to 0.022.

In [75], a model BF was studied which contained 100 dielectric layers of thickness 1 μm with alternating refractive indices $n_1 = 1.51$ and $n_2 = 1.49$ (the refractive index of the fibre core was $n_0 = n_1$ and the radius of the core cross section was varied from 2.5 to 3.25 μm). The main conclusions of paper [75] are that the TE modes should have the lowest optical losses in a glass BF, while the TM modes should have the highest losses (optical losses for hybrid modes are intermediate), which obviously contradicts to results [74].

In [76], the TE modes of a composite BF with a hollow core and a large refractive-index contrast in cladding layers $n_1 = 3$ and $n_2 = 1.5$ were analysed in the asymptotic approximation of large arguments of cylindrical functions (plane wave approximation). The layer thicknesses were set equal to 0.13 and 0.265 μm, respectively, and the core radius was 1 μm. The distributions of the longitudinal magnetic and azimuthal electric components of the lowest TE were found. It was pointed out that in the case of such a large refractive-index contrast in layers, the field amplitudes should decease with increasing the radial coordinate so rapidly that the optical loss related to radiation fiber modes ~ 0.2 dB/km can be achieved by using only twenty pairs of structure layers.

Note that multilayer dielectric waveguides were studied earlier in the microwave range in the plane wave approximation in paper of Russian researchers [77-81]. The theory developed in [81] was applied to the optical range as well and, unlike previous papers, it was found that the EH_{11} mode should have the lowest losses.

The transfer matrix method described in [82] for analysis of Bragg reflectors of cylindrical walls is analogous to the known method for plane multilayer mirrors [83]. The method allows one to find the geometrical parameters of the structure most efficiently reflecting cylindrical waves. It is pointed out that the method can be used to analyze multilayer cylindrical waveguides; however, concrete results are absent.

The waveguiding possibilities of a hollow BF with the refractive indices $n_1 = 4.6$ and $n_2 = 1.59$ in a broad IR range (5—16 μm) were demonstrated in [26]. As a rule, dielectrics with considerably different permittivities also have different coefficients of thermal expansion. It is rather difficult to fabricate a multilayer structure from such dielectrics in the technological process including the drawing of fibers from preforms. In [26], fibers were fabricated by depositing the components of a coaxial structure in layers (polymer and tellurium layers) on the external surface of a silica capillary followed by the dissolving of the later in hydrofluoric acid. The fabricated waveguide was not subjected to drawing and had, as a result, a comparatively large diameter of a hollow core, which was equal to the external diameter of the glass capillary (1.92 mm). It is obvious that this technology cannot be used to fabricate long waveguides. The investigations of this BF showed the presence of the transmission band between 8 and 11.5 μm, whose width was independent of the angle of incidence of radiation on the cladding, and also a comparatively small decrease in transmission even at a small radius of fibre bending (~ 1 cm).

Silica Bragg fibres were fabricated comparatively recently. In [27; 84], fibres with three pairs of coaxial glass layers and a glass core with the refractive index lower than those of cladding layers were studied. The length of fibres studied in [26; 27; 84] did not exceed, as a rule, ~ 1 m, so that experimental data on losses and other quantitative parameters of the fibres were absent.

Later [57], however, comparatively long (several metres) hollow BFs with a large permittivity contrast in layers were fabricated by using a chalcogenide glass As_2Se_3 with the refractive index of ~ 2.8 and a thermoelastic polymer with the refractive index of ~ 1.55, which had matching thermal properties. These fibres had different geometrical parameters (core diameter and thickness of a multilayer cladding) for different transmission ranges. In particular, BFs with the hollow core diameters 700—750 μm had the main transmission band in the wavelength region from 10 to 11 μm (the second transmission band was at ~ 5 μm). The optical losses at the CO_2 laser wavelength 10.6 μm were 0.95 dB/m, which is considerably smaller than optical

losses in As_2Se_3 (~ 10 dB/m) and is many of orders of magnitude smaller than optical losses in polymers.

After 2000, many papers devoted to theoretical and experimental studies of BFs were published (see, for example, [35, 85-110]). However, in none of the papers the fiber structure was optimized in detail to achieve minimal optical losses. It is possible that for this reason the optical properties of BFs were estimated quite differently in different papers, both rather optimistically [74; 89] and, on the contrary, pessimistically (for example, [73]). In our opinion, it is not definitely clear so far which of the modes in hollow and glass BFs is fundamental [75; 108; 109]. This situation stimulated us to reconsider this problem as a whole and to analyse the properties of BFs based on somewhat different concepts.

II.2 Theoretical part

The mechanism of formation of guided radiation in BFs, which differs from that inherent in usual fibers, should result in the different formulation of the problem of analyzing their properties. Instead of searching for the field distribution in a fiber with a preliminarily specified light-guiding structure, as is done for usual two-layer fibers and most of the theoretical studies of BFs, we will find, on the contrary, the structure of a fiber in which the field should not only satisfy the boundary conditions but also should be maximally localized in an optically less dense core.

II.2.1 Main equations and their solutions

We start, as usual, from Maxwell's equations, by representing them in the form of wave equations. We assume that light propagates in a dielectric medium with the magnetic susceptibility equal to unity everywhere and the permittivity ε invariable in time and uniform in each of the layers of the fibre cladding (step radial profile of the distribution of ε). The time dependences of the electric $\vec{E}_0$ and magnetic $\vec{H}_0$ components of the field can be written in the form $\vec{E}_0 = \vec{E}e^{-i\omega t}$ and $\vec{H}_0 = \vec{H}e^{-i\omega t}$.

Then, the vectors $\vec{E}$ and $\vec{H}$ in fibre cladding layers and core satisfy the wave equations

$$\left(\Delta + \frac{\omega^2 \varepsilon}{c^2}\right)\begin{Bmatrix}\vec{E}\\ \vec{H}\end{Bmatrix} = 0, \qquad (1)$$

Then we take into account the translation invariance of the field along its propagation direction *z*. This will define the dependence of field components on the longitudinal coordinate in the form of a factor $\exp(i\beta z)$, where β is the phase propagation constant (i.e. longitudinal component of the wave vector – the complex variable in general case).

Now let us represent each of vectors $\vec{E}$ and $\vec{H}$ by the sum of the longitudinal and the transverse components

$$\vec{E} = (\vec{e}_t + e_z \vec{z})\exp(i\beta z),$$
$$\vec{H} = (\vec{h}_t + h_z \vec{z})\exp(i\beta z),$$

(where $\vec{z}$ - a unit vector of the *z*-axis), and we found that any of longitudinal components of the field e_z or h_z (denoted by Q) validating the equation

$$(\Delta_\perp + k_j^2)Q = 0. \qquad (1^*)$$

Here $k_j^2 = \varepsilon_j \omega^2 / c^2 - \beta^2 = (2\pi n_j / \lambda)^2 - \beta^2$, k_j - transversal component of the wave vector (also is the complex variable in a general case) in a material of the waveguide with the refractive index $n_j = \sqrt{\varepsilon_j}$; $k_0 = 2\pi / \lambda$ - wave number of free space; λ - wavelength of light in vacuum; $\Delta_\perp = \Delta - \frac{\partial^2}{\partial z^2}$ - transversal Laplace operator. The relation of transversal and longitudinal components is defined by Maxwell equations [111].

Equations (1*) for the longitudinal field components E_z and H_z (denoted by Q) in the cylindrical coordinate system *(r,φ,z)* have the known form

$$\frac{1}{r}\frac{\partial}{\partial r} r \frac{\partial Q}{\partial r} + \frac{1}{r^2}\frac{\partial^2 Q}{\partial \varphi^2} + (\frac{\omega^2 \varepsilon_j}{c^2} - \beta^2)Q = 0. \qquad (2)$$

We assume that the cladding permittivity, which is uniform along *z* and *φ*, has only two values alternating in cladding layers.

Under these assumptions, the solution of (2) has the form:1

$$Q = R(r)(G_1 \cos m\varphi + G_2 \sin m\varphi)e^{i\beta z}, \qquad (3)$$

where m – is the azimuthal parameter (for axially symmetric fibres, m is an integer, including zero); G_1, G_2 - are integration constants; $R(r)$ – is the radial part of the coordinate dependence of Q.

For the function $R(r)$, we obtain from (2) the Bessel equation

$$\frac{d^2R}{dr^2} + \frac{1}{r}\frac{dR}{dr} + (k_j^2 - \frac{m^2}{r^2})R = 0, \qquad (4)$$

where $k_j^2 = \varepsilon_j \omega^2 / c^2 - \beta^2 = (2\pi n_j / \lambda)^2 - \beta^2$; k_j – are the transverse components of wave vectors in media with refractive indices $n_j = \sqrt{\varepsilon_j}$; λ - is the radiation wavelength in vacuum.

The solution of (4) in the general case is a combination of two linearly independent cylindrical functions. It is known that there exist several such combinations. Before choosing a particular solution of (4), note the following.

We will assume that the fibre core has the refractive index n_0 and the refractive indices of alternating coaxial cladding layers are n_1 and n_2, and for definiteness $n_1 > n_2 > n_0$. Assume also that material losses in the fibre are absent $(\mathrm{Im}\, n_j = 0; j = 0,1,2)$. In such a multilayer structure, numerous, both natural and quasi-natural waves can be excited. The natural waves are defined as slow waves with a discrete spectrum appearing due to total internal reflection and localised in optically dense cladding layers. The fields of quasi-natural, the so-called rapid waves are formed due to frustrated total internal reflection for cladding layers and are localised in the fibre core [81]. It is these radiation modes, which have the absolute maxima of the field components in the core but also possess some radiation losses, which we are interested in. The envelopes of radial distributions of the field components of such modes should be functions of r rapidly deceasing in magnitude. Only if this condition is fulfilled, the cladding properties of a mirror can be manifested. It is also clear the value of $k_0^2 = (2\pi n_0 / \lambda)^2 - \beta^2$ should be positive (k_0 is the transverse wave number in the fibre core). Otherwise, the argument $k_0 r$ of cylindrical functions in the solution of (4)

proves to be imaginary, and the solution itself is represented only by one modified Bessel function of the first kind $I_m(k_0 r)$, which monotonically increases with #r and has no the absolute extremum in the core (the second linearly independent cylindrical function $K_m(k_0 r)$ of the imaginary argument has a singularity for $r = 0$ and should be excluded from consideration). It follows from the above discussion that the main difference of a BF from a usual two-layer fibre is that the value of the effective mode refractive index $\bar{n} = \beta\lambda / 2\pi$ in the usual fibre lies between the refractive indices of the fibre core and cladding, whereas this value for the BF should be smaller than the refractive index of the optically less dense core material, i.e. $\bar{n} < n_0$ (for a hollow BF, $\bar{n} < 1.0$).

It is easy to see that the condition $k_0^2 > 0$ is fulfilled for purely imaginary values of the propagation constant β; however, they are of no interest because for such β there is no wave propagating along *z*.

It is clear that the complete absence of radial energy transfer would be corresponded to a structure representing an ideal cylindrical mirror. It is known that in this case a standing wave is formed along the radial coordinate, while the absence of energy transfer in it means that the time-averaged radial component S_r of the Poynting vector $\vec{S} \sim \mathrm{Re}[\vec{E}\vec{H}^{\bullet}]$ is zero. Recall that the electric energy in a standing wave completely transforms to the magnetic energy during a quarter of the period of electromagnetic oscillations and during the next quarter – vice versa, the magnetic energy transforms to the electric energy. In this case, the energy migrates from the antinodes of the electric field to the phase-shifted (by $\pi/2$) antinodes of the magnetic field and backward. The energy flux through the nodes of the electric and magnetic fields is identically zero (i.e. at any arbitrary instant of time). Each layer of the medium of optical thickness λ/4 from a node of the electric field to the nearest node of the magnetic field does not exchange energy with the environment. In a real, not ideally reflecting multilayer structure of a finite thickness (with a finite number of layers), a "quasi-standing" wave is formed, which is a superposition of a standing wave and a

wave travelling in the radial direction and determines optical losses. In other words, we define the "quasi-standing" wave as a wave with the radial energy flux somewhat different from zero. In this respect, we can say only about a partial localisation of light in the BF core. Therefore, in the general case even in the absence of material losses in fibre layers, the propagation constant β is a complex quantity with the positive imaginary part. This imaginary part in turn should be a function of the radiation wavelength and the number of dielectric layers in the fibre cladding.

Each BF structure has the maximum reflectance of a cladding at a specific wavelength λ_0 of guided radiation. The shift of any side of λ_0, as a decrease in the number of layers in the cladding, leads, as will be shown below, to an increase in $\mathrm{Im}\beta$, increasing thereby optical losses (the real part of the exponent in the factor $e^{i\beta z} = e^{z(i\,\mathrm{Re}\beta - \mathrm{Im}\beta)}$) increases. Below, it makes sense to analyse only BF structures with $\mathrm{Im}\beta << \mathrm{Re}\beta$; therefore, the condition $\bar{n} < n_0$ should be fulfilled for $\bar{n} \approx \lambda\,\mathrm{Re}\beta/2\pi$ with good accuracy.

According to the above consideration, we will write the solution of (4) in the form of a linear combination of linearly independent Bessel and Hankel functions of the first kind, which gives for Q:

$$Q(r,\varphi,z) = (G_1 \cos m\varphi + G_2 \sin m\varphi)\left[C_1 J_m(kr) + C_2 H_m^{(1)}(kr)\right]e^{i\beta z}, \qquad (5)$$

where C_1, C_2 - are two additional integration constants. For the time dependence of the field components that we use ($\sim e^{-i\omega t}$), the Hankel function $H_m^{(1)}$ determines a wave diverging from the symmetry axis. The superposition of the standing and travelling waves instead of the functions J_m and $H_m^{(1)}$ can be, of course, also described by other pairs of linearly independent cylindrical function, in particular, $H_m^{(2)}$ and $H_m^{(1)}$ or, as in [13], by J_m and N_m (N_m is the Neumann function).

Taking into account that $H_m^{(1)}(kr)$ has a singularity at r = 0, it is necessary to assume that $C_2 = 0$ for the cladding region in (5).

We further assume that the layered part of the cladding is surrounded by a very thick dielectric layer with the refractive index n_2 (or n_1). Based on physical consid-

erations, the solution of (5) in this region should be represented only by the function $H_m^{(1)}$ (assuming that $C_1 = 0$). Indeed, here in the absence of interfaces between different media, there are no reflections of light and only diverging waves can exist. The latter statement is true if either the thickness of the external non-layered part of the cladding is infinite or the field intensity in it small. In reality, the entire glass structure of a fibre is covered with a protective jacket made of polymers or other materials (in particular, metals). Therefore, the reflection of light from the additional glass—protective jacket interface should be taken into account in the number of cases [110].

The necessity of fulfilment of boundary conditions for any values of the azimuthal coordinate φ determines the constants G_1 and G_2 in (3) and (5), which are not arbitrary in this case. In other words, the solutions of (2) represent two variants of dependences on transverse coordinates (or two classes of waves) containing simultaneously either upper or lower trigonometric functions in braces in the expressions

$$E_z = \left[AJ_m(kr) + BH_m^{(1)}(kr)\right]\begin{Bmatrix}\cos m\varphi \\ \sin m\varphi\end{Bmatrix} e^{i\beta z},$$

$$H_z = \left[CJ_m(kr) + DH_m^{(1)}(kr)\right]\begin{Bmatrix}\sin m\varphi \\ \cos m\varphi\end{Bmatrix} e^{i\beta z}, \qquad (6)$$

where *A, B, C,* and *D* are arbitrary constants.

By defining E_z and H_z in the form (6), we find with their help from Maxwell's equations the rest of the field components. Thus, the solution of equations (1) is represented by two sets of relations in accordance with the two possible variants of solutions (6):

$$E_z = \left[A_i J_m(k_j r) + B_i H_m^{(1)}(k_j r)\right]\begin{Bmatrix}\cos m\varphi \\ \sin m\varphi\end{Bmatrix},$$

$$E_r = \frac{i\omega}{ck_j^2}\left(\overline{n}\frac{\partial E_z}{\partial r} + \frac{1}{r}\frac{\partial H_z}{\partial \varphi}\right) =$$

$$= \frac{i\beta}{k_j}\left\{\left[A_i J_m'(k_j r) + B_i H_m^{(1)\prime}(k_j r)\right] + \frac{m}{\alpha k_j r}\left[C_i J_m(k_j r) + D_i H_m^{(1)}(k_j r)\right]\right\}\begin{Bmatrix}\cos m\varphi \\ \sin m\varphi\end{Bmatrix},$$

$$E_\varphi = \frac{i\omega}{ck_j^2}\left(\frac{\bar{n}}{r}\frac{\partial E_z}{\partial \varphi} - \frac{\partial H_z}{\partial r}\right) =$$

$$= \frac{i\beta}{k_j}\left\{\frac{m}{k_j r}\left[A_i J_m(k_j r) + B_i H_m^{(1)}(k_j r)\right] + \frac{1}{\alpha}\left[C_i J_m{}'(k_j r) + D_i H_m^{(1)}{}'(k_j r)\right]\right\}\begin{Bmatrix}-\sin m\varphi \\ \cos m\varphi\end{Bmatrix},$$

$$H_z = \left[C_i J_m(k_j r) + D_i H_m^{(1)}(k_j r)\right]\begin{Bmatrix}\sin m\varphi \\ \cos m\varphi\end{Bmatrix},$$

(7)

$$H_r = \frac{i\omega}{ck_j^2}\left(-\frac{\varepsilon_j}{r}\frac{\partial E_z}{\partial \varphi} + \bar{n}\frac{\partial H_z}{\partial r}\right) =$$

$$= \frac{i\beta}{k_j}\left\{\frac{m\varepsilon_j}{\alpha k_j r}\left[A_i J_m(k_j r) + B_i H_m^{(1)}(k_j r)\right] + \left[C_i J_m{}'(k_j r) + D_i H_m^{(1)}{}'(k_j r)\right]\right\}\begin{Bmatrix}\sin m\varphi \\ \cos m\varphi\end{Bmatrix},$$

$$H_\varphi = \frac{i\omega}{ck_j^2}\left(\varepsilon_j\frac{\partial E_z}{\partial r} + \frac{\bar{n}}{r}\frac{\partial H_z}{\partial \varphi}\right) =$$

$$= \frac{i\beta}{k_j}\left\{\frac{\varepsilon_j}{\alpha}\left[A_i J_m{}'(k_j r) + B_i H_m^{(1)}{}'(k_j r)\right] + \frac{m}{k_j r}\left[C_i J_m(k_j r) + D_i H_m^{(1)}(k_j r)\right]\right\}\begin{Bmatrix}\cos m\varphi \\ -\sin m\varphi\end{Bmatrix},$$

where the subscript j = 0, 1, 2 according to the definition of k_j and n_j; $\alpha = \pm\beta c/\omega = = \pm\bar{n}$; and the common factor $\exp(i\beta z)$ for all field components is omitted in (7). The subscript *i* of integration constants indicates that the corresponding solution belongs to the *i-th* layer so that $r_{i-1} \le r \le r_i$, where r_i are coordinates of the interfaces between layers with different refractive indices, *i = 1, 2,...N; N* is the number of interfaces equal to the doubled number of layers with the high refractive index n_1, if the non-layered part of the cladding has the refractive index n_2; when this part has the refractive index n_1, N is larger by unity; $r \le r_1$ corresponds to the core region. The prime at cylindrical functions means differentiation with respect to the argument. Solutions (7) are classified so that $\alpha = \bar{n}$ and $\alpha = -\bar{n}$ correspond to the group with upper and lower, respectively, trigonometric functions in braces at the right.

The boundary conditions to which the solutions of the electrodynamic problem should satisfy require the continuity of the filed components $(E_z, E_\varphi, H_z, H_\varphi)$ tangen-

tial to medium interfaces. It follows from (7) that in the general case (m≠0) these boundary conditions have the form

$$
\begin{aligned}
A_{l-1}J_m(x_{jl}) + B_{l-1}H_m^{(1)}(x_{jl}) &= A_lJ_m(x_{pl}) + B_lH_m^{(1)}(x_{pl}),\\
\frac{m}{x_{jl}^2}\left[A_{l-1}J_m(x_{jl}) + B_{l-1}H_m^{(1)}(x_{jl})\right] + \frac{1}{\alpha x_{jl}}\left[C_{l-1}J_m'(x_{jl}) + D_{l-1}H_m^{(1)\prime}(x_{jl})\right] &=\\
= \frac{m}{x_{pl}^2}\left[A_lJ_m(x_{pl}) + B_lH_m^{(1)}(x_{pl})\right] + \frac{1}{\alpha x_{pl}}\left[C_lJ_m'(x_{pl}) + D_lH_m^{(1)\prime}(x_{pl})\right],&\\
C_{l-1}J_m(x_{jl}) + D_{l-1}H_m^{(1)}(x_{jl}) &= C_lJ_m(x_{pl}) + D_lH_m^{(1)}(x_{pl}),\\
\frac{n_j^2}{\alpha x_{jl}}\left[A_{l-1}J_m'(x_{jl}) + B_{l-1}H_m^{(1)\prime}(x_{jl})\right] + \frac{m}{x_{jl}^2}\left[C_{l-1}J_m(x_{jl}) + D_{l-1}H_m^{(1)}(x_{jl})\right] &=\\
= \frac{n_p^2}{\alpha x_{pl}}\left[A_lJ_m'(x_{pl}) + B_lH_m^{(1)\prime}(x_{pl})\right] + \frac{m}{x_{pl}^2}\left[C_lJ_m(x_{pl}) + D_lH_m^{(1)}(x_{pl})\right],&
\end{aligned}
\qquad (8)
$$

Where $x_{jl} = k_j r_l$; $x_{pl} = k_p r_l$; the subscripts j and p correspond to two media separated by a cylindrical interface of radius r_l. In this case, the inmost interface has the radius r_1, so that $k_j = k_0$ and $k_p = k_1$ in it. Then, for $l = 2$, $k_j = k_1, k_p = k_2$, and for *l>2* values of k_j and k_p alternate.

II.2.2 Dispersion equations

Boundary conditions (8) are a system of 4N linear homogeneous algebraic equations for 4N integration constants $A_0, A_1, ..., A_{N-1}$; $B_1, B_2, ..., B_N$; $C_0, C_1, ..., C_{N-1}$; $D_1, D_2, ..., D_N$ (recall that $B_0 = D_0 = 0$ in the fibre core and $A_N = C_N = 0$ behind the layered structure). The nontrivial solution of this system exists if only its determinant is zero. The zero determinant represents a nonlinear dispersion equation determining the dependence of β on ω (or λ) for the known fibre geometry (the known coordinates r_l) or, vice versa, the equation relating the propagation constant β with the structure geometry for fixed λ. Let us find this dispersion equation.

The calculation of the 4N×4N determinant for large values of N is quite time-consuming. However, in our case the calculation is simplified and is reduced to operations with quadratic 4 x 4 matrices. Indeed, boundary conditions (8) can be written in the matrix form

$$\begin{pmatrix} A_l \\ B_l \\ C_l \\ D_l \end{pmatrix} = M(r_l) \begin{pmatrix} A_{l-1} \\ B_{l-1} \\ C_{l-1} \\ D_{l-1} \end{pmatrix}, \tag{9}$$

where

$$M(r_l) = -\frac{i\pi x_{pl}}{2}(m_{ks}), \tag{10}$$

is the 4 x 4 matrix; *k* is the line number; and *s* is the column number. By using (8), it is easy to show that matrix elements in (10) are

$$m_{11} = J_m(x_{jl})H_m^{(1)\prime}(x_{pl}) - \frac{\varepsilon_j x_{pl}}{\varepsilon_p x_{jl}} J_m'(x_{jl})H_m^{(1)}(x_{pl}),$$

$$m_{12} = H_m^{(1)}(x_{jl})H_m^{(1)\prime}(x_{pl}) - \frac{\varepsilon_j x_{pl}}{\varepsilon_p x_{jl}} H_m^{(1)\prime}(x_{jl})H_m^{(1)}(x_{pl}),$$

$$m_{13} = \frac{\alpha m}{\varepsilon_p}\left(\frac{1}{x_{pl}} - \frac{1}{x_{jl}}\frac{x_{pl}}{x_{jl}}\right) J_m(x_{jl})H_m^{(1)}(x_{pl}), \qquad m_{14} = m_{13}H_m^{(1)}(x_{jl})/J_m(x_{jl}),$$

$$m_{21} = \frac{\varepsilon_j x_{pl}}{\varepsilon_p x_{jl}} J_m'(x_{jl})J_m(x_{pl}) - J_m(x_{jl})J_m'(x_{pl}),$$

$$m_{22} = \frac{\varepsilon_j x_{pl}}{\varepsilon_p x_{jl}} H_m^{(1)\prime}(x_{jl})J_m(x_{pl}) - H_m^{(1)}(x_{jl})J_m'(x_{pl}),$$

$$m_{23} = -m_{13}J_m(x_{pl})/H_m^{(1)}(x_{pl}), \qquad m_{24} = -m_{14}J_m(x_{pl})/H_m^{(1)}(x_{pl}), \tag{11}$$

$$m_{31} = m_{13}\varepsilon_p, \qquad m_{32} = m_{14}\varepsilon_p,$$

$$m_{33} = J_m(x_{jl})H_m^{(1)\prime}(x_{pl}) - \frac{x_{pl}}{x_{jl}} J_m'(x_{jl})H_m^{(1)}(x_{pl}),$$

$$m_{34} = H_m^{(1)}(x_{jl})H_m^{(1)\prime}(x_{pl}) - \frac{x_{pl}}{x_{jl}} H_m^{(1)\prime}(x_{jl})H_m^{(1)}(x_{pl}),$$

$$m_{41} = m_{23}\varepsilon_p, \qquad m_{42} = m_{24}\varepsilon_p,$$

$$m_{43} = \frac{x_{pl}}{x_{jl}} J_m{}'(x_{jl}) J_m(x_{pl}) - J_m(x_{jl}) J_m{}'(x_{pl}),$$

$$m_{44} = \frac{x_{pl}}{x_{jl}} H_m^{(1)}{}'(x_{jl}) J_m(x_{pl}) - H_m^{(1)}(x_{jl}) J_m{}'(x_{pl}).$$

The elements of the matrix $M(r_l)$ are also presented in [13]. However, the matrix elements presented in [1] for $m \neq 0$ are incorrect, and we present here correct expressions.

One can see that the transformation (9) of the field components is performed at each of the interfaces of the layered structure. By starting from the fibre core and performing these transformations he required number of times, we obtain

$$\begin{pmatrix} A_l \\ B_l \\ C_l \\ D_l \end{pmatrix} = M \begin{pmatrix} A_0 \\ 0 \\ C_0 \\ 0 \end{pmatrix}, \qquad (12)$$

for an arbitrary *l-th* layer, where M is determined by the product of cofactors of type (10) and is also a 4 x 4 matrix $M = M(r_l) \cdot M(r_{l-1}) \cdot \ldots \cdot M(r_1)$.

For $l = N$, matrix relation (12) is equivalent to a system of four linear homogeneous algebraic equations for constants A_0, C_0, B_N, D_N. Their nontrivial solution exists only under the condition

$$\overline{m}_{11}\overline{m}_{33} - \overline{m}_{31}\overline{m}_{13} = 0, \qquad (13)$$

where $\overline{m}_{ks}$ are the elements of the matrix M in (12) for $l = N$.

The obtained dispersion equation (13) is the required one. It satisfies the general boundary conditions and is valid for any geometry of a layered cladding and all the modes, both eigenmodes (cladding modes) and radiation modes (core modes).

Our problem now is to select from a set of solutions (7) satisfying general conditions (8) the solutions for which the cladding has the maximum reflection at a wavelength of λ_0.

We begin with the analysis of the simplest the TM- and TE-mode families. These symmetric modes in (6)—(8), (11) correspond to *m = 0*, and only three components among a total set of field components (7) are nonzero. In particular, we have for the TM modes (upper trigonometric functions)

$$E_z = \left[A_i J_0(k_j r) + B_i H_0^{(1)}(k_j r)\right],$$

$$H_\varphi = -\frac{i\varepsilon_j \omega}{c k_j}\left[A_i J_1(k_j r) + B_i H_1^{(1)}(k_j r)\right], \qquad (14)$$

$$E_r = \frac{\overline{n}}{\varepsilon_j} H_\varphi,$$

and for the TE modes (lower trigonometric functions),

$$H_z = \left[C_i J_0(k_j r) + D_i H_0^{(1)}(k_j r)\right],$$

$$E_\varphi = \frac{i\omega}{c k_j}\left[C_i J_1(k_j r) + D_i H_1^{(1)}(k_j r)\right], \qquad (15)$$

$$H_r = -\overline{n} E_\varphi.$$

The boundary conditions for these modes also have the simpler form than (8)

$$A_{l-1} J_0(x_{jl}) + B_{l-1} H_0^{(1)}(x_{jl}) = A_l J_0(x_{pl}) + B_l H_0^{(1)}(x_{pl}),$$

$$\frac{\varepsilon_j}{x_{jl}}[A_{l-1} J_1(x_{jl}) + B_{l-1} H_1^{(1)}(x_{jl})] = \frac{\varepsilon_p}{x_{pl}}[A_l J_1(x_{pl}) + B_l H_1^{(1)}(x_{pl})], \qquad (16)$$

for the TM modes and

$$C_{l-1} J_0(x_{jl}) + D_{l-1} H_0^{(1)}(x_{jl}) = C_l J_0(x_{pl}) + D_l H_0^{(1)}(x_{pl}),$$

$$\frac{1}{x_{jl}}[C_{l-1} J_1(x_{jl}) + D_{l-1} H_1^{(1)}(x_{jl})] = \frac{1}{x_{pl}}[C_l J_1(x_{pl}) + D_l H_1^{(1)}(x_{pl})]. \qquad (17)$$

for the TE modes. Unlike (8), conditions (16) and (17) are the systems of 2N linear homogeneous algebraic equations for 2N constants $A_0, A_1, ..., A_{N-1}, B_1, ..., B_N$ or $C_0, C_1, ..., C_{N-1}, D_1, ..., D_N$, respectively.

The matrix $M(r_l)$ for the TM modes in (9) and (10) is the 2 x 2 matrix of the form

$$M(r_l) = -\frac{i\pi x_{pl}}{2}\begin{pmatrix} m_{11} & m_{12} \\ m_{21} & m_{22} \end{pmatrix}, \qquad (18)$$

where the matrix elements (m_{ks}) have the form

$$m_{11} = \frac{\varepsilon_j x_{pl}}{\varepsilon_p x_{jl}} J_1(x_{jl}) H_0^{(1)}(x_{pl}) - J_0(x_{jl}) H_1^{(1)}(x_{pl}),$$

$$m_{12} = \frac{\varepsilon_j x_{pl}}{\varepsilon_p x_{jl}} H_1^{(1)}(x_{jl}) H_0^{(1)}(x_{pl}) - H_0^{(1)}(x_{jl}) H_1^{(1)}(x_{pl}), \qquad (19)$$

$$m_{21} = J_0(x_{jl}) J_1(x_{pl}) - \frac{\varepsilon_j x_{pl}}{\varepsilon_p x_{jl}} J_1(x_{jl}) J_0(x_{pl}), \qquad m_{22} = H_0^{(1)}(x_{jl}) J_1(x_{pl}) - \frac{\varepsilon_j x_{pl}}{\varepsilon_p x_{jl}} H_1^{(1)}(x_{jl}) J_0(x_{pl}).$$

Instead of (13), the dispersion equation takes the form

$$\overline{m}_{11} = 0, \qquad (20)$$

where $\overline{m}_{11}$ - is the element of the product matrix $M = M(r_N) \cdots M(r_1)$ for factors of type (18).

For the TE modes, we obtain the same equations as (18)—(20); however, the ratio $\varepsilon_j / \varepsilon_p$ in expressions for the elements of the matrix $M(r_l)$ in (18) and (19) should be replaced by unity.

II.2.3 Principles of optimization of multilayered BF structure

Note first that the Floquet—Bloch theorem in the cylindrical geometry, which is used, as rule, to analyse periodic structures, can be applied only in the asymptotic approximation [76]. The field components in the rectangular geometry are determined by the combinations of trigonometric functions with the invariable spatial period. Therefore, such a periodic structure can be described as a whole by using the Floquet—Bloch theorem. However, in the cylindrical geometry the field is represented by cylindrical functions with a period depending on the radial coordinate. Therefore, the thicknesses of layers of a multilayer BF cladding with alternating val-

ues of the refractive index should be the functions of this coordinate. In the general case the structure is quasi-periodic and only at large arguments of the functions the thicknesses of layers become asymptotically almost equal in each of the two their sequences. This specific feature of the cylindrical geometry should be taken into account in the rigorous consideration of this problem.

In the absence of material losses, optical losses in a fibre (due to radiation modes) and the degree of light localisation in the fibre core are determined by the radial component of the Poynting vector S_r. Therefore, the minimisation of S_r is the most natural way for obtaining the optimal geometry of a multilayer cladding. It is possible, for example, to require the maximum reflection of light from each of the layer interfaces. This method assumes the determination of total reflection (transmission) both in all previous (with respect to the symmetry axis) and all structure layers behind this interface. This method for calculating reflection and transmission in a multilayer coaxial structure is described in most detail probably in [112]; however, the optimisation of the structure geometry for obtaining maximum reflection was not discussed in this paper (see also [82]). In addition, it is clear that minimal optical losses can be also found by minimising the radial energy flux propagating behind the layered cladding for r> r_N and explicitly determining radiation losses.

It seems that the two above-mentioned methods for minimising S_r are equivalent; however, we will not prove it, but simply will use the second method.

It was shown in papers [13; 75; 89; 95; 97; 98] that an important property of BFs is that they can be used as efficient mode filters and the TE_{01} mode in hollow BFs should have the highest Q factor. The latter is confirmed by the results of our calculations presented below. Therefore, when we are dealing with the optimisation of the multilayer structure of hollow BFs, it is reasonable to optimise it only for the lowest of the TE modes. The rest of the modes in this optimised BF should have considerably higher losses.

Let us write the expression for the time-averaged radial component of the energy flux vector $S_r = \mathrm{Re}\left(E_\varphi H_z^\bullet / 2\right)$ for the TE modes on the last interface r_N of the layered cladding. This expression follows from (15), (17)—(19) and has the form

$$S_r(r_N) = -\frac{r_N \omega C_0^2}{2c}\left|\frac{\overline{m}_{21}}{x_N}\right|^2 \mathrm{Im}\left\{H_1^{(1)}(x_N)\left[x_N H_0^{(1)}(x_N)\right]^\bullet\right\}, \qquad (21)$$

where $\overline{m}_{21}$ - is the element of the product matrix $M = M(r_N)\cdots M(r_1)$ for factors of type (18); $x_N = r_N k_2$ for even N and $x_N = r_N k_1$ for odd N. Because $S_r(r_N)$ is the function of coordinates of all layer interfaces, the optimisation of the cladding structure for obtaining the minimum radial energy flux is equivalent to the determination of the minimum of the right-hand side of (21) over N variables $r_1, r_2, ..., r_N$. It is possible to do it in a standard way by setting equal to zero all the first-order partial derivatives from (21) with respect to r_i (the necessary but not sufficient condition for the existence of the multidimensional extremum of the function). The system of homogeneous nonlinear equations for $r_1, r_2, ..., r_N$ obtained in this way should be closed with dispersion equation (20).

II.2.4 Genetic algorithm in the task of BF optimization

The solution of such a system of equations for high enough N is, as a rule, a challenging independent problem. We preferred another method and found the minimum of S_r with the help of the so-called genetic algorithm (see, for example, [113]), which is based on a direct analogy of the optimisation process with selection processes occurring in nature. The genetic algorithm operates by the "populations" of potential solutions, by applying the survival principle to them and taking part in the formation of the "descendants" of the most adapted solutions. The adaptability of each of the potential solutions is determined by the value of its target function [in or case, (21), (20)] estimating the difference of this solution from the required result. The higher the adaptability of the solution, the higher probability that the useful features of the descendants obtained with the help of this solution and determining the adaptability will be manifested greater. "The vector of variables" in the genetic algo-

rithm plays the same role as a genotype in biology. The algorithm does not require the knowledge of the relief of a multidimensional surface on which an extremum is sought, it can come from local extrema, can be simply realised, does not require large computational resources and has been already tested by solving many problems (see details in [113]).

Thus, the optimal geometry of a BF is determined in the following way. The radius of the fibre core r_1 and the values of n_0, n_1, n_2,N are assumed known for the specified wavelength λ_0 of guided radiation in the fibre. By using the genetic algorithm, the minimum of function (21) of variables $r_2, r_3, ..., r_N, \beta$ is sought when equation (20) is valid (optimisation of the BF to the TE mode). To each value of β, its own optimal geometry of the layered structure of the cladding corresponds, and therefore the propagation constant is included to the list of variables to be optimised. The solution of the problem should be the choice of the values of $r_2, r_3, ..., r_N, \mathrm{Re}\,\beta, \mathrm{Im}\,\beta$, which, on the one hand, would provide the absolute minimum of function (21) and, on the other, satisfy equation (20). In this case, because Eq. (20) for an arbitrary geometry ($r_2, r_3, ..., r_N$) has a set of roots β, the root with the smallest possible value of $\mathrm{Im}\,\beta$ corresponds to the lowest TE_{01} mode of a hollow fibre.

II.2.4.1 Definition of "initial" values of layers coordinates for hollow BF in optimization procedure for TE-mode

Not also that the genetic algorithm operates the better, the smaller the region of changing the variables of the function being optimised. In other words, both the initial values of coordinates $r_2, r_3, ..., r_N$ and $\mathrm{Re}\,\beta$ should be closer as possible to their real values. The condition $\mathrm{Im}\,\beta = 0$ corresponds, as mentioned above, to the presence of a standing wave along the cross-section radius, when the time-averaged radial energy flux is zero for all values of r, which is possible only for a cladding consisting of the infinite number of alternating layers. To find the approximate parameters of the structure of a multilayer BF with a finite number of cladding layers under the condition

$\mathrm{Im}\,\beta << \mathrm{Re}\,\beta$, when the radial energy flux is generally speaking nowhere equal to zero, we will assume, nevertheless, that S_r=0 at all the nodes tangential to the interfaces of the field component layers. This means that we assume that the cladding of a real fibre consists of the infinite number of layers. We place the layer interfaces at the same nodes. The latter is achieved by solving the system of coupled equations following from (15) for the case of TE modes:

$$\begin{aligned}
&E_{\varphi 1} = \frac{i\omega}{ck_0} C_0 J_1(k_0 r_1) = 0,\\
&H_{z2} = C_1 J_0(k_1 r_2) + D_1 H_0^{(1)}(k_1 r_2) = 0,\\
&E_{\varphi 3} = \frac{i\omega}{ck_2}\left[C_2 J_1(k_2 r_3) + D_2 H_1^{(1)}(k_2 r_3)\right] = 0,\\
&H_{z4} = C_3 J_0(k_1 r_4) + D_3 H_0^{(1)}(k_1 r_4) = 0,\\
&\cdots\cdots\cdots\cdots\cdots\cdots\cdots\cdots\cdots\cdots\cdots\cdots\cdots\cdots\cdots\cdots\cdots\cdots\\
&E_{\varphi(N-1)} = \frac{i\omega}{ck_2}\left[C_{N-2} J_1(k_2 r_{N-1}) + D_{N-2} H_1^{(1)}(k_2 r_{N-1})\right] = 0,\\
&H_{zN} = C_{N-1} J_0(k_1 r_N) + D_{N-1} H_0^{(1)}(k_1 r_N) = 0.
\end{aligned} \tag{22}$$

Equations (22) can be solved in real quantities (in this case, $\mathrm{Im}\,\beta \approx 0$) and the first of them, for the known r_1, gives

$$\mathrm{Re}\,\bar{n} \approx \sqrt{n_0^2 - \left(\frac{\delta_1 \lambda_0}{2\pi r_1}\right)^2}, \tag{23}$$

where $\delta_1 = 3.83171$ is the first nonzero root of the function $J_1(x)$.

According to (12) and (18), coefficients C_1 and D_1 in the second relation in (22) are

$$C_1 = -\frac{i\pi k_1 r_1}{2} m_{11} C_0, \qquad D_1 = -\frac{i\pi k_1 r_1}{2} m_{21} C_0,,$$

where m_{11} and m_{21} are defined by expressions (19).

By substituting the expressions for C_1, D_1, and $\mathrm{Re}\,\bar{n}$ in the condition $H_{z2} = 0$ = 0, we obtain the equation for r_2 in the form

$$J_0(k_1 r_2)N_1(k_1 r_1) - J_1(k_1 r_1)N_0(k_1 r_2) = 0. \qquad (24)$$

Similarly, from the relation for $E_{\varphi 3}$ in (22) we obtain the equation

$$J_1(k_2 r_3)N_0(k_2 r_2) - J_0(k_2 r_2)N_1(k_2 r_3) = 0, \qquad (24a)$$

from which r_3 can be determined from already known $\mathrm{Re}\,\bar{n}$ and r_2, etc.

By solving successively equations (22), the "starting" values of variables required for the genetic algorithm are found. From a set of solutions with increasing values of each of the equations of type (24) and (24a), we choose the value of the desired coordinate that is closest to the required value corresponding to the particular optical thickness of the cladding layer (for example, the quarter-wavelength one or more).

In the large argument approximation, we can use the asymptotic form of cylindrical functions [114]. In this case, Eq. (24), for example, proves to be equivalent to the equation $\sin[k_1(r_2 - r_1) + \pi/2] = 0$. It follows from this that $r_2 = r_1 + \pi(2p-1)/(2k_1)$. By using (23), we obtain

$$k_1 = \frac{2\pi}{\lambda_0}\sqrt{n_1^2 - n_0^2 + \left(\frac{\delta_1 \lambda_0}{2\pi r_1}\right)^2}, \qquad (25)$$

As a result, we have

$$r_2 = r_1 + \frac{(2p-1)\lambda_0}{4}\left[n_1^2 - n_0^2 + \left(\frac{\delta_1 \lambda_0}{2\pi r_1}\right)^2\right]^{-1/2}, \quad (p = 1,2,3,\ldots). \qquad (26)$$

Note that the same expression (26) is obtained by using the well-known result [83], which is the condition of the maximum reflection of light from a plane—parallel plate of thickness h $(= r_i - r_{i-1})$,

$$h = \frac{(2p-1)\lambda_0}{4\cos\theta \cdot n},,$$

where θ is the angle between the wave vector in a layer and the normal to its boundary, and n is the refractive index of the layer material. In particular, for the cladding layer closest to the fibre core, we have $n = n_1$ in the latter relation and

$$\cos\theta = \sqrt{1-(n_0/n_1)^2 + [\delta_1\lambda_0/(2\pi n_1 r_1)]^2}\ .$$

Recall, however, that expression (26) is approximate and corresponds (as in [83]) to a planar geometry (asymptotics of cylindrical functions).

One can see that the thickness of the first layer of the cladding in asymptotics is approximately proportional to an odd number of $\lambda_0/4$ (this result is approximate due to the presence of the third, generally speaking, small term in brackets). In this case, depending on the refractive-index contrast, the proportionality coefficient can be noticeably greater than unity, i.e. the real thickness of layers can exceed by several times $\lambda_0/4$ in vacuum, which is important for practical realisation of quarter-wavelength structures.

A similar dependence also takes place for optically less dense layers. In particular, to obtain the approximate value of r_3 in (24a), it is simply necessary to make the replacements $r_2 \to r_3,\ r_1 \to r_2,\ n_1 \to n_2$ in (26).

The method for determining initial values of $\mathrm{Re}\,\bar{n}$ and r_i described above is most efficient and allows one to obtain the values of variables that are very close to real ones. The genetic algorithm further "corrects" these values and finds their set providing, together with the required minimal $\mathrm{Im}\,\bar{n}$, the global minimum of $S_r(r_N)$ and satisfying equation (20).

To determine other radiation modes in a fibre optimised for the TE_{01} mode, the found geometry of the fibre is fixed. Then, the next root of Eq. (2) closest to the value of β for the TE_{01} mode will define the TE_{02} mode (this root has a greater value of $\mathrm{Im}\,\beta$ than the first root), the root following after the second root (with greater $\mathrm{Im}\,\beta$) will define the TE_{03} mode, etc. It is clear that this sequence of roots should be found from the dispersion equation only without using the genetic algorithm.

By using the dispersion equation for the TM modes in the same fibre optimised to the TE_{01} mode, all the sequence of the complex propagation constants of the TM_{0n} modes can be also determined. Similarly, by replacing Eq. (20) by dispersion equa-

tion (13), hybrid modes can be found. In this paper, we performed some calculations only for the lowest hybrid modes with the azimuthal parameter m = 1.

II.2.4.2 Definition of "initial" values of layers coordinates for solid core BF in optimization procedure for hybrid HE_{11} mode

However, the optimisation of the structure of a BF with a glass core is somewhat complicated because the fundamental mode in such BFs is not the TE_{01} mode but the doubly degenerate lowest hybrid HE_{11} mode (see below). The start values of variables for optimisation are found here also from the condition that the radial component of the Poynting vector vanishes at all the interfaces in the layered cladding. In particular, in the same approximation HE_{11}, the equality $S_r(r = r_1) = 0$ and the independence of S_r of the azimuthal angle φ for all *r* specify the relation between amplitudes in expressions for the field components, for example, in (12) and also allow one to determine $\mathrm{Re}\,\bar{n}$ from the equation

$$J_0(k_0 r_1) = \frac{J_1(k_0 r_1)}{k_0 r_1}\left(1 - \frac{\mathrm{Re}\,\bar{n}}{n_0}\right), \qquad \text{where } k_0 = \frac{2\pi n_0}{\lambda_0}\sqrt{1 - \left(\frac{\mathrm{Re}\,\bar{n}}{n_0}\right)^2}. \tag{27}$$

It is easy to see that this equation can be quite accurately replaced by the equation $J_0(k_0 r_1) \cong 0$, because, as a rule, $\mathrm{Re}\,\bar{n}/n_0 \approx 1$, and $|J_1(k_0 r_1)/(k_0 r_1)| < 1$.

Unlike (24) and (24a), the equations for determining coordinates of layer interfaces in the cladding, which also follow from equations, $S_r(r = r_i) = 0$ $(i = 2,3,...,N)$ have a more complicated form. However, in the approximation of low-contrast refractive indices in cladding layers, these equations are reduced to expressions of type (24), (24a), and at the large arguments of cylindrical functions – to (26). In particular, the equation for determining r_2 has the form

$$J_1(k_1 r_2)N_0(k_1 r_1) - J_0(k_1 r_1)N_1(k_1 r_2) \approx 0. \tag{28}$$

Note that the procedure somewhat similar to the approximate method for determining the fibre structure geometry described above was applied in paper [87]

where the authors determined the thickness of cladding layers by dividing intervals between the neighbouring roots of functions $J_0(x)$ and $J_1(x)$ by the values of the transverse wave number k_j. corresponding to the given layer. Note, however, that such an approach cannot be used to optimise BFs for the TE or TM modes.

II.2.5 Some remarks concerning the optimization procedures of BF with the large core radius.

In a BF with a large core radius, when the arguments of cylindrical functions in the cladding are large, the period of a photonic crystal (the sum of thicknesses of two adjacent layers) in the entire cladding becomes approximately the same, and the optimisation of such BFs is reduced to the determination of the optimal values of the period and the thickness of layers in them. This does not mean, however, that the number of variables in the optimisation procedure noticeably decreases. Indeed, each additional layer in the cladding causes the redistribution of the field in the fibre and the corresponding change in the optimal geometry of the entire structure. It is obvious that the period changes with increasing N the stronger the lower the value of #N itself. In other words, for large N, when the field behind the layered cladding becomes small, both the period and $\mathrm{Re}\,\bar{n}$ virtually become independent of N. As a result, the dependence $\mathrm{Re}\,\bar{n}(N)$ has the form of a function saturating with increasing N. Waveguide losses continue to decease with increasing N.

If necessary, the approach described above can be used to optimise the BF structure for any mode. However, it is not obvious that this mode will “survive” upon excitation of such a BF. It is most likely that some modes will propagate in the fibre with lower losses.

II.2.6 Definition of the fundamental mode in hollow core and solid core BFs.

After the consideration of various methods for optimising BFs with hollow and glass cores, it is pertinent to discuss in more detail the question of which of the BF modes is fundamental. According to the definition of the fundamental mode as a mode with the lowest optical losses in a given fibre, either the TE_{01} or HE_{11} mode can be the fundamental mode in a BF. Let us present some relevant arguments.

On the one hand, it follows from (23) and (27), for example, that for any BF structure with a fixed r_1, the HE_{11} mode has the greatest real part of the propagation constant among all the modes. Indeed, from approximate equation (27) ($J_0(k_0 r_1) \approx 0$), we have with good accuracy for $\mathrm{Re}\,\bar{n}_{HE}$

$$\mathrm{Re}\,\bar{n}_{HE} \approx \sqrt{n_0^2 - \left(\frac{\delta_2 \lambda_0}{2\pi r_1}\right)^2}, \qquad (29)$$

where $\delta_2 = 2{,}40483$ is the first root of the function $J_0(x)$. By comparing (23) with (29), we see that $\mathrm{Re}\,\bar{n}_{HE} > \mathrm{Re}\,\bar{n}_{TE}$. It also follows from this that the transverse component of the wave vector of the HE_{11} mode is the smallest, while the angle of its incidence on the core—cladding interface is the largest of all the angles of incidence of the guided modes in the fibre.

On the other hand, the dependence of the Fresnel coefficient R^2 of light power reflection from the plane interface between different media on the incident radiation polarisation is well known [83]. Indeed, if the electric vector of a wave is perpendicular to its plane of incidence, the dependence of R^2 on the angle of incidence θ has the form of a monotonically increasing (up to unity) function. But if the electric vector of the wave is parallel to the plane of incidence, the function $R^2(\theta)$, which also increases up to unity, is nonmonotonic and passes through the zero minimum at the Brewster angle. As a result, although both these dependences begin at the same point (for $\theta = 0$) and terminate at the same point (for $\theta = \pi/2$), the reflection coefficient is everywhere higher for the first polarisation than for the second one (except the two extreme points).

To use the result from [83], we will assume with good approximation that the TE_{01} and HE_{11} modes are plane waves and the core—cladding interface is a plane. Note also that the fields of TE modes have only the azimuthal electric component, which is perpendicular to the plane of incidence of light on the first cladding layer, and therefore are not subjected to the Brewster effect. However, the HE_{11} mode field consists of two fields with orthogonal polarisations, and the second of these components (parallel) should be reflected weaker than the first one. Despite the grazing incidence of the HE_{11} mode, the presence of this radiation component reduces the total Fresnel reflection of the HE_{11} mode from the cladding, so that the TE_{01} mode proves to be the fundamental mode of the fibre. The general polarisation properties of Fresnel reflection mentioned above depend considerably on the contrast between refractive indices of the core and the first cladding layer. For comparatively high contrasts (for example, for hollow BFs), the dependences of the reflection coefficient on the angle of incidence for two polarisations noticeably differ (Fig. 2a), and the TE_{01} mode is reflected most strongly from the cladding, being the fundamental mode in this case. The HE_{11} mode, in which a part of energy corresponds to polarisation parallel to the plane of incidence, is reflected worse as a whole and to a great extent is refracted to the cladding. If the contrast of refractive indices of the fibre core and cladding is small $(\Delta n \le 0{,}1)$ the influence of polarisation effects is considerably reduced and dependences of the reflectance on the angle of incidence for both polarisations become close, having small values of R^2 up to angles ~ 70^{o} (Fig. 2b).

In this case, the advantages of the TE_{01} mode over the HE_{11} mode are lost to a great extent.

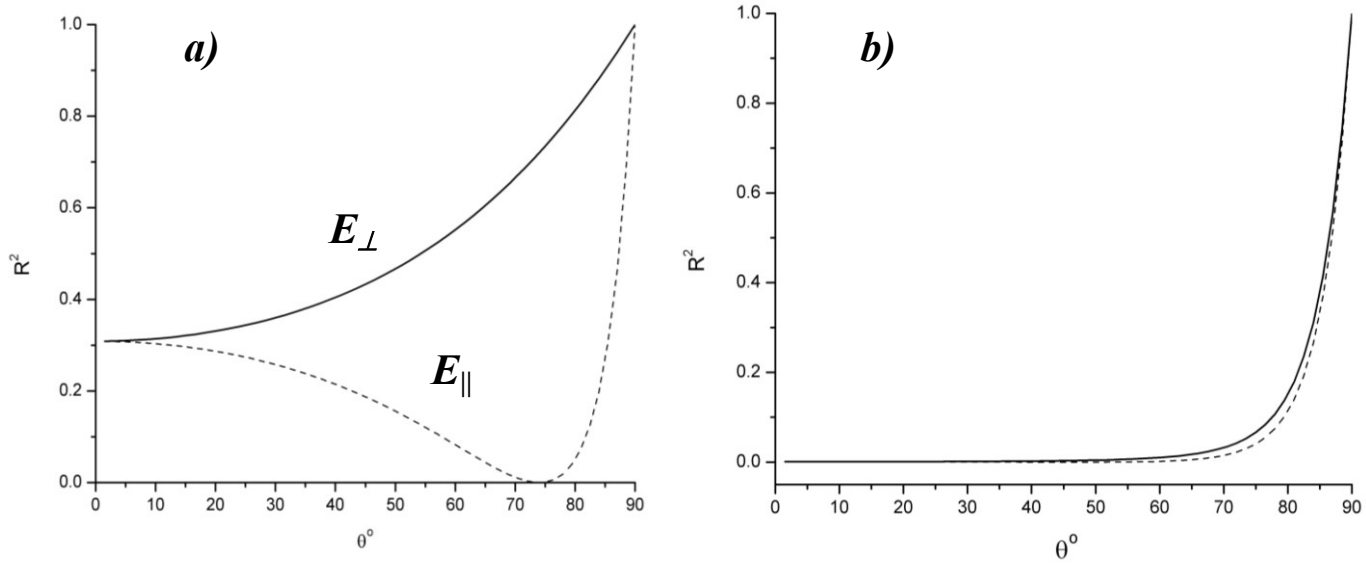

Fig. 2: *Dependences of the power coefficient of reflection from the interface of two media on the angel of incidence of light polarised in the plane of incidence (dashed curves) and in a plane perpendicular to the plane of incidence (solid curves). The contrast of the refractive indices of the media is* $\delta n = (n_1 - n_2)/n_1$, $(n_1 > n_2)$, *a)* $\delta n = 0.714$, *b)* $\delta n = 0.057$.

The analysis performed above, which was based on the consideration of interaction of light with only one interface, is, of course, approximate, however, it comparatively simply explains the essence of the phenomenon. To obtain the quantitative relation between losses for the TE_{01} and HE_{11} modes at a low refractive-index contrast, it is necessary, of course, to take into account all other interfaces between cladding layers. Here, it is probably important that the angle of incidence of the HE_{11} mode (which is the fundamental mode in this case) on the layered structure is the greatest. In this case, losses for the TE_{01} mode can be comparable with those for the HE_{11} mode.

For the illustration of the described above influence of the refractive index contrast on the core-cladding interface on definition of the fundamental mode in BF loss spectrums were calculated for the hollow and for the solid core BFs. In this case the contrast value of $\delta n = 0.714$ (as on Fig.2a) was related to the hollow core BF and the contrast value $\delta n = 0.057$ (as on Fig.2b) was related to the solid core BF.

Corresponded RIPs are presented on Fig.3. Let us note that the geometry for the hollow core BF was chosen optimal for the hybrid HE_{11} mode (by means of pro-

posed in *II.2.4.2* scheme) and the geometry for the solid core BF – optical for the TE_{01} mode (by means of proposed in *II.2.4.1* scheme).

Calculated losses spectrums are shown on Fig.4. It is clearly that in case of the hollow BF the losses for HE_{11} mode are higher than for the TE_{01} mode despite the fact that the geometry was chosen optimal for the HE_{11} mode. And here the fundamental mode is TE_{01} mode as expected. Similarly, in case of the solid core BF the losses for the TE_{01} mode are higher than for the HE_{11} mode despite the fact that here the geometry was chosen optimal for the TE_{01} mode. And now the fundamental mode is the HE_{11} mode.

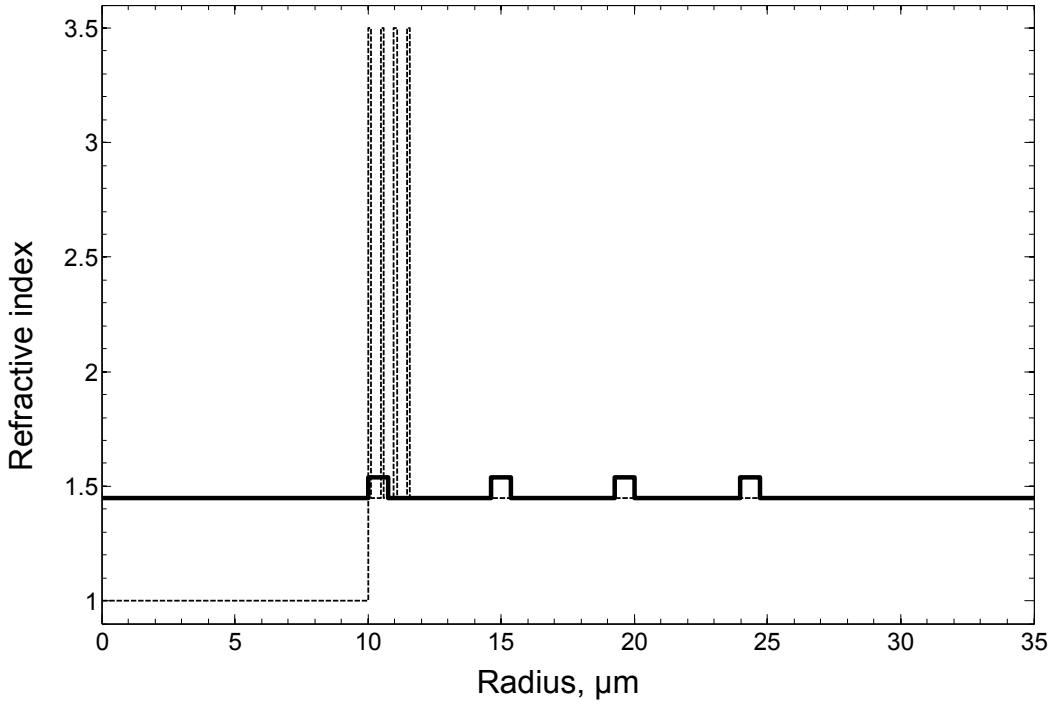

Fig. 3: *RIPs of BFs that were used in the illustration of influence of the refractive index contrast at the core-cladding interface.*
Dashed line –RIP for the hollow BF $\delta n = (n_1 - n_0)/n_1 = 0.714\,(n_0 = 1,\ n_1 = 3.5, n_2 = 1.45)$
Thick solid line –RIP for the solid core BF
$\delta n = (n_1 - n_0)/n_1 = 0.057\ \ (n_0 = 1.45,\ n_1 = 1.538, n_2 = 1.45)$. *Geometries were chosen when wavelength was fixed at* $\lambda_0 = 1.55\ \mu m$

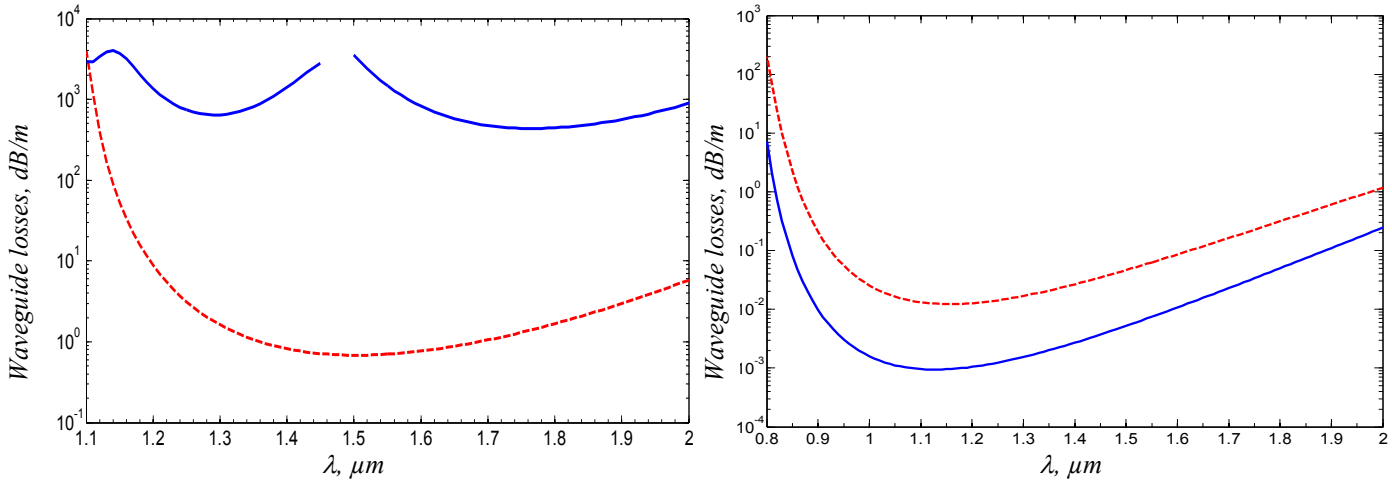

Fig. 4: *Waveguide losses for BFs from Fig.3*
a)waveguide losses in the hollow BF b) waveguide losses for the solid core BF
dashed lines always are corresponded to the TE_{01} mode

II.2.7 Losses in BF

By changing the wavelength to both sides of λ_0 for any of the radiation modes at a fixed geometry, the dependences $\mathrm{Re}\,\beta(\lambda)$ and $\mathrm{Im}\,\beta(\lambda)$ are determined. The mode dispersion is found from the first of them. Calculations in the complex plane allow us to take into account both material losses (by introducing the imaginary parts depending on λ to expressions for the refractive indices n_0, n_1, n_2 of the structure) and the material dispersion by assuming that the real parts of n_0, n_1, n_2 depend on λ. Optical losses γ are defined as losses of the radiation intensity, i.e. $\gamma = 2 \cdot \mathrm{Im}\,\beta = (4\pi\,\mathrm{Im}\,\bar{n})/\lambda$. Thus, losses in the units of dB/km can be found from the known relation (see, for example, [115])

$$\gamma = \frac{4 \cdot 10^{10} \pi \lg e}{\lambda} \mathrm{Im}\,\bar{n}, \qquad (30)$$

where λ is expressed in μm. One can see from (30) that, for example, to losses ~ 1 dB/km at λ = 1.5 μm, very low values of $\mathrm{Im}\,\bar{n}$ correspond (~$3 \cdot 10^{-11}$). This justifies with a great margin the applicability of the approximation $\mathrm{Re}\,\bar{n} >> \mathrm{Im}\,\bar{n}$ used everywhere.

Note that the radial distributions of the field components for modes in a BF are presented below in the normalised form. In the case of hybrid odes, the relation between A_0 and C_0 required for normalisation is presented below.

II.3 Results of calculations and discussion

The optical properties of guided radiation in BFs are analysed in the literature based on the geometry of the multilayer fibre cladding used in each of the studies. The thickness of cladding layers is, as a rule, close to the quarter-wavelength one and is estimated by assuming the grazing incidence of light on the core—cladding interface. In this approximation, the relation between the thickness h_1 of denser layers and the thickness h_2 of less dense layers has the form (see, for example, [89])

$$\frac{h_1}{h_2} = \sqrt{\frac{n_2^2 - 1}{n_1^2 - 1}}. \qquad (31)$$

The geometrical parameters of a BF can be determined more accurately by solving equations of type (22). We will show below that the deviations of the layer thickness from the quarter-wavelength one appearing due to approximations can sometimes noticeably affect optical losses in BFs.

II.3.1 Optimization of well-known from literature structures

We will illustrate the results of optimisation of the BF geometry by comparing them with the data known from the literature. The optical properties of a BF with a hollow core of large radius and a large refractive-index contrast in periodic layers of the cladding were calculated in [89]. The fibre parameters were N = 17, λ_0 = 1.55 μm, r_1 = 13.02 μm, h_1 = 0.09444 μm (n_1 = 4.6), and h_2 = 0.33956 μm (n_2 = 1.6). The minimal waveguide losses calculated for the TE_{01} mode in this fibre were ~ $6 \cdot 10^{-4}$ dB/km (this minimal value should correspond to the wavelength λ_0, whereas in [89] it corresponds for unknown reason to $\lambda \approx 1.66$ μm). By using the same initial values of r_1, n_1, n_2, N, and λ_0 as in [89] and optimising the cladding structure geometry, we

obtained h_1 = 0.086375 μm and h_2 = 0.3085 μm and minimal losses ~ $2.9 \cdot 10^{-4}$dB/km at λ_0 = 1.55 μm. This example convincingly demonstrates a strong dependence of waveguide losses on the periodic cladding structure geometry – the change in the layer thickness only by 10% reduces losses more than by half.

Note that waveguide losses characterise the degree of localisation of radiation guided in the fibre core. In the given case, waveguide losses are very small and the degree of light localisation is so high that material losses in cladding layers can be neglected with high accuracy.

There also exist papers in which the geometry of a multilayer cladding is very close to optimal; however, as a rule, the authors do not substantiate the choice of this geometry. For example, the parameters of a hollow BF in [95] were N = 32, λ_0 = 1 μm, r_1 = 1.3278 μm, h_1 = 0.2133 μm (n_1= 1.49) and h_2 = 0.346 μm (n_2 = 1.17). For the TE_{01} mode in this fibre, the authors calculated $\bar{n} = 0{,}891067 + i \cdot 1{,}4226 \cdot 10^{-8}$ (γ = 776.4 dB/km), whereas for the geometry optimised by us (h_1 = 0.2146, h_2 = 0.3241 μm) for the same parameters, we obtained γ = 600 dB/km for this mode (i.e. losses were smaller only by ~ 30%). A similar result was obtained for another variant of the fibre with r_1 = 1.8278 μm calculated in [95] (other parameters were the same). In this case, the difference between optimised and non-optimised losses for the TE_{01} mode was also small (~ 32%). The found values of $\mathrm{Re}\,\bar{n}$, as expected, coincided with good accuracy with the values calculated by expression (23).

Note also that calculations in [95] were performed by using the above-mentioned model [112]. If we calculate $\bar{n}$ for the periodic structure geometry used in [95] without the optimisation procedure, the results will exactly coincide with those obtained in [95]. This confirms the expressed assumption about the equivalence of our method for the calculation of the BF modes by using 4 x 4 matrices and the 2 x 2 matrix method applied in [112].

As another example we compare our results with calculations [98] of the lowest modes and their losses in a hollow BF with a cladding consisting of four pairs

(N = 8) of layers made of Si (n_1 = 3.5) and Si_3N_4 (n_2 = 2.0). The authors of [98] calculated optical losses in the wavelength range from 1.5 to 1.7 μm in a BF fibre with the core radius r_1 = 7.5 μm and cladding layer thicknesses h_1 = 0.11 μm and h_2 = 0.21 μm. By optimising the geometry of this fibre, we obtained h_1 = 0.1157 μm and h_2 = 0.235 μm by assuming that λ_0 = 1.7 μm. This wavelength corresponds to the minimum of losses $\gamma \approx 0.62$ dB/cm in the dependence presented in [30]. Our calculations give $\gamma(\lambda_0) \approx$ 0.57 dB/cm.

So far we considered fibres with claddings made of quarter-wavelength dielectric layers or having a similar structure. Such BFs have a transmission band with two bands with very large losses located on each side of it. The width of the long-wavelength band is infinite, whereas the short-wavelength band has a finite spectral width. In such fibres optimised to the specified wavelength λ_0, radiation at $\lambda > \lambda_0$ cannot propagate, and transmission bands exist only at shorter wavelengths. In the terminology of photonic crystals, transmission bands of BFs correspond to the so-called photon-forbidden bands in which light cannot propagate across the periodic structure of a photonic crystal and propagates only over its defects (in our case, a defect is the BF core). A photonic crystal is transparent in other spectral ranges, light is not reflected from the cladding and is not localised in the core, corresponding to BF bands with large losses.

II.3.2 Optical properties of ARROW BF

In the short-wavelength spectral region, where the conditions $r_1 > \lambda$ and $h = h_1 + h_2 > \lambda$ are fulfilled, new properties of BFs are manifested, which are not typical for quarter-wavelength structures. Planar waveguides with a large cladding period proposed earlier [116; 117; 66] were called ARROW (anti-resonant reflecting optical waveguide). They differ from waveguides with a quarter-wavelength layer cladding by a weak dependence of the spectral position of maxima of waveguide losses on h down to the radiation wavelength $\lambda \approx h$. As a whole it is assumed that the spectral parameters of an ARROW are mainly determined by the parameters of a layer closest to

the core with a large refractive index (by its thickness and the refractive-index contrast in layers).

The properties of ARROWs are explained by the fact that the structure layers can be compared with Fabry—Perot (FP) resonators (or their cylindrical analogue). Indeed, it is clear from physical considerations that if the fibre cladding has spectral regions resonant with the given radiation wavelength, the radiation will be distributed in the fibre cross section so that its great fraction will be localised in these resonance regions. As a result, the resonance spectral bands (modes) of the FP cladding correspond to a weak transmission of light in the fibre because the redistribution of the radiation field due to its localisation in resonance regions reduces the radiation intensity in the core. And vice versa, the absence of resonances in the cladding corresponds to the spectral bands with the maximum transmission (hence the name ARROW for waveguides of this type). Physically, the resonance bands are related to a standing wave in a FP resonator.

II.3.2.1 Influence of coupled resonators on loss spectrum of ARROW BF

In the general case the transmission spectrum of an ARROW should be determined by the resonance properties of optically denser and less dense cladding layers. Moreover, natural resonances (modes) are inherent both in a cladding period representing a complex FP resonator, which contains two dielectric media, and in a combination of many closely spaced layers. The number of possible resonators rapidly increases with increasing N. The discrete eigenfrequencies (modes) of each complex resonator do not coincide in the general case with frequencies for individual layers and frequencies of other resonators. Therefore, the cladding can have a considerable number of resonance frequencies in a particular spectral range. The resonance frequencies of individual layers can be easily estimated analytically, whereas the determination of the eigenfrequencies of multilayer resonators is a more complicated problem, which is beyond the scope of our paper.

Thus, the quarter-wavelength structure of the cladding corresponds to the absence of FP resonances when the ARROW transmission is maximal. If the thickness of layers is a multiple of even numbers of a quarter of the wavelength (of integers of half-waves), the conditions of FP resonances are realised, and an ARROW with such a structure does not virtually transmit radiation. The intermediate values of layer thicknesses correspond to intermediate regions between bands with high and low ARROW losses.

Radiation mode losses rapidly decrease with increasing the number of layer periods, but, as mentioned above, the addition of these new periods does not change the spectral position of maxima of losses in fibres if h > λ.

The properties of planar ARROWs considered above also inherent in cylindrical waveguides, which were studied in a number of papers (see, for example, [93; 94; 99]). The theoretical analysis of BFs of the ARROW type does not differ in principle from our analysis presented above. Therefore, we will not consider them as a separate class of BFs, but simply will illustrate their properties by a number of examples.

Thus, Fig. 5 presents the transmission spectrum of an ARROW with arbitrarily chosen parameters. Resonance conditions for an optically dense layer (with n_1) have the form $k_1 h_1 = \pi m$ (here, $m = 1,2,3...$) is an integer of radiation half-wavelength fitting in the resonator length h_1. By using (25), we find for the TE modes the approximate resonance wavelengths in optically dense cladding layers

$$\lambda_{1,m} = \frac{2h_1\sqrt{n_1^2 - n_0^2}}{\sqrt{m^2 - \left(\delta_1 h_1 / \pi r_1\right)^2}}. \qquad (32)$$

The wavelengths $\lambda_{1,m}^{(a)}$ corresponding to the absence of resonances in these layers (anti-resonance) are also well described by (32) with the replacement $m \to m + 1/2$.

One can see from Fig. 5 that the spectrum has several forbidden bands (bands with small losses) even within a range of moderate width and all the resonances determined from (32) fall into ARROW bands with the smallest transmission. Note at the same time that not all anti-resonances of the first cladding layer determined by (32) correspond to photon-forbidden bands. Thus, according to Fig. 5, the loss level

at wavelengths $\lambda_{1,8}^{(a)} = 1.583$; $\lambda_{1,9}^{(a)} = 1.415$; $\lambda_{1,11}^{(a)} = 1.168$; $\lambda_{1,12}^{(a)} = 1.075$ μm corresponding to anti-resonances in (32) with m=8,9,11,12 is $2 \cdot 10^4$-$5 \cdot 10^5$ dB/km, whereas these losses at other resonances (m=7,10,13 с $\lambda_{1,7}^{(a)} = 1.795$; $\lambda_{1,10}^{(a)} = 1.28$; $\lambda_{1,13}^{(a)} = 0.995$ μm) are 6—7 orders of magnitude lower.

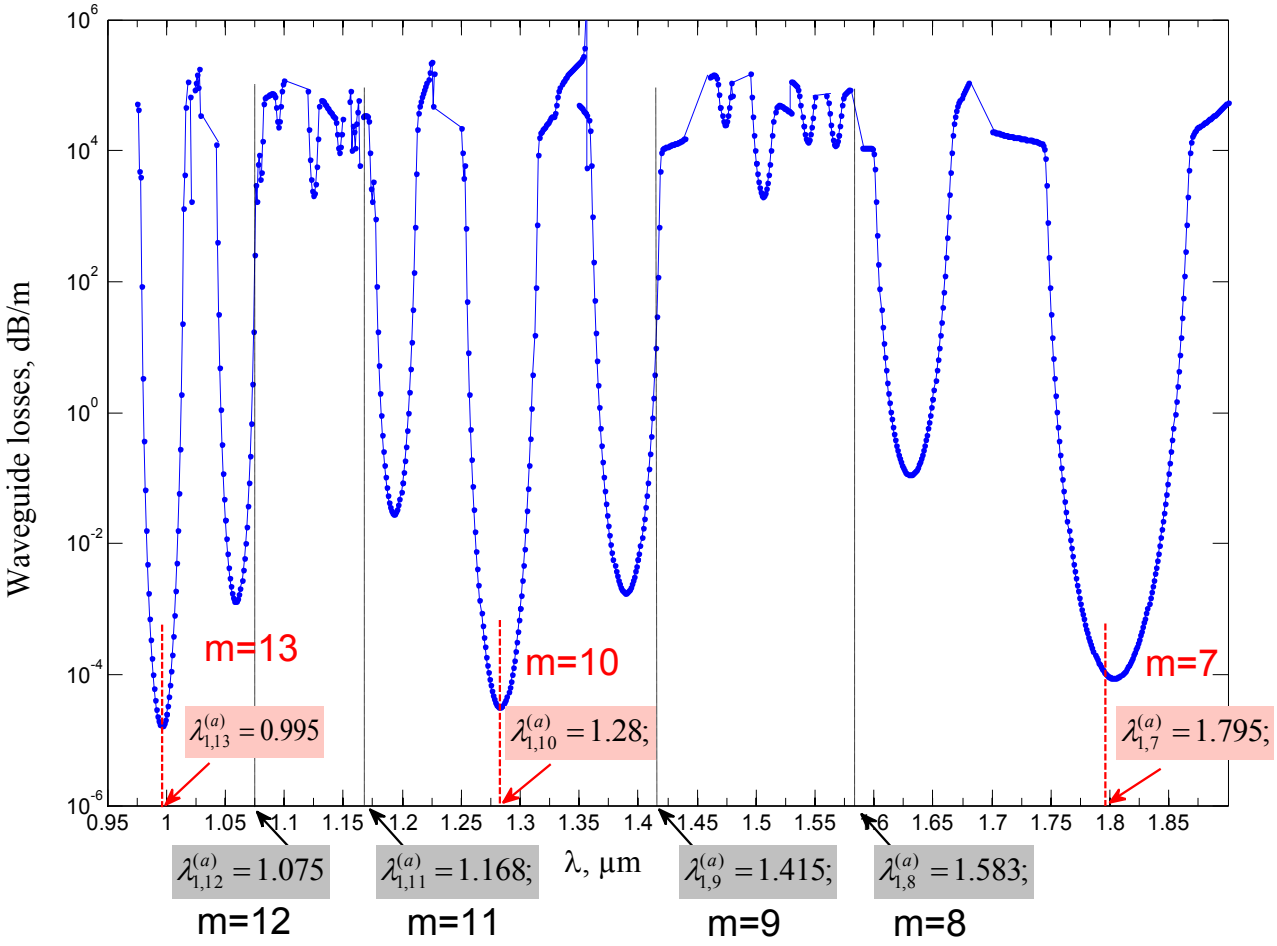

Fig. 5: *Calculated transmission spectrum for the TE_{01} mode in an ARROW;* $n_0 = 1$; $n_1 = 3.5$; $n_2 = 1,5$; $h_1 = h_2 = 2$ μm; $r_1 = 4$ μm; $N = 20$.

Such a difference can be explained only by the fact that at wavelengths close to anti-resonances with m = 8, 9, 11, and 12 there exist resonances (cladding modes) in other, more complex resonators, which were mentioned above. The interaction of these cladding modes with the anti-resonances of the first layer leads, as a rule, to the spectral shift of the low-loss bands with respect to its position predicted by expression (32). For example, the expected loss minimum at $\lambda_{1,8}^{(a)} = 1.583$ μm appears at a wavelength of 1.625 μm. A similar behaviour is observed for anti-resonances at m =

9, 11, 12. As a result, not all the optical properties of an ARROW are found to be determined by the parameters of only one first layer.

The FP resonances of optically less dense ARROW layers (with n_2) can affect the width of bands with large losses. Indeed, the positions of these additional resonances, similarly to (32), can be found from the expression

$$\lambda_{2,p} = \frac{2h_2\sqrt{n_2^2 - n_0^2}}{\sqrt{p^2 - \left(\delta_1 h_2 / \pi r_1\right)^2}}, \quad p = 1,2,3... \ . \qquad (33)$$

One can see from (33) and Fig. 5 that the resonance wavelengths $\lambda_{2,p}$ for the given particular parameters of the fibre are close to the corresponding $\lambda_{1,m}$ and fall into the same minimal transmission ARROW bands. But even all resonances (32) and (33) cannot completely explain the calculated spectrum. Spectral bands with high losses should be determined by some other resonances (modes) which can be caused, for example, by the presence of more complex resonances in the structure, which were neglected in the model.

Because the analysis of the spectrum as a whole in Fig. 5 is quite complicated, we consider one of the anti-resonance bands (photon-forbidden bands) with minimal losses at $\lambda_{1,10}^{(a)} = 1.28\,\mu\text{m}$ at the enlarged wavelength scale (Fig. 6). The shape of this curve is typical for the wavelength dependence of the TE_{01} mode losses in BFs. The ARROW properties are discussed below by the example of this forbidden band.

Fig. 7 presents the radial distributions of one of the two field components (H_z) determining the radial energy flux (waveguide losses) $S_r = \text{Re}\left(E_\varphi H_z^\bullet / 2\right)$ in a hollow ARROW. The distributions are presented at the points of the spectrum (see Fig. 5) with minimal losses in the photon-forbidden band shown in Fig. 6 and at one of the points in the high-loss band adjacent to this band.

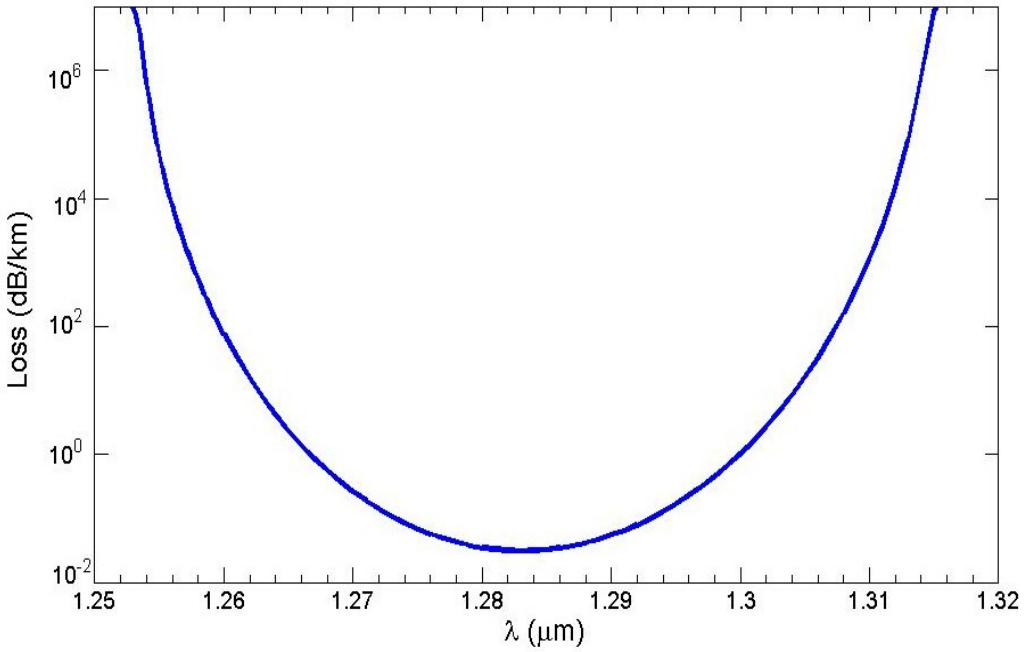

Fig 6: *Photon-forbidden band in an ARROW with minimal losses at* $\lambda_{1,10}^{(a)} = 1.28\ \mu m$ *(see Fig.5)*

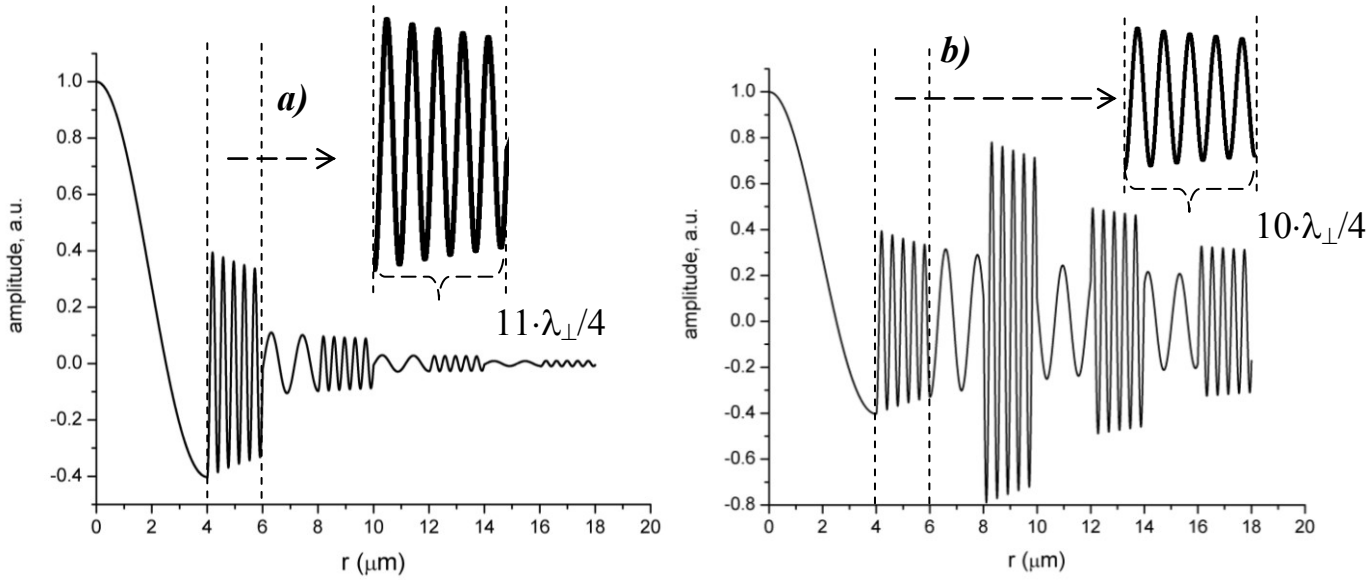

Fig. 7: *Radial distributions of* H_z *normalised to the maximum for the minimal losses in an ARROW at* $\lambda_{1,10}^{(a)} = 1.28\ \mu m$ *(a) and for large losses at* $\lambda_{1,10} = 1.344\ \mu m$ *(b) (see Fig. 5).*

One can see from Fig. 7a that in the "anti-resonance" case, neither of the cladding layers contains an integer of radiation half-wavelengths. However, despite comparatively low losses in the fibre, the field amplitudes in layers closest to the fibre

core are large enough. This can indicate that although the cladding geometry, which we have chosen arbitrarily, gives minimal losses at a wavelength of 1.28 μm, it does not exactly correspond to the quarter-wavelength structure for this wavelength and can be in principle optimised. The optimisation should reduce the field amplitude in the cladding and losses. The latter assumption is confirmed by calculations from which it follows that the decrease in the thickness of cladding layers down to the optimal value 1.976 μm reduces losses at least by a factor of one and a half.

The radial distribution of the second field component (E_φ) determining S_r exhibits a similar behaviour. The field distribution for the resonance wavelength $\lambda_{1,m} =$ 1.344 μm (m=10) presented in Fig. 7b shows that the field is indeed concentrated to a great extent in cladding layers. In this case, the thickness of each optically dense layer fits ten half-wavelengths, as should be in the resonance case. One can also see that layers with the smaller refractive index n_2 do not contain an integer of half-wavelengths and resonances are absent, which follows, by the way, from (33). Note, however, that the field amplitudes decrease nonmonotonically both in optically denser and less optically dense layers. In our opinion, this is explained by the fact that each of the layers, being an independent FP resonator, also serves as a component of a number of complex resonators consisting of several successive layers. Because the eigenfrequencies of such numerous resonators are different, the total contribution of these frequencies to the resonance response of each cladding layer to the given radiation wavelength is also different.

We see that there exist a number of spectral properties of ARROWs that can be explained only by considering the influence of composite resonators forming the cladding. Their substantial role is indirectly confirmed in paper [110] where it was shown that the resonance properties of a new layer added to the cladding structure (although with parameters different from those of regular cladding layers) considerably changed the ARROW spectrum.

Microstructure fibres of different types, in which instead of coaxial cladding layers with a high refractive index n_1 the cylindrical rods of radius $R > \lambda$ with the

same refractive index n_1 are located around the optically less dense core, have spectral properties similar to those of ARROWs. The positions of resonance spectral bands in such structures are related to the cut-off wavelengths of the eigenmodes of the rods in the cladding photonic crystal [33; 34; 118-121].

II.3.3 Calculation of dispersion in BF

As for the group velocity dispersion in BFs, by assuming that the material dispersion is absent, we are dealing with the waveguide dispersion only. This dispersion is completely determined by the properties of a particular photon-forbidden band. The dispersion parameter D is defined as

$$D = -\frac{2\pi c}{\lambda^2}\frac{d^2\,\mathrm{Re}\,\beta}{d\omega^2} = -\frac{\lambda}{c}\frac{d^2\,\mathrm{Re}\,\bar{n}}{d\lambda^2}, \qquad (34)$$

i.e. the photon-forbidden band is characterised by the dependence $\mathrm{Re}\,\bar{n}(\lambda)$.

The effective mode refractive index for the photon-forbidden band under study (see Fig. 6) is presented in Fig. 8.

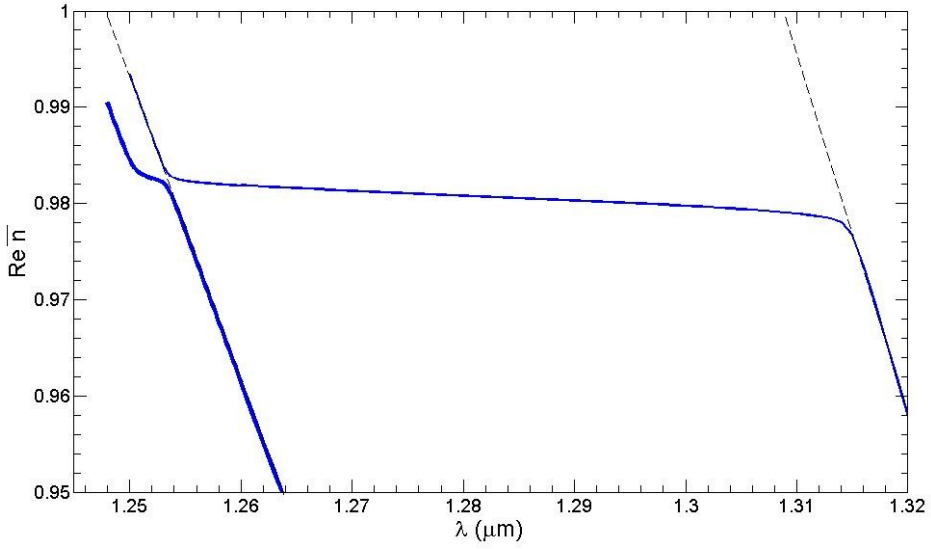

Fig. 8: *Wavelength dependence of the real part of the effective mode refractive index in the photon-forbidden band in Fig. 6 (the TE_{01} mode). The boundaries of the photon-forbidden band are shown by dashed straight lines.*

The straight dashed lines show the boundaries of the photon-forbidden band. The strong interaction of modes in the fibre core with cladding modes (resonances of all possible FP resonators in the cladding) leads to numerous "anti-crossings" of the dispersion curves of interacting modes, one of which is shown near a wavelength of ~ 1.25 μm. The boundaries of the photon-forbidden band are determined by the loci of the anti-crossings. A similar dependence for the HE_{11} mode is located somewhat higher than the dependence shown in Fig. 8 (but, of course, lower than the unit level), while the dependence for the TE_{02} mode is located lower. However, these modes have considerably higher optical losses than the TE_{01} mode, and we will not discuss them here.

The mode dispersion $D(\lambda)$ calculated from (34) by using the function $\mathrm{Re}\,\bar{n}(\lambda)$ in Fig. 8 is presented in Fig. 9.

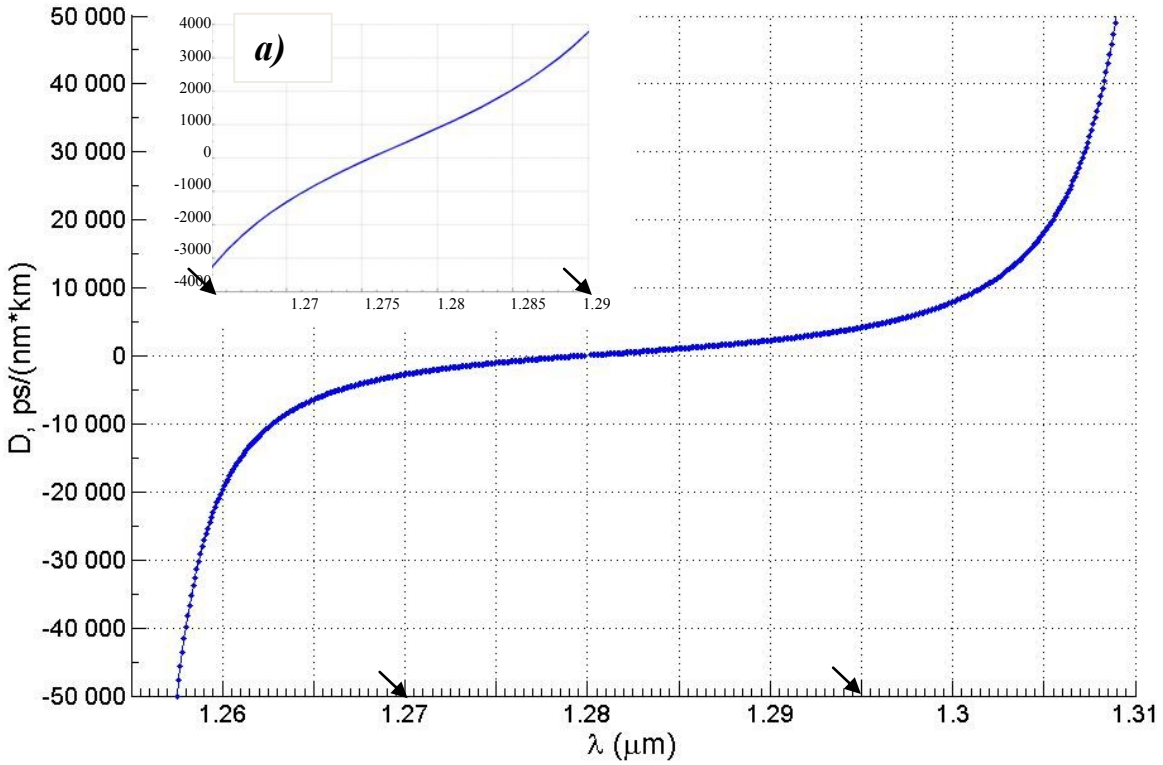

Fig.9: *Dispersion parameter D calculated for mode TE_{01} in the photonic-bandgap showed on* ***Fig.6****.*
Inset ***a)****: here is showed the dispersion parameter D in the wavelength range of 1.27-1.295 μm corresponded to waveguide losses ≤ 1 dB/m*

This dependence is also typical for BFs and is characterised by very large absolute values of dispersion near the boundaries of the photon-forbidden band, but unfortunately they are characterised by very large optical losses. At the same time, dispersion values in the region of acceptable losses are still large, as the inset in Fig. 9 shows. This property of BFs can be used to control dispersion in various optical devices.

Recall now that we calculated the dependence $\mathrm{Re}\,\bar{n}(\lambda)$ by neglecting the material dispersion. In the spectral region where hollow BFs have low optical losses, the wavelength dependence of the material refractive index can be neglected because the fraction of light propagating in the cladding material is quite small. At the same time, the spectral position of the zero dispersion in glass BFs can be found sufficiently accurately only by taking into account the material dispersion.

II.4 Conclusions

We have considered in detail one of the most efficient methods for calculating the optical properties of Bragg optical fibres. The method can be used not only to find the mode composition of radiation, optical losses and dispersion in fibres with the specified geometry of a multilayer cladding but, in conjunction with the genetic algorithm, also to determine the optimal cladding structure providing minimal optical losses at a particular wavelength. It has been explained simply which of the modes should be fundamental in BFs with high and low contrasts between refractive indices of the fibre core and cladding. The possibility of using BFs as efficient mode filters is confirmed, especially, in the case of a high refractive-index contrast. Such BFs with a hollow cladding can have in principle very low optical losses for the fundamental TE_{01} mode. The basic properties of BFs of the ARROW type have been described and it has been shown that these properties are determined not only by the parameters of the cladding layer nearest to the core but also by resonances of the cladding as a whole and of layered resonators comprising the cladding. Interest in BFs of the ARROW type is caused by practical considerations because it is possible to fabricate fi-

bres with comparatively broad transmission bands (a few tens of nanometres) with acceptable optical losses (see, for example, Fig. 6).

Note that, being potentially single-mode and guiding only one cylindrically symmetric and nondegenerate TE_{01} mode, hollow BFs are not subjected to the influence of the polarisation mode dispersion.

Chapter III. Analysis of optical properties of 2-D MOF

In present Chapter the analysis of optical properties of 2-D MOF is carried out. At the beginning the multipole method chosen for analysis was described sequentially and quite detailed. Then a concrete MOF type was investigated by means of this method. Namely, dispersion characteristics and waveguide losses of HF with the solid core made of tellurite glass were calculated. An influence of geometric parameters on optical properties was investigated. Finally, conditions of a singlemode regime realization in tellurite HF were obtained.

Main results of this Chapter were published in following works: [2; 3; 5].

III.1 Introduction

The theoretical analysis of optical properties of microstructured fibers, as of many other problems of electrodynamics, is based on the solution of Helmholtz wave equation for longitudinal components of the field. There are several semi-analytic methods for its solution, which use the expansion of the general solution in different bases of orthogonal functions. In particular, bases of trigonometric functions are used in the plane wave expansion method [122], the bases of orthogonal polynomials, for example, Hermite - Gaussian polynomials [123], etc. However, to obtain good convergence of the solution, many harmonics should be taken into account in its expansion, which deteriorates the calculation efficiency (its rate and accuracy). The number of harmonics in the expansion can be substantially reduced (thereby increasing the calculation efficiency) taking into account the fact that, as a rule, the elements of a structure under study have the circular symmetry.

At first time a similar technique was used in [124] where the field distribution in the system of two parallel cylinders was investigated. In [125] the problem of mode finding in the infinite array of hexagonally packed cylinders was considered. Further, in [126] the task was made more complicated and the system consisted of three parallel arranged cylinders with their cross-section centers lying in vertexes of

equilateral triangles was considered. However, in above mentioned tasks a specific notation for the general solution in the form of the cylindrical function expansion authors were used without proof of its validity. Theoretical proof of the possibility for such representation of a general solution was proposed later in [127]. While developing the method in [128] a more general case when the cladding consists of few high-index cylindrical inclusions was considered. And, finally, in [129; 130] a case of holey fibers with low-index (compared with a matrix refractive index) inclusions was investigated. Here the cylindrical functions expansion method (or multipole method) takes on its closed form.

By means of the multipole method it's possible to calculate structures consisted of the cylindrical elements having circular [129; 130] or elliptical [131] forms of transverse cross sections. Also it's possible to place each element into its own "local" cladding [132]. There are not imposed restrictions on a relative displacement of these elements in the transverse cross section so that one can analyze 2-D waveguide structures with arbitrary arrangement of circular holes generally speaking with different diameters. In this more general case the field in the arbitrary point of the cross section is represented by a sum of partial contributions from each of the different elements of the structure, while the symmetrical arrangement of holes allows one to consider the problem only within some sector of the fiber cross section. The required solution can be found by subjecting the field components to the boundary conditions at the interfaces between sectors. Depending on a symmetry class, the calculation rate can be increased by several times compared to the general case. With slight modifications the methodology described in [129; 130] allows also to spread out the analysis to waveguides based on photonic bandgap both with hollow and solid cores.

III.2 Theoretical part

III.2.1 Main equations and their solutions

Geometry of the considered general task is shown on Fig. 10. It represents the transverse cross section of the waveguide in *(x, y)* plane. The waveguide is considered infinite along *oz* axis direction which is coincided with a light's propagation direction. Thus the structure is representing by itself a circular glass rod with the refractive index *n* and radius R_0, which has *N* through cylindrical holes parallel to each other.

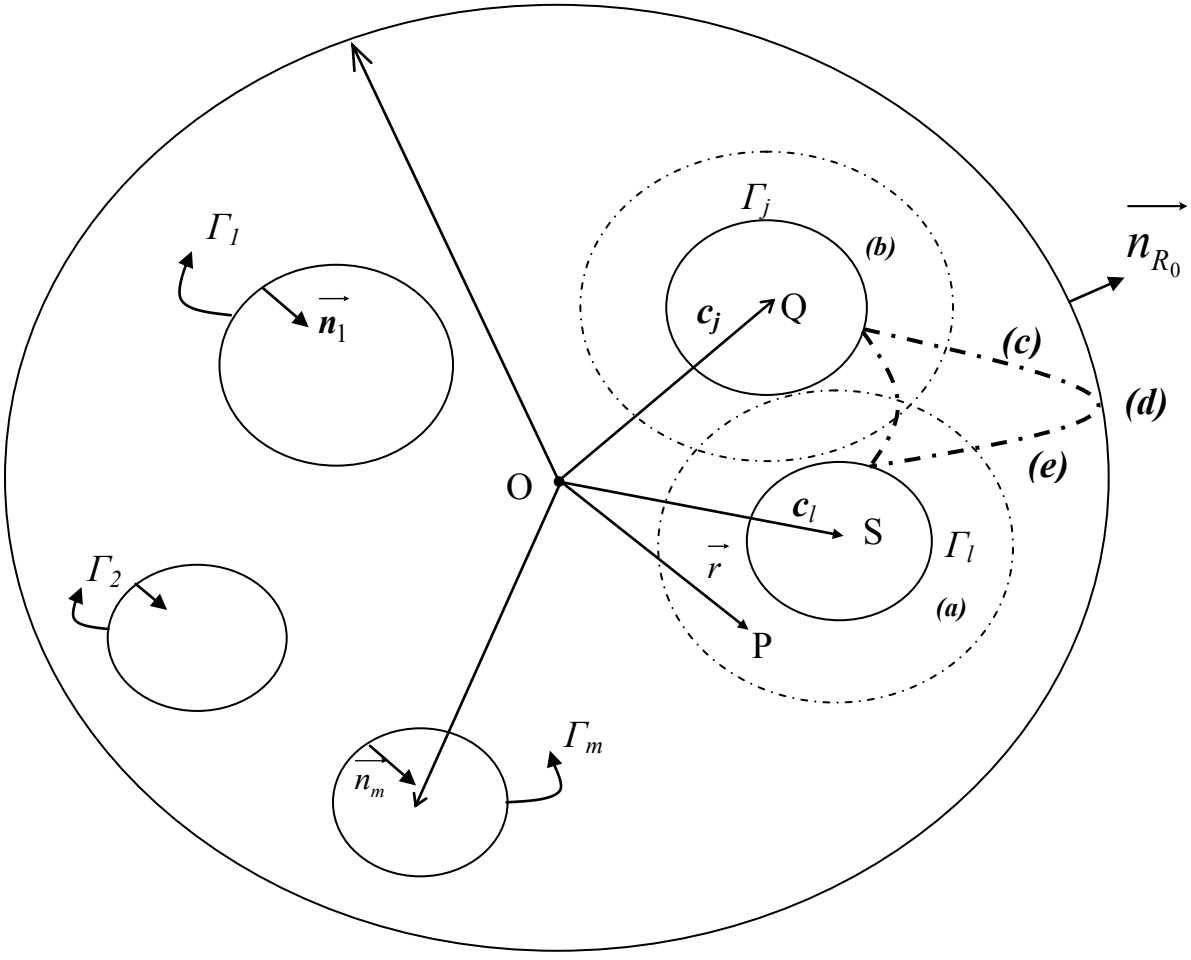

Fig. 10: *General view of waveguide's transverse cross section. Dashed curves – convergence regions for corresponding field expansions. Solid curves – physical boundaries. $QP=r_j$; $SP=r_l$; $OP=r$.*

The center of *i-th* cylinder has coordinates *(c_i,arg(c_i)),* diameter d_i, refractive index n_i (in case of holes filled with air $n_i = 1$). The region with holes (so called "matrix of refractive index *n*" further in text) has an external cladding (r > R_0) made of a different material with the refractive index n_0.

As in the previous chapter we assume that light propagates in a medium with the magnetic susceptibility equal to unity everywhere and the dielectric constant ε independent of time and homogeneous in each of the components of the fiber (glass, air, and cladding).

Following a general course and designations of the Chapter 2, in further analysis again we start from Maxwell equations represented in the form of wave equation for electromagnetic field:

$$\left(\Delta + \frac{\omega^2 \varepsilon}{c^2}\right)\begin{Bmatrix}\vec{E}\\ \vec{H}\end{Bmatrix} = 0, \qquad (1)$$

III.2.2. General solution in the form of two equivalent expansions

Let us represent e_z and h_z in the matrix near arbitrary *i-th* hole by means of linear combination of fundamental solutions of the wave equation for the longitudinal components (formulae II.1*) in local coordinates with the center in a point with radius-vector $\vec{c}_l$:

$$\vec{r}_l = (r_l, \theta_l) = \vec{r} - \vec{c}_l\,. \qquad (2)$$

At the same time for the electrical field we have:

$$e_z = \sum_m [A_m^{El} J_m(kr_l) + B_m^{El} H_m^{(1)}(kr_l)]\exp(im\theta_l)\,, \qquad (3)$$

where $k = \left(k_0^2 n^2 - \beta^2\right)^{1/2}$; $J_m(x)$ and $H_m^{(1)}(x)$ - Bessel and Hankel functions of the first kind and *m-th* order, correspondingly. The magnetic field h_z has analogous form, but with the expansion coefficients A_m^{Kl}, B_m^{Kl}.

In (3) summands described by the bounded everywhere function $J_m(x)$ can be interpreted as a part R^{El} of the field e_z incident on to the *l-th* cylinder. The summand

with functions $H_m^{(1)}(x)$ (source's summand) describing the field O^{El} scattering by the *l-th* cylinder. In other words $e_z = R^{El} + O^{El}$.

The local expansion (3) is valid only in the annular region extended from the surface of *l-th* cylinder to the surface of its nearest neighbour (region (a) on Fig.10). The same expansion also describes the field around the cladding-matrix interface further designated with index 0 (region (d) on Fig.10). The expression for the field which is valid in the all matrix region was proposed in [124], where a light propagation in an infinite medium with two parallel cylindrical rods was investigated.

It was considered that the field in some region can be presented as a superposition of waves outgoing from all sources in this region (there were two cylinders in [124] etc). If waves originate from sources outside considered region then they described by means of *J-Bessel functions* which have not the source.

When there are not two, but *N* cylindrical inclusions in a medium, then the field expansion is being written in a manner of [124] and it is:

$$e_z = \sum_{l=1}^{N}\sum_{m}[B_m^{El} H_m^{(1)}(k|\vec{r_l}|)\exp(im\arg(\vec{r}-\vec{c_l}))] + \sum_m A_m^{E0} J_m(kr)\exp(im\theta). \qquad (4)$$

Each summand in the double sum, composed of a series in terms of *m*, describes the field of the outgoing wave source of which is *l-th* cylinder. The last summand with index 0 describes the field reflected from the matrix-cladding interface.

It is obvious, that in annular region around *l-th* hole where (3) is valid, both expansions (3) and (4) describe the same field. An equivalence of (3) and (4) will be used for a finding of coefficients at sources terms (B_m^l) in a text below.

III.2.3. Obtaining multipole coefficients in fields expansions

Let us use both the equivalence of expressions (3), (4) in a vicinity of the arbitrary *l-th* cylinder and the boundary conditions on mediums interfaces for finding multipole coefficients in the fields expressions.

Expressions (3) and (4) describe the same field in the annular region around the *l-th* cylinder. Therefore we can equate them. Thus, taking into account that the summands with $H_m^{(1)}(kr_j)$ disappears when *j=l* because they are common, we obtain the equation:

$$\sum_m A_m^{El} J_m(kr_l)\exp(im\theta_l) = \sum_{\substack{j=1 \\ j\neq l}}^{N}\sum_m \left[B_m^{Ej} H_m^{(1)}(kr_j)\exp\left(im\arg(\vec{r}-\vec{c}_j)\right)\right] + \sum_m A_m^{E0} J_m(kr)\exp(im\theta) \quad (5)$$

All summands in (5) are related to different "local" coordinate systems. That's why in order to reduce the considered task to the eigenvalue problem let us transform these summands by help of Graf's summation theorem for cylindrical functions (look for example [133], p. 993). This question is discussed in more detail in works [3; 129] from which we have following transformation of summands from (5):

a) let us start from defining a contribution from the field scattered by the *j-th* cylinder into the local, regular (without singularity) field in a vicinity of the *l-th* cylinder (curve (b) on Fig. 10). This contribution (the sum by *m* in the first summand on the right of (5)) has the form:

$$\sum_m B_m^{Ej} H_m^{(1)}(kr_j)\exp(im\theta_j) = \sum_n A_n^{Elj} J_n(kr_l)\exp(in\theta_l), \quad (6)$$

where

$$A_n^{Elj} = \sum_m \mathrm{H}_{nm}^{lj} B_m^{Ej}, \qquad \mathrm{H}_{nm}^{lj} = H_{n-m}^{(1)}(kc_{lj})\exp\left[-i(n-m)\arg(\vec{c}_{lj})\right], \qquad \vec{c}_{lj} = \vec{c}_j - \vec{c}_l. \quad (7)$$

Introducing vector and matrix designations $\mathbf{A^{Elj}}=[A_n^{Elj}]$, $\mathbf{B^{Ej}}=[B_m^{Ej}]$, $\mathbf{H^{lj}}=[\mathrm{H}_{nm}^{lj}]$, let us represent the bases transformation (7) in the matrix form:

$$\mathbf{A^{Elj}}=\mathbf{H^{lj}}\mathbf{B^{Ej}}. \quad (8)$$

b) by a similar way we will show that the contribution (curve (e) on Fig.10) into the regular field (external, having no sources field) incident on the *l-th* cylinder and creating due to presence of a outer cladding has the form:

$$\sum_m A_m^{E0} J_m(kr)\exp(im\theta) = \sum_n A_n^{El0} J_n(kr_l)\exp(im\theta_l), \quad (9)$$

where $A_n^{El0} = \sum_m \Im_{nm}^{l0} A_m^{E0}$, or in the matrix form

$$\mathbf{A^{El0}}=\Im^{\mathbf{l0}}\mathbf{A^{E0}}, \quad (10)$$

and $\mathfrak{I}^{\mathbf{l0}}=\left[\mathfrak{I}_{nm}^{l0}\right]=\left\{(-1)^{n-m}J_{n-m}(kc_l)\exp\left[-i(n-m)\arg(\vec{c}_l)\right]\right\}$.

As a result of transformations of the clauses a) and b) all summands on the right in equation (5) are reduced to the coordinate system (r_l,θ_l) related with the arbitrary cylinder l and relatively of which the Fourier-Bessel expansion is considered. The equation (5) in this case in the annular region around the *l-th* cylinder (region (a) on Fig.10) with taking into account (8), (10) can be written in the form:

$$\mathbf{A}^{\mathbf{El}}=\sum_{\substack{j=1\\ j\neq l}}^{N}\mathbf{A}^{\mathbf{Elj}}+\mathbf{A}^{\mathbf{El0}}=\sum_{\substack{j=1\\ j\neq l}}^{N}\mathbf{H}^{\mathbf{lj}}\mathbf{B}^{\mathbf{Ej}}+\mathfrak{I}^{\mathbf{l0}}\mathbf{A}^{\mathbf{E0}} \qquad (11)$$

An analogous expression occurs also for the magnetic field's component h_z.

c) For outgoing field from arbitrary *l-th* cylinder in a vicinity of the cladding-matrix interface we have (curve (c) on Fig.10):

$$\sum_m B_m^{El}H_m^{(1)}(kr_l)\exp(im\theta_l)=\sum_n B_n^{E0l}H_n^{(1)}(kr)\exp(in\theta), \qquad (12)$$

where

$$B_n^{E0l}=\sum_{m=-\infty}^{\infty}\mathfrak{I}_{nm}^{0l}B_m^{El},\ \text{or in the matrix form:}$$

$$\mathbf{B}^{\mathbf{E0l}}=\mathfrak{I}^{\mathbf{0l}}\mathbf{B}^{\mathbf{El}}, \qquad (13)$$

Therewith

$$\mathfrak{I}^{\mathbf{0l}}=\left[\mathfrak{I}_{nm}^{0l}\right]=\left\{J_{n-m}(kc_l)\exp\left[-i(n-m)\arg(\vec{c}_l)\right]\right\}.$$

The transformation (12) is the transformation of the field outgoing from the local coordinate origin of an arbitrary cylinder to the field of an outgoing wave in the vicinity of the matrix-cladding interface.

Summing a contribution from all cylindrical sources lets rewrite the firs summand in the expansion (4) in the form that is valid only in cladding (region (d) on Fig.10)

$$\sum_{l=1}^{N}\mathbf{O}^{\mathbf{El}}=\sum_n B_n^{E0}H_n^{(1)}(kr)\exp(in\theta)=\mathbf{O}^{\mathbf{E0}},\ \text{where}$$

$$\mathbf{B}^{\mathbf{E0}}=\sum_{l=1}^{N}\mathbf{B}^{\mathbf{E0l}}=\sum_{l=1}^{N}\mathfrak{I}^{\mathbf{0l}}\mathbf{B}^{\mathbf{El}}. \qquad (14)$$

The analogous expression occurs also for the magnetic field's component h_z.

III.2.4 Dispersion equation

Here, accounting of boundary conditions also can be made by means of a matrix language but in slightly different way compared with Chapter 2. For doing so, let us consider a cylinder having a circular shape of the transverse cross section and with radius *a*. A refractive index of the cylinder material we have designated as n_-, but a refractive index of the surrounding material as n_+. Let's represent the longitudinal components of the field e_z and h_z in the form of a Fourier-Bessel expansion as in (3) inside and outside from the cylinder:

$$e_z^{\pm} = \sum_{m=-\infty}^{+\infty} [A_m^{E\pm} J_m(k^{\pm} r) + B_m^{E\pm} H_m^{(1)}(k^{\pm} r)] \exp(im\theta), \qquad (15)$$

where the sign (-) is related to the region where $r < a$, and a sign (+) where $r > a$. The analogous expression occurs also for the magnetic field component h_z. Here $k^{\pm} = (k_0{}^2 n_{\pm}^2 - \beta^2)^{1/2}$, and an interpretation of the summand with *J* and *H* Bessel functions is given earlier.

In the light of the said above, let's introduce vectors for amplitudes of the field components $\mathbf{A^{E\pm}} = [A_m^{E\pm}]$, $\mathbf{A^{K\pm}} = [A_m^{K\pm}]$, $\mathbf{B^{E\pm}} = [B_m^{E\pm}]$, $\mathbf{B^{K\pm}} = [B_m^{K\pm}]$. On the cylindrical dielectric interface a partial reflection and transmission of light occur. And amplitudes of transmitted and reflected fields can be represented by matrix relations due to linear nature of Maxwell equations:

$$\begin{aligned} \widetilde{\mathbf{A}}^{-} &= \widetilde{\mathbf{T}}^{-}\widetilde{\mathbf{A}}^{+} + \widetilde{\mathbf{R}}^{-}\widetilde{\mathbf{B}}^{-} \\ \widetilde{\mathbf{B}}^{+} &= \widetilde{\mathbf{R}}^{+}\widetilde{\mathbf{A}}^{+} + \widetilde{\mathbf{T}}^{+}\widetilde{\mathbf{B}}^{-} \end{aligned}, \qquad (16)$$

where $\widetilde{\mathbf{A}}^{\pm}$ and $\widetilde{\mathbf{B}}^{\pm}$ - vectors with components $(\mathbf{A^{E\pm}},\mathbf{A^{K\pm}})$ и $(\mathbf{B^{E\pm}},\mathbf{B^{K\pm}})$, correspondingly; $\widetilde{\mathbf{R}}^{-}, \widetilde{\mathbf{R}}^{+} (\widetilde{\mathbf{T}}^{-}, \widetilde{\mathbf{T}}^{+})$ - inner and outer reflection (transmission) matrices of the cylinder. Let us note that transmission matrices are not necessitated in cases considered below.

Let's obtain expressions for matrix elements $\widetilde{\mathbf{R}}^{-}, \widetilde{\mathbf{R}}^{+}$ by means of boundary conditions, i.e. continuity of the tangential field components on the two dielectric's interface.

a) At first, we considering $A_m^{E+} = A_m^{K+} = 0$ (or $\tilde{\mathbf{A}}^{+}$=0), that corresponds to an absence of external field sources. In this case elements of the inner reflection matrix $\widetilde{\mathbf{R}}^{-}$ can be found (in particular, from the matrix-cladding interface). At the same time, from general relations (16) (first of them) the summand having the transmission matrix falls out.

And it's possible to write:

$$A_m^{E-} = R_m^{EE-} B_m^{E-} + R_m^{EK-} B_m^{K-},$$
$$A_m^{K-} = R_m^{KE-} B_m^{E-} + R_m^{KK-} B_m^{K-},$$

that corresponds to

$$\begin{bmatrix} \mathbf{A}^{\mathbf{E-}} \\ \mathbf{A}^{\mathbf{K-}} \end{bmatrix} = \begin{bmatrix} \mathbf{R}^{\mathbf{EE-}} & \mathbf{R}^{\mathbf{EK-}} \\ \mathbf{R}^{\mathbf{KE-}} & \mathbf{R}^{\mathbf{KK-}} \end{bmatrix} \begin{bmatrix} \mathbf{B}^{\mathbf{E-}} \\ \mathbf{B}^{\mathbf{K-}} \end{bmatrix}, \qquad \text{or} \qquad \widetilde{\mathbf{A}}^{-} = \widetilde{\mathbf{R}}^{-} \widetilde{\mathbf{B}}^{-}, \qquad (17)$$

where $\mathbf{R}^{\mathbf{EE-}}$, $\mathbf{R}^{\mathbf{EK-}}$, $\mathbf{R}^{\mathbf{KE-}}$, $\mathbf{R}^{\mathbf{KK-}}$ - diagonal matrices. Their *m-th* diagonal elements are follows:

$$R_m^{EE-} \frac{1}{\delta_m} \left[\left(\alpha_{J^- H^+}^{+} - \alpha_{H^+ J^-}^{-} \right) \left(n_-^2 \alpha_{H^- H^+}^{+} - n_+^2 \alpha_{H^+ H^-}^{-} \right) - \left(m\tau H_m^{+} \right)^2 J_m^{-} H_m^{-} \right],$$
$$R_m^{EK-} = \frac{1}{\delta_m} \frac{2m\tau}{\pi k_0 a} \frac{k^{+}}{k^{-}} \left(H_m^{+} \right)^2, \qquad (18)$$
$$R_m^{KE-} = -n_-^2 R_m^{EK-},$$
$$R_m^{KK-} = \frac{1}{\delta_m} \left[\left(\alpha_{H^- H^+}^{+} - \alpha_{H^+ H^-}^{-} \right) \left(n_-^2 \alpha_{J^- H^+}^{+} - n_+^2 \alpha_{H^+ J^-}^{-} \right) - \left(m\tau H_m^{+} \right)^2 J_m^{-} H_m^{-} \right].$$

Let's note, that in [129] in the expression for R_m^{KK-}, the second summand in square brackets is incorrect because it has a positive sign.

Earlier we considered that field amplitudes for the matrix-cladding interface have index 0. That's why the expression (17) in such designations we must write as follows:

$$\widetilde{\mathbf{A}}^0 = \widetilde{\mathbf{R}}^0 \widetilde{\mathbf{B}}^0. \qquad (19)$$

A physical meaning of the last relation is so that the field $\widetilde{\mathbf{B}}^0$ created by all sources (i.e. by cylinders here) reflects by the cladding and gives the contribution into the regular field $\widetilde{\mathbf{A}}^0$ that is incident onto each of cylinders.

b) Now we considering $B_m^{E-} = B_m^{K-} = 0$ (or $\widetilde{\mathbf{B}}^- = 0$) in (16). In this case elements of the outer reflection (from the interface of the arbitrary cylinder) matrix $\widetilde{\mathbf{R}}^+$ are being founded. It's clear that terms with Hankel functions *H* which are related with sources were not to be in inner regions of cylinders. The summand with the transmission matrix also falls out in the second relation of (16) when $\widetilde{\mathbf{B}}^- = 0$.

Similarly to a) we can obtain:

$$B_m^{E+} = R_m^{EE+} A_m^{E+} + R_m^{EK+} A_m^{K+},$$
$$B_m^{K+} = R_m^{KE+} A_m^{E+} + R_m^{KK+} A_m^{K+},$$

that as in (17) corresponds to:

$$\begin{bmatrix} \mathbf{B}^{E+} \\ \mathbf{B}^{K+} \end{bmatrix} = \begin{bmatrix} \mathbf{R}^{EE+} & \mathbf{R}^{EK+} \\ \mathbf{R}^{KE+} & \mathbf{R}^{KK+} \end{bmatrix} \begin{bmatrix} \mathbf{A}^{E+} \\ \mathbf{A}^{K+} \end{bmatrix}, \quad \text{or} \quad \widetilde{\mathbf{B}}^+ = \widetilde{\mathbf{R}}^+ \widetilde{\mathbf{A}}^+. \qquad (20)$$

Consequently we obtain that for the field scattered by the arbitrary cylinder *m-th* diagonal elements of the matrices $\mathbf{R}^{EE+} = diag\left(R_m^{EE+}\right)$, $\mathbf{R}^{EK+} = diag\left(R_m^{EK+}\right)$ and so on, are following:

$$R_m^{EE+} \frac{1}{\delta_m} \left[\left(\alpha_{J^- H^+}^+ - \alpha_{H^+ J^-}^- \right) \left(n_-^2 \alpha_{J^- J^+}^+ - n_+^2 \alpha_{J^+ J^-}^- \right) - \left(m\tau J_m^- \right)^2 J_m^+ H_m^+ \right],$$

$$R_m^{EK+} = \frac{1}{\delta_m} \frac{2m\tau}{\pi k_0 a} \frac{k^-}{k^+} \left(J_m^- \right)^2, \qquad (21)$$

$$R_m^{KE+} = -n_+^2 R_m^{EK+},$$

$$R_m^{KK+} = \frac{1}{\delta_m} \left[\left(\alpha_{J^- J^+}^+ - \alpha_{J^+ J^-}^- \right) \left(n_-^2 \alpha_{J^- H^+}^+ - n_+^2 \alpha_{H^+ J^-}^- \right) - \left(m\tau J_m^- \right)^2 J_m^+ H_m^+ \right].$$

Let's note again that few errors are committed in expressions for these matrix elements in [129]. So, there is H_m^- instead of using J_m^--function in the second summand of the right-hand part of the expression for R_m^{EE+} in [129]. The same misprint is in the second summand of the expression for R_m^{KK+}. In addition the sign of the value R_m^{KK+} by itself is opposite.

So, now we have all relations (11), (14), (19), (20) which are necessary for reducing the considered task to the eigenvalue problem.

At first, with taking into account introduced above vectors $\widetilde{\mathbf{A}}$ and $\widetilde{\mathbf{B}}$, the relation (11) which was found earlier we write in the following form:

$$\widetilde{\mathbf{A}}^{\mathbf{l}} = \sum_{\substack{j=1 \\ j\neq l}}^{N} \widetilde{\mathbf{H}}^{\mathbf{lj}} \widetilde{\mathbf{B}}^{\mathbf{j}} + \widetilde{\mathfrak{I}}^{\mathbf{l0}} \widetilde{\mathbf{A}}^{\mathbf{0}} \qquad (22)$$

where $\widetilde{\mathbf{H}}^{\mathbf{lj}} = diag(\mathbf{H}^{\mathbf{lj}}, \mathbf{H}^{\mathbf{lj}}), \widetilde{\mathfrak{I}}^{\mathbf{l0}} = diag\,(\mathfrak{I}^{\mathbf{l0}}, \mathfrak{I}^{\mathbf{l0}})$.

The equation (22) represents by itself the system of *N* equations for amplitudes of fields in the vicinity of cylindrical elements of the structure. These equations defines the regular field incident onto the arbitrary *l-th* cylinder by means of fields amplitudes from all remaining sources (i.e. cylinders) and also with taking into account the contribution introduced by the reflection from the cladding ($\widetilde{\mathbf{A}}^{\mathbf{0}}$). Let's introduce matrices:

$$\mathbf{A} = [\widetilde{\mathbf{A}}^{l}],\ \mathbf{B} = [\widetilde{\mathbf{B}}^{l}],\ \widetilde{\mathbf{H}} = [\widetilde{\mathbf{H}}^{lj}]\ (\ \widetilde{\mathbf{H}}^{ll} \equiv 0\ ),\ \widetilde{\mathfrak{I}}^{B0} = [\widetilde{\mathfrak{I}}^{l0}] = [(\widetilde{\mathfrak{I}}^{10})^T, (\widetilde{\mathfrak{I}}^{20})^T, ..., (\widetilde{\mathfrak{I}}^{N0})^T]^T,$$

$l, j = 1, ..., N,$

where upper index *T* designates a matrix transpose.

Then in consideration of all cylinders the equation (22) takes the form:

$$\mathbf{A} = \widetilde{\mathbf{H}} \cdot \mathbf{B} + \widetilde{\mathfrak{I}}^{\mathbf{B0}} \cdot \widetilde{\mathbf{A}}^{\mathbf{0}} \qquad (23)$$

Similarly, for the components $\widetilde{\mathbf{B}}^0$ of the field created by all sources in the vicinity of cladding-matrix interface from the equation (14) we have:

$$\widetilde{\mathbf{B}}^{\mathbf{0}} = \sum_{l=1}^{N} \widetilde{\mathfrak{I}}^{0l} \widetilde{\mathbf{B}}^{l} = \widetilde{\mathfrak{I}}^{0B} \mathbf{B},$$
$$\widetilde{\mathfrak{I}}^{0B} = [\widetilde{\mathfrak{I}}^{0l}] = [\widetilde{\mathfrak{I}}^{01}, \widetilde{\mathfrak{I}}^{02}, ..., \widetilde{\mathfrak{I}}^{0N}]. \qquad (24)$$

Further, we designate

$$\widetilde{\mathbf{R}}^{+} \overset{обозн}{=} \widetilde{R}^{l} \text{ и } \Re \overset{обозн}{=} diag(\widetilde{R}^{1}, \widetilde{R}^{2}, ..., \widetilde{R}^{N}).$$

Then from (20) follows, that

$$\mathbf{B} = \Re \cdot \mathbf{A}.$$

From (19) and (24) correspondingly we obtain:

$$\widetilde{\mathbf{A}}^{0} = \widetilde{\mathbf{R}}^{0}\widetilde{\mathbf{B}}^{0} = \widetilde{\mathbf{R}}^{0}\widetilde{\Im}^{0B}\mathbf{B}.$$

After, in considering of (23) we have:

$$\mathbf{B} = \Re \cdot (\widetilde{\mathbf{H}} \cdot \mathbf{B} + \widetilde{\Im}^{\mathbf{B0}} \cdot \widetilde{\mathbf{A}}^{\mathbf{0}}) = \Re \cdot (\widetilde{\mathbf{H}} \cdot \mathbf{B} + \widetilde{\Im}^{\mathbf{B0}} \cdot \widetilde{\mathbf{R}}^{0}\widetilde{\Im}^{0B}\mathbf{B}).$$

Or, by carrying out all terms into the left-hand side, finally we obtain required homogeneous system of algebraic equations on coefficients $\widetilde{\mathbf{B}}^{l}$:

$$[I - \Re \cdot (\widetilde{\mathbf{H}} + \widetilde{\Im}^{\mathbf{B0}} \cdot \widetilde{\mathbf{R}}^{0}\widetilde{\Im}^{0B})]\mathbf{B} = \aleph \cdot \mathbf{B} = 0 \qquad (25)$$

The nontrivial solution of the system (25) corresponds to the field propagating along *z* direction. And this solution corresponds to guided (or may be leaky) modes of the considered waveguide because of this field exists in absence of external sources.

The system (25) corresponds to the nontrivial vector $\mathbf{B}$, under the condition of equality of the related determinant to zero. When geometry and wavelength are fixed this determinant depends only on the propagation constant or, that is equivalent, on the effective refractive index. Therefore, for a given waveguide a mode searching process is related with finding of zeros of complex function $det(\aleph)$ of complex variable n_{eff}.

In practice, a treatment of quite complex structures with large amount of holes is necessary as a rule. Sometimes an increasing of the field expansion order is required while varying of geometrical parameters (hole diameter, pitch, etc.). In these cases difficulties in numerical calculation arise. Namely, the determinant dimension is increasing because of $dim(\aleph) = 2(2M+1)N_c$, where M - field's expansion order, N_c - amount of cylinders. If the considered structure having symmetry then taking this into account allows us to use a group theory methodology. At first it's possible to categorize modes of the structure with respect to its symmetry classes and degeneracy and at second to decrease the determinant dimension. This allows to investigate more

complex structures using personal computer. More detailed explanation of the method of using symmetry in calculations is given in works [3; 130] on the example of a structure having C_6^v symmetry group.

III.3 Optical properties of holey fibers based on tellurite glass

General overview of HF and their possibilities was done in Chapter 1, and here we will concentrate on the analysis of optical properties of tellurite HF. Dispersion properties, waveguide losses, conditions of obtaining of the singlemode regime of light propagation in such waveguides are investigated in depending on geometrical parameters of the structure – total amount of holes, their size and pith between them.

The $Te0_2$ glass used in holey fibers studied in the paper is quite promising for fiber optics. First, its refractive index is greater approximately by a factor of one and a half than that of a silica glass (see, for example, [134]) and, therefore, the cladding-core contrast Δn is greater, which simplifies the control of chromatic dispersion. Second, tellurite glasses also have higher nonlinear properties (the third-order susceptibility of some of them can be ~ 40 times higher than that for silica glasses [135]), which makes holy fibers promising for the use in various nonlinear radiation frequency converters. Note also that the melting temperature of tellurite glasses is much lower [134] than that of silica glasses, which can be important for the manufacturing technology of fibers.

Although at present the material optical losses in tellurite glasses (~ 1 dB/m [134]) still greatly exceed their assumed low fundamental losses, a study of the optical properties of tellurite fibers is of current interest in connection with the expected progress in technologies.

III.3.1 Waveguide's geometry

The cross section of a typical microstructure fiber considered here is shown in Fig. 11. The fiber is a circular glass rod with the refractive index n and radius R_0, which has N through cylindrical holes of diameter d (the same for all the holes in our case). The arrangement of holes in the cross section of typical microstructure fibers corresponds to the hexagonal symmetry with the distance Λ between the centers of the adjacent holes. The central region in this symmetric structure, where a hole is absent, and its nearest surrounding play the role of the fiber core. In practice, the glass rod has an external cladding ($r > R_0$) made of a different material with the refractive index n_{ext}. Usually R_0 is considerably exceeding sizes of nonuniformities

($R_0 >> \Lambda$). Therefore calculations are carried out with good approximation in assumption that $R_0 \to \infty$.

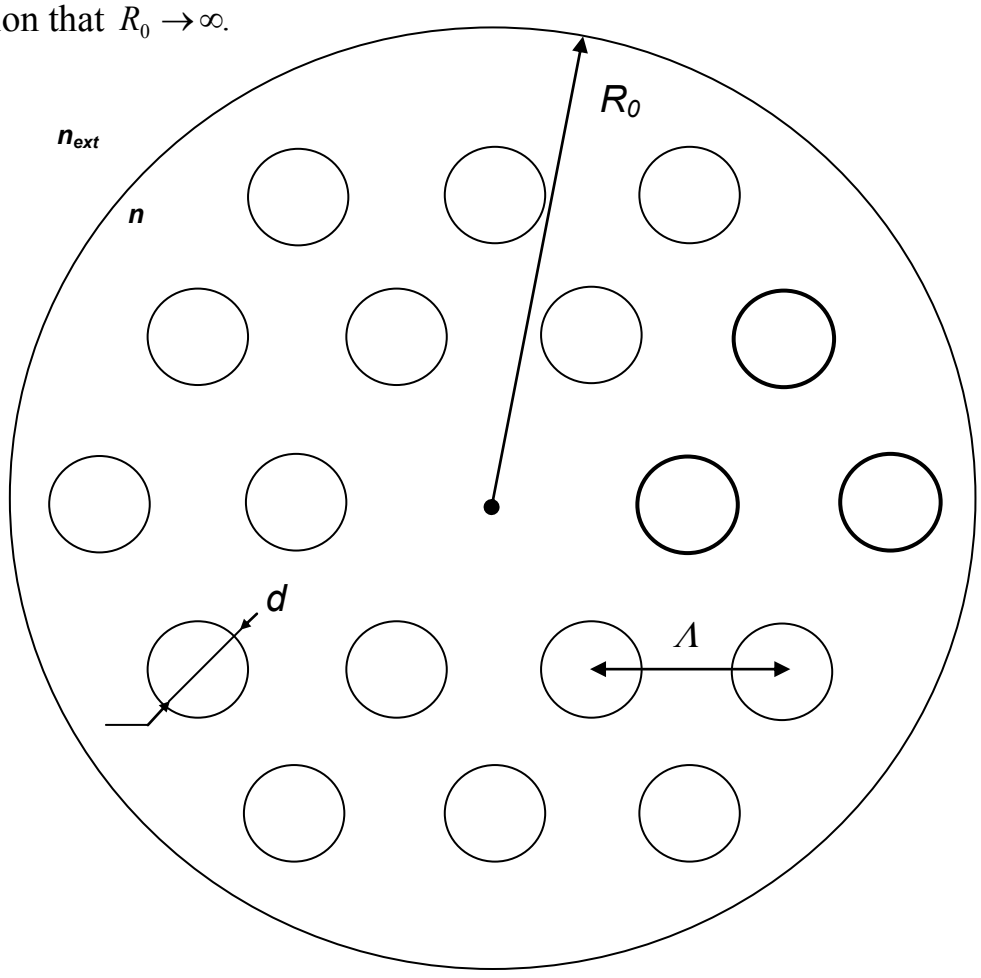

Fig. 11: *Cross section of a holey fiber (in this example, with two rows of holes around the fiber core).*

III.3.2 Analysis of dispersion properties

Of all the tellurite glasses we considered a particular glass of the $0{,}8TeO_2$-$0{,}2WO_3$ chemical composition (the numerical coefficients denote molar fractions). The material dispersion of this glass determined by the Sellmeyer dependence

$$n^2(\lambda) = A + B/\left(1 - C/\lambda^2\right) + D/\left(1 - E/\lambda^2\right), \qquad (26)$$

is known [136]. Here, $A=2.4909866;\ B=1.9515037;\ C=5.6740339\cdot10^{-2};\ D=3.0212592;\ E=225;$ and the wavelength is measured in micrometers.

Roots of the dispersion equation were calculated in complex plane. For its numerical solution it's necessary to truncate field expansions (3) i.e. $m \in [-M,...,0,...,M]$. A criterion for a truncation error is numerical difference of expansions (3) and (4) on cylindrical interfaces. An amount of accountable terms increases with increasing of holes diameters as it follows from [130]. A value of M is chosen based on analysis of an error arising while truncation of series in fields expansions on cylindrical functions. This error was analyzed by means of comparing expansions (3) and (4) which must coincide in the limit when $M \to \infty$. In [130] a conclusion was made that M must exceed approximately in *1.5* times a largest argument of used Bessel functions. Then cylindrical functions in last terms will have power law providing a fast convergence with increasing of m. The largest argument of used Bessel functions is $k_1 \cdot a,$ where $k_1 = \left((k_0 n_1)^2 - \beta^2\right)^{1/2}, \beta = n_{eff} \cdot k_0, n_1$ – refractive index of a matrix glass, a – hole's radius. In case of tellurite fibers and wavelength for example assumed to be 1.55 μm then the real part of $k_1 \sim 2$ that's why for radii $a \sim$ up to *2 μm* the value of *M=5* can be not increased.

The following method was used for the plotting of dispersion curves. The effective refractive index $n_{eff}(\lambda_0)$ was found for desired mode at some fixed wavelength λ_0. Then the effective index was founding at wavelength $\lambda_0 + \Delta_\lambda, \Delta_\lambda << \lambda_0$, where $n_{eff}(\lambda_0)$ was using as a first approximation. The rest effective indices at the wavelengths $\lambda_0 + m\Delta_\lambda, m = 2,3,...$ were found doing in exactly the same way varying over all demanded spectral range.

In this case, because no data on the spectral dependence of optical losses in tellurite glasses are available in the literature, the material losses were neglected, and the values of $\mathrm{Im}\, n_{eff}$ obtained in the solution were completely determined by waveguide losses. In the future, when the reliable experimental data of material losses will be obtained, these losses can be readily taken into account by introducing the imaginary part into dependence (26).

The group velocity v_g

$$\frac{v_g}{c} = \left(\mathrm{Re}\, n_{eff} - \lambda \frac{d\, \mathrm{Re}\, n_{eff}}{d\lambda} \right)^{-1}, \qquad (27)$$

and the dispersion parameter D

$$D = -\frac{\lambda}{c} \frac{d^2\, \mathrm{Re}\, n_{eff}}{d\lambda^2}, \qquad (28)$$

were found from the calculated real part $\mathrm{Re}\, n_{eff}$ while the waveguide losses (in dB/km) were calculated from the expression

$$\alpha = 20 k_0 \lg e \cdot \mathrm{Im}\, n_{eff} \ [137], \qquad (29)$$

where k_0 is measured in km^{-1}.

It is obvious that the main optical properties of holey fibers made of tellurite glass and of holey silica fibers should be qualitatively similar. However, from the practical point of view it is important to have an idea of their quantitative difference. This difference is illustrated by the calculated optical characteristics of tellurite holey fibers presented in Figs 12-16.

One of the most important features of holey fibers is a strong dependence of their dispersion properties on the structure geometry. Of no less interest is also their ability to maintain the single-mode propagation of radiation in a much broader spectral range than in conventional fibers. In this case, the cross-section area of the field mode can be varied in a very broad range.

Fig. 12 presents the spectral dependences of the effective mode refractive index $\mathrm{Re}\, n_{eff}$, the group velocity, and the dispersion parameter for the fundamental mode

of fibers with different geometries. One can see, in particular, that the greater is the air content in the cladding than the greater is the difference of dispersion properties of the fiber from those of the bulk glass. This difference is increasing with the wavelength of light. The latter is clear, because the longer is the wavelength, the less sensitive is irradiation to structural inhomogeneities when the fiber geometry is being fixed. In this case, the field is more and more homogeneously distributed in the cladding whose refractive index tends to some averaged value determined by the relative content of air. Correspondingly, the refractive-index contrast of the fiber core and cladding monotonically increases with increasing λ. An vice versa, the shorter is the wavelength (λ is smaller than the characteristic size of structural inhomogeneities), the stronger is the field localization in glass regions of the fiber (mainly due to TIR) and the weaker is its penetration into air holes. The effective refractive index gradually approaches the refractive index of the glass, resulting in a decrease in the contrast Δn. However, this does not lead in the limit to the loss of waveguide properties of the structure because, as the values of Δn and λ decrease simultaneously, the dimensionless characteristic parameter V of the fiber tends to a constant value.

One can see from Fig. 12b that the zero value of the material chromatic dispersion in a tellurite glass corresponds to a considerably longer wavelength (~ 2.2 μm) than for a silica glass. In fibers, the waveguide dispersion is added to the material dispersion, and the zero value of D, as in the case of holey silica fibers, shifts to the blue.

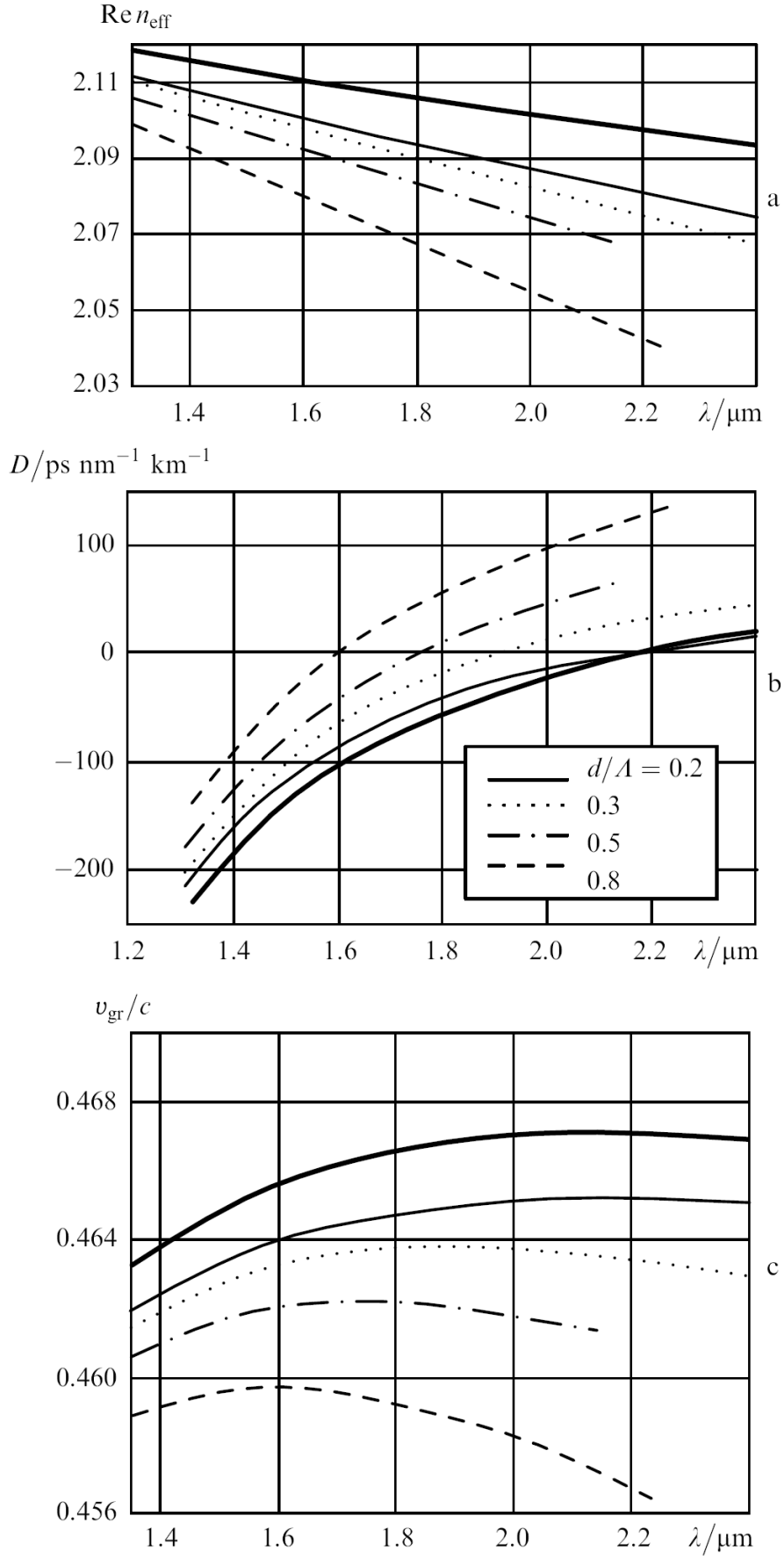

Fig. 12: *Spectral dependencies of the effective refractive index* $\mathrm{Re}\, n_{eff}$ *(a), the dispersion parameter D (b), and the ratio* v_g / c *of the group velocity to the speed of light in vacuum (c) on the air content in the fiber cladding (the* d / Λ *ratio) for a holey fiber with three rows of holes around the fiber core for* $\Lambda = 2.3$ *μm. The calculations are presented for the fundamental mode of the fiber. The solid thick curves show the dependences corresponding to the purely material dispersion (26) for a bulky glass.*

III.3.3 Waveguide losses

The number of rows (layers) of holes around the fiber core (two or more) almost does not affect the dispersion characteristics of fibers; however, it affects considerably the waveguide losses. The value of these losses is demonstrated in Figs 13 and 14. In particular, one can see from Fig. 13 that the waveguide losses rapidly decrease with increasing the air content in the cladding (with increasing the d/Λ ratio), large distances between the holes being preferable at fixed *d*. Figure 14 shows losses in fibers with two and three rows of holes. The qualitative result of this comparison is obvious in advance and is determined by the air content in the cladding. Our calculations show that the waveguide losses in a fiber with three rows of holes are so small that the total losses, even in the case of expected low material losses, will be determined by the latter. Therefore, it seems unlikely that tellurite holey fibers with three rows of holes will be required.

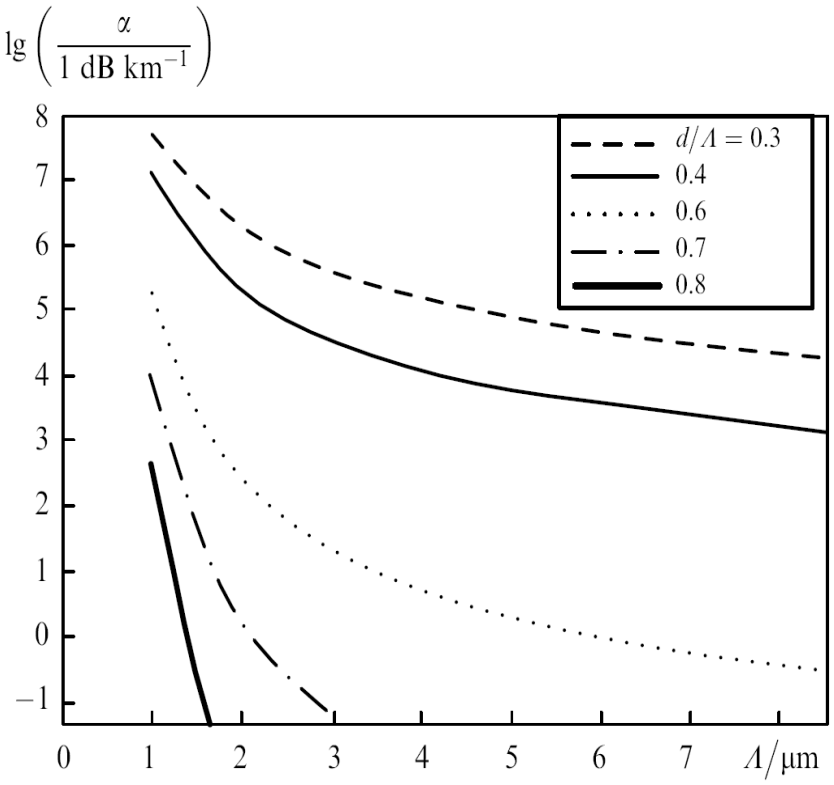

Fig. 13: *Dependences of the waveguide losses on the distance* Λ *between the centers of the adjacent holes for different ratios* d/Λ *holey fibers with two rows of holes. The calculations were performed (the radiation wavelength* $\lambda = 1.55$ *μm*

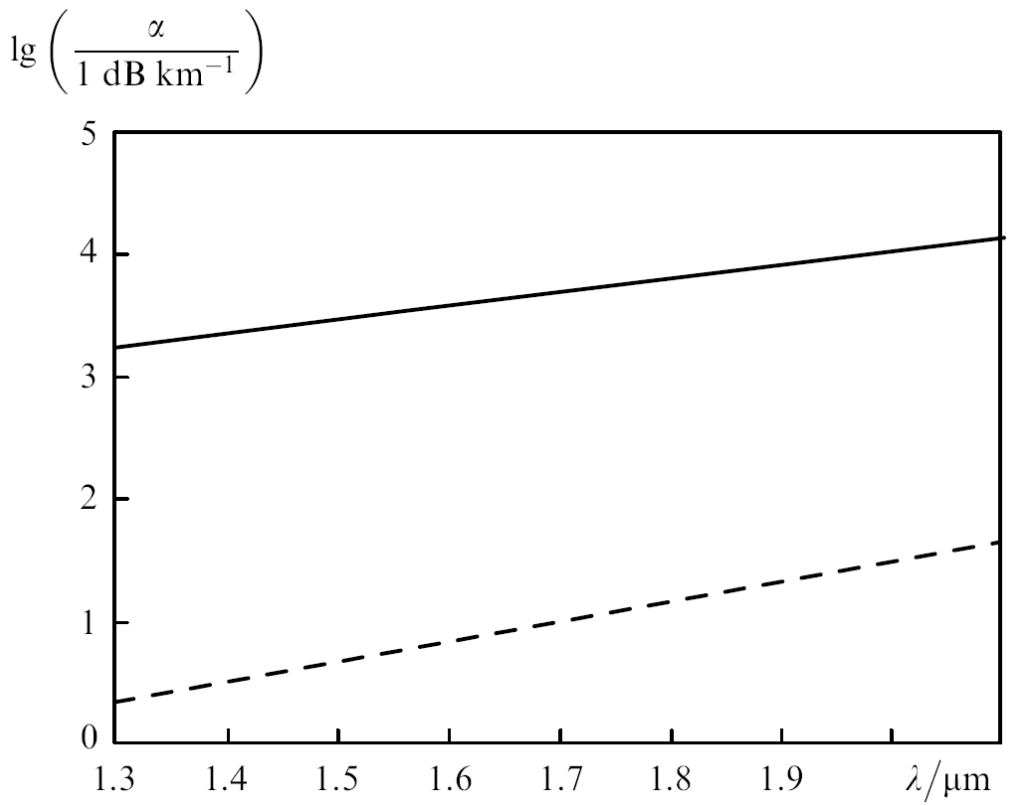

Fig. 14: *Waveguide losses for the fundamental mode of a holey tellurite glass fiber with two (upper straight line) and three (lower straight line) rows of holes as functions of the radiation wavelength. The curves are obtained for* Λ *=2.5 μm and* $d/\Lambda = 0.5$.

III.3.4 Singlemode and multimode regions

To find the region of variation of geometrical parameters of tellurite glass holey fibers in which the single-mode propagation of radiation can be realized, we plotted the dependences of losses for the fundamental and first higher modes of the fiber on the distance Λ between the centers of adjacent holes for different ratios d/Λ. The results of some calculations are presented in Figs 15-17.

Figure 15 shows the change in the intensity of the fundamental mode of the fiber (the real part of the longitudinal component of the Poynting vector) with decreasing the parameter Λ. One can see that, beginning from some values $\Lambda < \lambda$, the process of delocalization and disappearance of the mode gradually develops. For the most descriptive presentation of this process, the most optimal scales for the mode intensity and the transverse dimensions of the mode field were used in each picture.

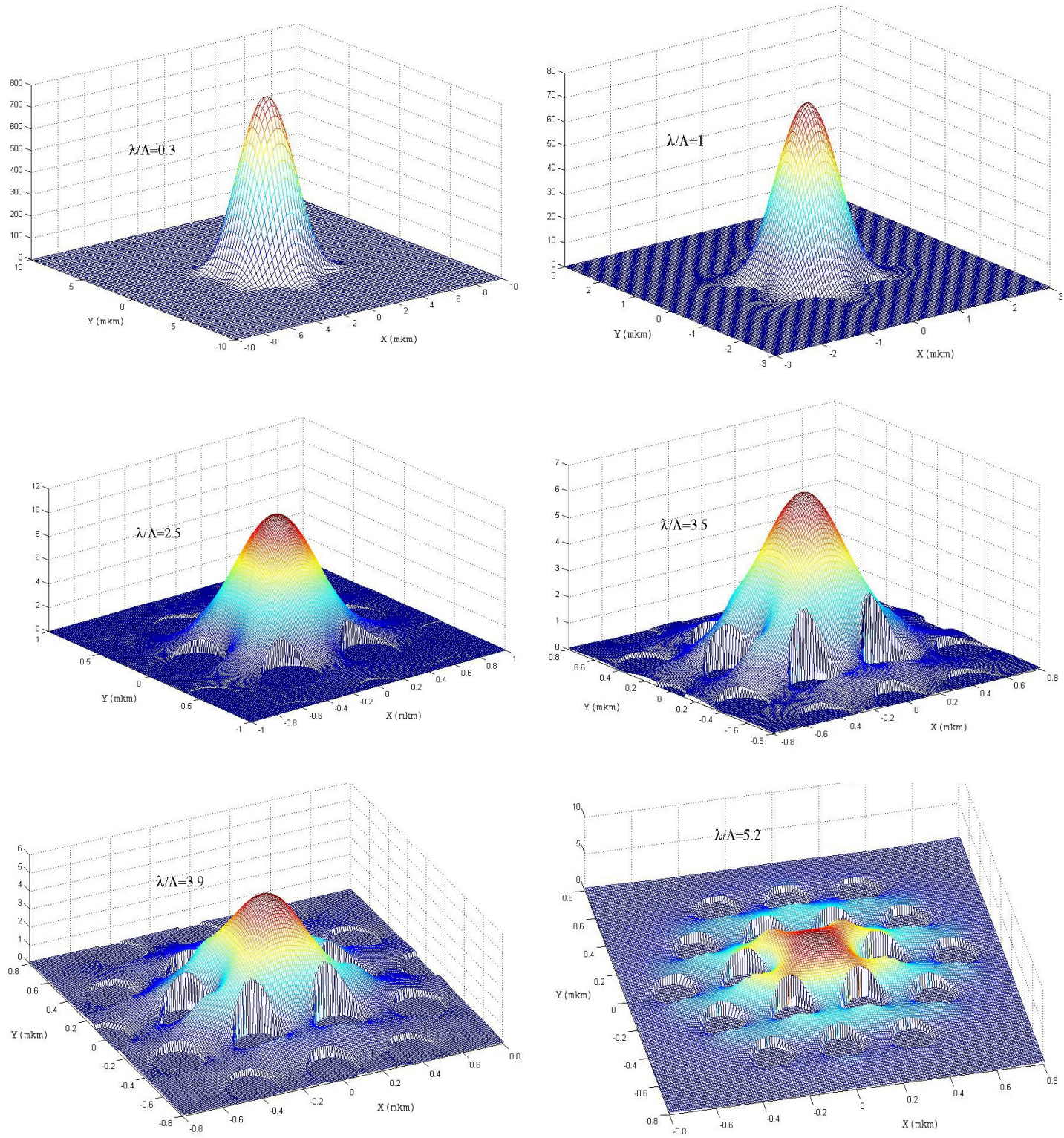

Fig. 15: *Dependence of the fundamental mode intensity in a tellurite HF with two rows of holes on the ratio* λ / Λ *for* $d / \Lambda = 0.6$ *and* $\lambda = 1.55$ *μm.*

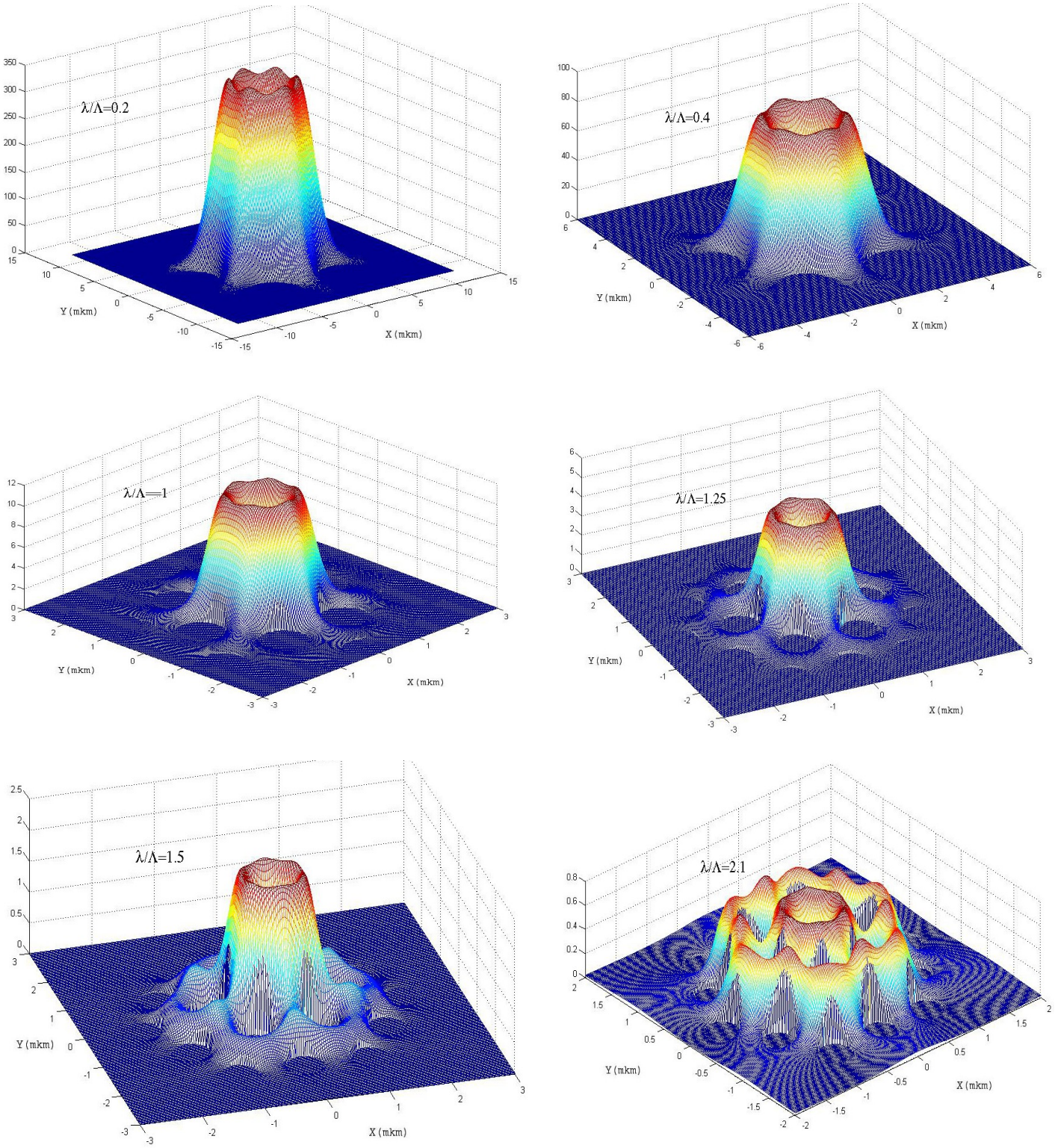

Fig. 16: *Same as in Fig. 15, but for the next (after the fundamental) mode.*

Figure 16 shows a similar behavior for the first of the higher modes of the fiber. By comparing Figs 15 and 16, we see that the higher modes are delocalized noticeably faster than the fundamental mode (the range of variation in the parameter Λ required for delocalization is noticeably narrower). The effective refractive index n_{eff} for higher modes decreases faster with increasing λ than that for the fundamental mode, these modes are no longer guided in the fiber and the fiber becomes single-mode. On a Figure 17 results of parameters searching for investigated tellurite holey fiber that allowing the possibility of its working in singlemode and multimode regimes are presented. One cans see that the singlemode region is quite wide as in holey fibers made of silica glass.

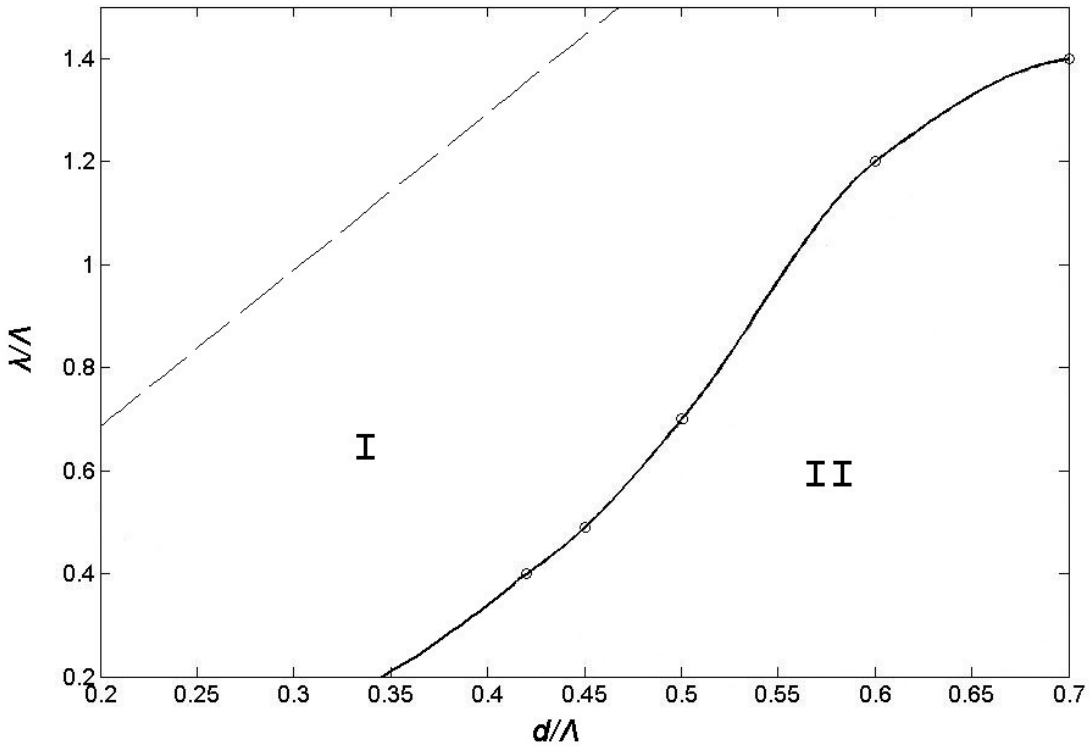

Fig. 17: *Regions of the single-mode (I) and multimode (II) regimes of radiation propagation in a tellurite holey fiber with two rows of holes. The dashed straight line is the upper boundary of the single-mode regime region (delocalization of the fundamental mode).*

III.4 Conclusions

In this Chapter optical properties of fibers with the solid core and with 2-D photonic crystal cladding were investigated by means of the multipole method.

For waveguides made of tellurite glass the influence of geometric parameters on optical properties of such structures was examined. The following results were obtained:

- a possibility of zero-dispersion point shifting both to the short-wavelength and to the long-wavelength spectral range compared with standard fibers.

-a behavior of dependence of waveguide losses on pitch, on air filling ratio and on number of considered cladding layers were obtained

-geometric parameters ranges were found where singlemode regime can be realized in wide spectral diapason

Main advantages of the multipole method in the analysis of MOF were demonstrated based on this work:

-high accuracy of a calculated propagation constant and fields distributions with not great system resources requirements if the waveguide has appropriate cladding layers (i.e. when material losses becomes predominating over waveguide losses)

-symmetry of the structure taking into account while method realization therefore there are not questions about polarization degeneracy of the modes.

Chapter IV. High power Yb-doped fiber laser based on all-solid LMA BF

This chapter is devoted to creation of the fiber laser based on the active BF doped by Yb^{3+} ions and with pumping into the cladding. Investigations results of modal composition of the active BF and of an influence of the inaccuracy of the cross-section form on output intensity field pattern were presented. The mechanism that provides a singlemode lasing was described. Influence of the waveguide macro bending on form and quality of the mode shape of the output irradiance was investigating.

Main results of this chapter were published in following works: [8-10; 138].

IV.1 BF as LMA waveguides

Creation of pulsed or continuous wave fiber lasers of high output power is related with a problem of initiation of undesirable nonlinear effects (mainly it's Stimulated Raman Scattering - SRS). Increase in SRS threshold necessitate the mode field diameter increasing [139] while simultaneous preserving a singlemodeness of the output irradiation.

There are a variety of LMA waveguides constructions existing at present and used as active mediums in creation of fiber lasers. High-order modes filtration there is reached by different methods. In [140], for example, a multimode waveguide is coiled with the definite bent radius due to a fact that a critical bent radius is smaller for the fundamental mode than for all high-order modes when a leakage into the cladding occurs. In [141] the helical core introduced additional losses for high-order modes was used [142]. In [143] a chirally-coupled core (i.e. straight core twisted by an additional core's spiral) was used to filter high-order modes by means of an avoided interaction between high-order modes of main and additional cores. Using of active waveguides with negative contrast of refractive index in the core was shown in [144]. Singlemodeness in such fibers is achieved by a fact that the compensation of

the losses by the amplification occurs earlier for the fundamental "leaky" mode than for the high-order modes.

Holey fibers are used as LMA waveguides also. Here, increasing of the core diameter, while keeping the singlemodeness of an output irradiation, demands decreasing of the refractive index contrast on core/cladding interface as in case of using of standard step-index fibers. Hence, it appears that all these holey structures are too bent sensitive. Consequently all being created fiber lasers based on these holey waveguides become quasi-solid state.

However, recently a possibility of reducing the bend sensitivity while preserving the mode field diameter with help of using of another type of MOF – a solid core BF was demonstrated in works [35; 145]. This led to formulation of task of realization of the active BF with subsequent creation of the fiber laser based on the similar structure.

IV.2 Geometry choosing for active LMA BF

Geometry for the active BF is chosen quite similar to that used in work [35]. For the sake of simplicity, index of the core is chosen to be equal to that of the pure silica low-index layers. The high-index layers are GeO_2-doped. Such preform can be made by the MCVD process. As the proposed fiber is a leaky waveguide, a trade-off regarding the modes' attenuation coefficients must be found: the first Gaussian mode must exhibit low (<1 dB/m) loss while the HOMs must exhibit high (>100 dB/m) loss at a specified wavelength. This requirement can be fulfilled by engineering the index profile. Degrees of freedom are core diameter D, lattice constant Λ, thickness d and index contrast Δn of high-index layers and number N of bilayers. To optimize an index profile we need to choose core diameter as well as index in each section of the profile. For the high-power fiber laser application, $D > 20$ μm is chosen. Indices are chosen considering the MCVD process requirements ($\Delta n < 0.05$). At a specified wavelength λ, the radiation must resonate in the core. This leads to a certain value of the mode effective index ($neff_{01}$) together with the transverse wavenumbers in the *i-th*

cladding layer $\beta_i = k_0\sqrt{n_i^2 - neff_{01}^2}$. Under the quarter-wave stack condition, it is then straightforward to determine Λ and d. Then, the design space reduces to {*D, Δn, N*}. For such a triplet, attenuation coefficients of LP_{01} and LP_{11} modes are computed using the transfer matrix method. An example of results is shown in Fig. 18b for *D = 20 μm*. Obviously, the attenuation coefficients of both modes decrease with *N* and Δn. A strong discrimination against HOMs will necessitate α_{11} > 100 dB/m while a quasi-lossless propagation of LP_{01} is preferred. Graphically, we can determine that for *D = 20 μm, Δn = 0.015 and N = 3* are well suited. The bend influence was also computed using a full-vector finite element algorithm. A conformal transformation was applied to simulate the propagation in the bent fiber. A perfectly-matched layer was added to evaluate the radiation loss due to bend. The critical bend radius defined as the radius leading to a 3-dB/m loss for the fundamental mode was computed to 8 cm for the design proposed. This bend radius does not affect the effective mode area (~170 μm²). A preform was then manufactured and drawn down to the double-clad fiber.

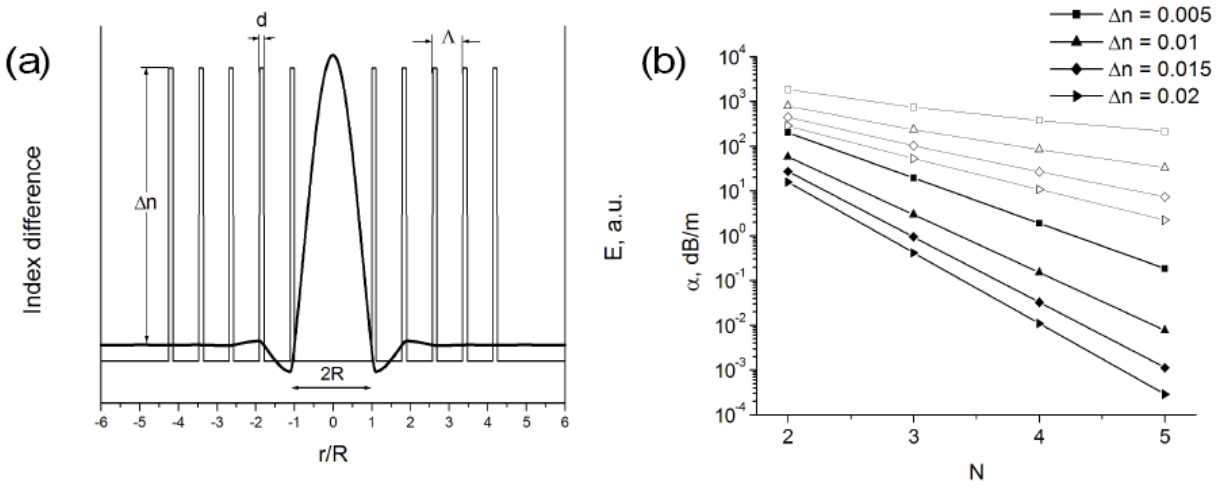

Fig.18: *(a) Theoretical refractive index profile of solid-core BF. The design space includes the core diameter D, the cladding index contrast Δn, the number N of bilayers. Also reported is an example of electric field distribution (b) Attenuation coefficients computed when D = 20 μm for various Δn in the range (0.005, 0.01, 0.015, 0.02) as functions of N. Hollow symbols: LP_{11}, filled symbols: LP_{01}*

IV.3 Investigation of the active LMA BF

Preforms of the active BF were created in Institute of Chemistry of High Purity Substances (ICHPS), Nizhny Novgorod. There were few collapsing regimes during preforms fabrication due to complexity of the active structure realization. Further, after drawing, samples were investigated and it was found that in some samples an axially symmetric geometry is broken:

1. The first layer of the structure is deformed due to attempt to lower the preform's collapsing temperature (see Fig. 19).

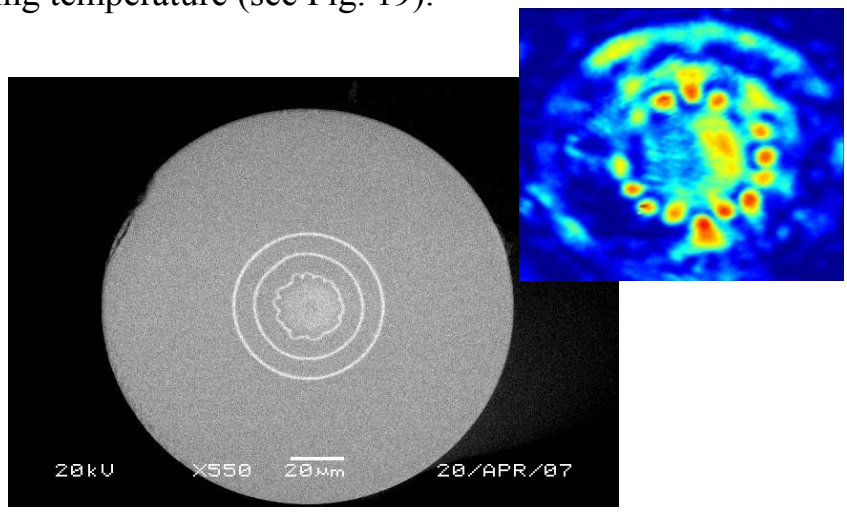

Fig. 19: *SEM image of a fiber end-face with distorted first layer. In-set: A typical distribution of mode field intensity in this fiber (λ=1.06 µm)*

2. The dip in the core center arisen while the process of preform collapsing (see Fig.20).

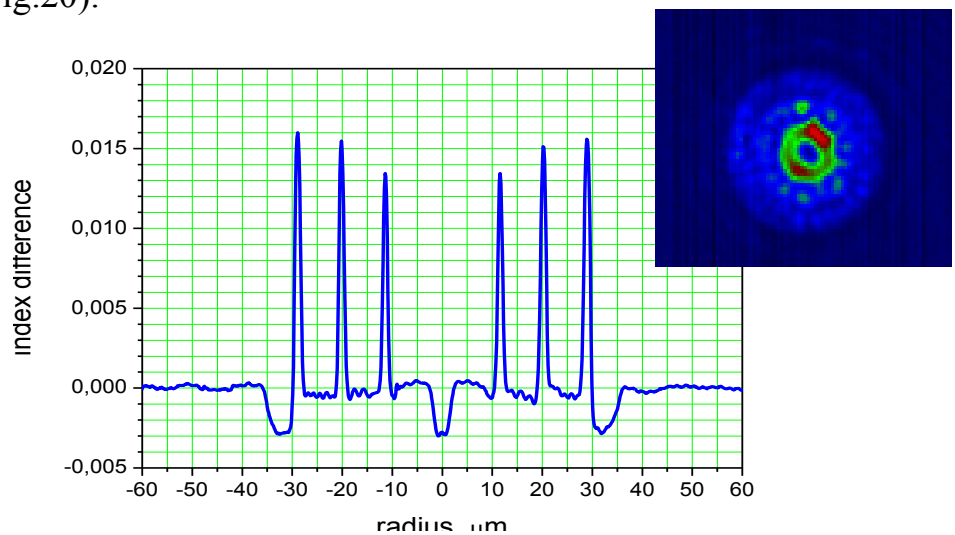

Fig. 20: *RIP in a sample with a dip in the core's centre. In-set: A typical distribution of mode field intensity in this fiber (λ=1.06 µm)*

3. In the attempt of making the outer cladding in a shape of square (to break axial symmetry with the aim to increase pump mixing and hence pump absorption) the shape of cladding layers reproduced the outer cladding shape. (Fig. 21)

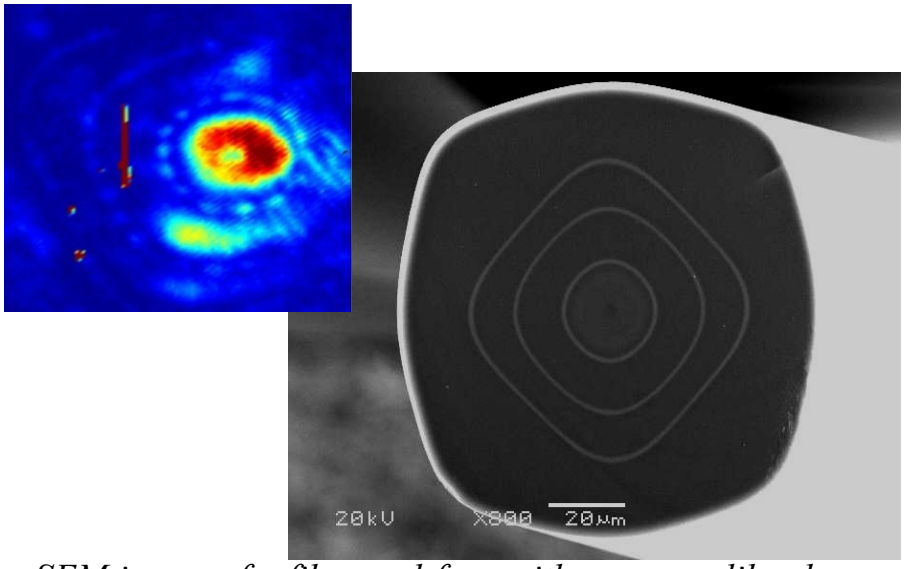

Fig. 21: *SEM image of a fiber end-face with a square-like shape of the outer cladding. In-set: A typical distribution of mode field intensity in this fiber (λ=1.06 µm)*

In all three cases the fundamental Bragg mode is being broken and makes impossible obtaining of the singlemode lasing.

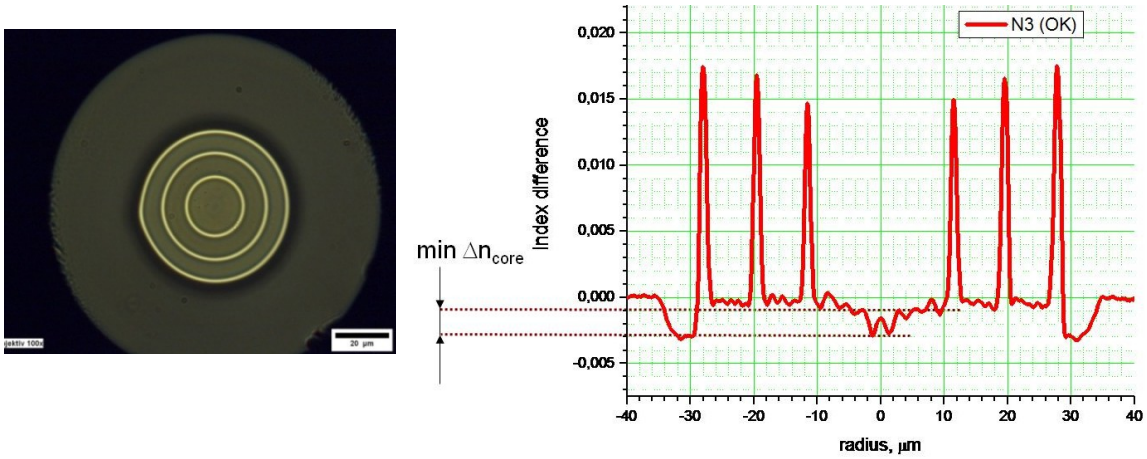

Fig. 22: *RIP in the sample with the minimal dip in the core's centre (on the right). SEM image of this sample (on the left).*

However, for one more sample it was succeeded to maximally suppress the dip in the core without breaking of axial symmetry at the same time (see Fig. 22).

Characteristics of the chosen sample are following (Fig. 23):

- Preform was made by MCVD method
- $\Delta n_{BF} \sim 15.10^{-3}$ (GeO_2);
- $[Yb^{3+}] \sim 1$ % by weight;
- whole doped core;

For implementation of the cladding pumping the Bragg structure was placed into the outer cladding made of a reflecting polymer (NA=0.48).

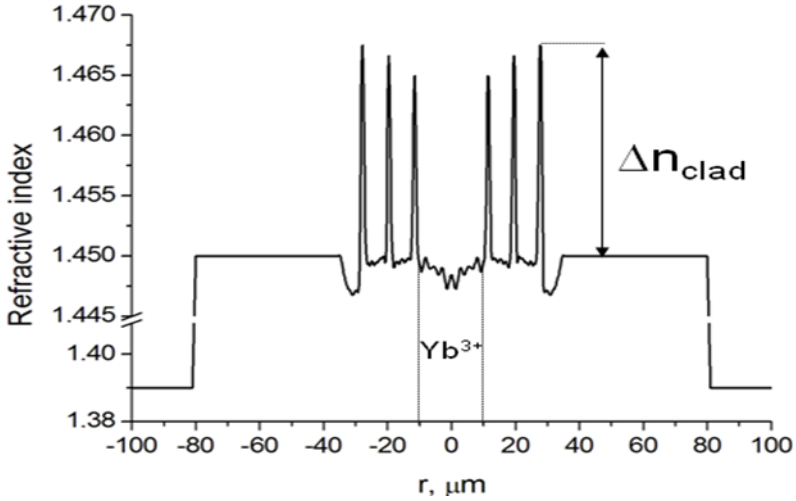

Fig. 23: *RIP of the BF from Fig. 22 which is placed into an outer cladding made of reflecting polymer*

Appearance of the reflecting polymer leads to the double-clad structure - an ordinary multimode waveguide in general case. Hence we can't talk about waveguide losses of the whole structure because now all modes become "guided". Here waveguide losses of BF structure define the part of power in the core for the correspondent mode in the double-clad structure. Therefore it's possible to associate for a concrete mode its part of power in the core with waveguide losses of the corresponded Bragg structure.

Experimental and theoretical RIP's that were used in the estimation of waveguide losses of BF without reflecting polymer are shown on Fig. 24.

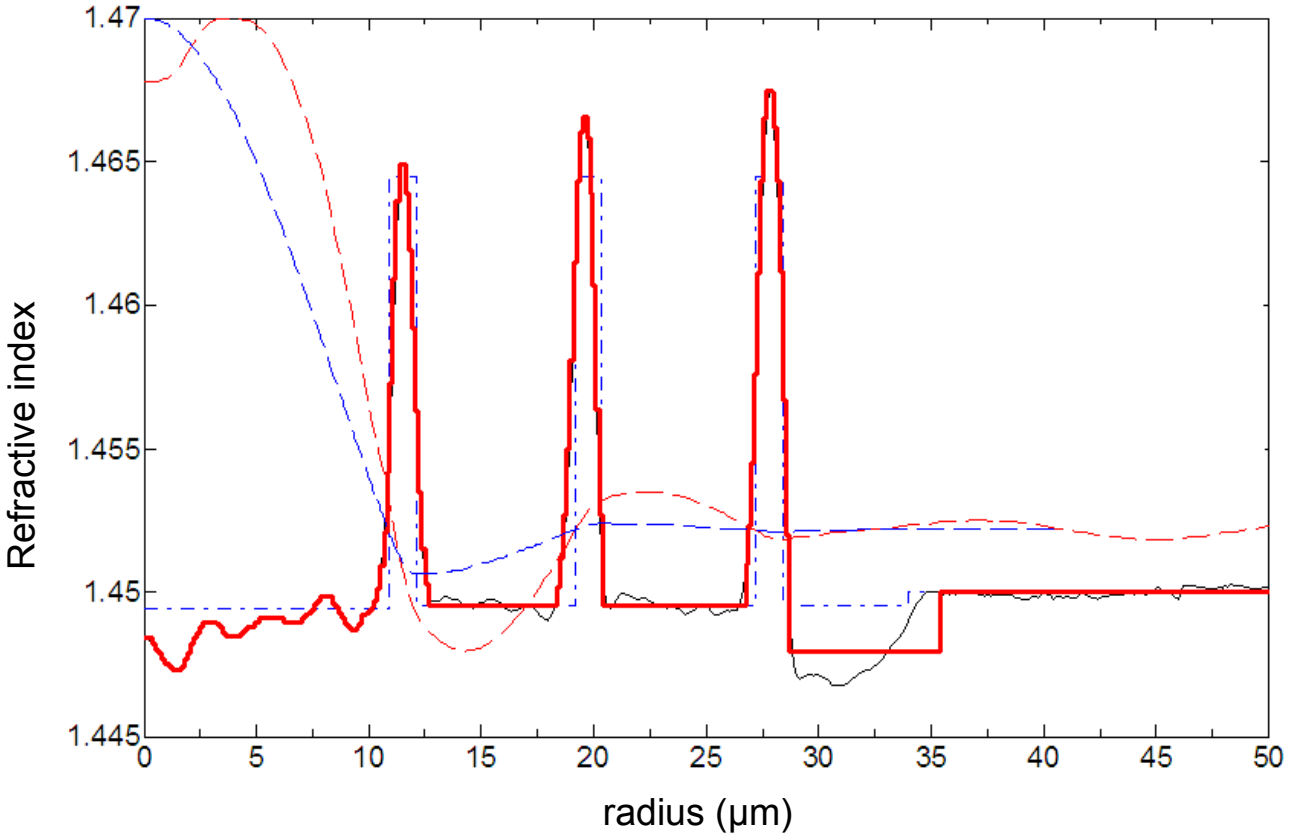

Fig. 24:

Solid thin curve – experimental RIP

Dashed-dot curve – ideal theoretic RIP

Solid thick curve – theoretical RIP maximally approximated to the experimental one which was used in estimation of waveguide losses of BF from Fig. 22

Dashed line was used for representing an axial component E_φ of an electric field. (a) – corresponds to the ideal RIP, (b) – corresponds to the RIP maximally approximated to the experimental one)

Calculated spectrums of waveguide losses of the fundamental mode HE_{11} and of the first high-order mode TE_{01} for the ideal RIP and for the RIP closest to the experimental one are shown on Fig.25. One can see from this figure that with taking into account the experimental RIP the loss ratio of the fundamental mode and of the first high-order mode increasing approximately in order and provided to be equal:

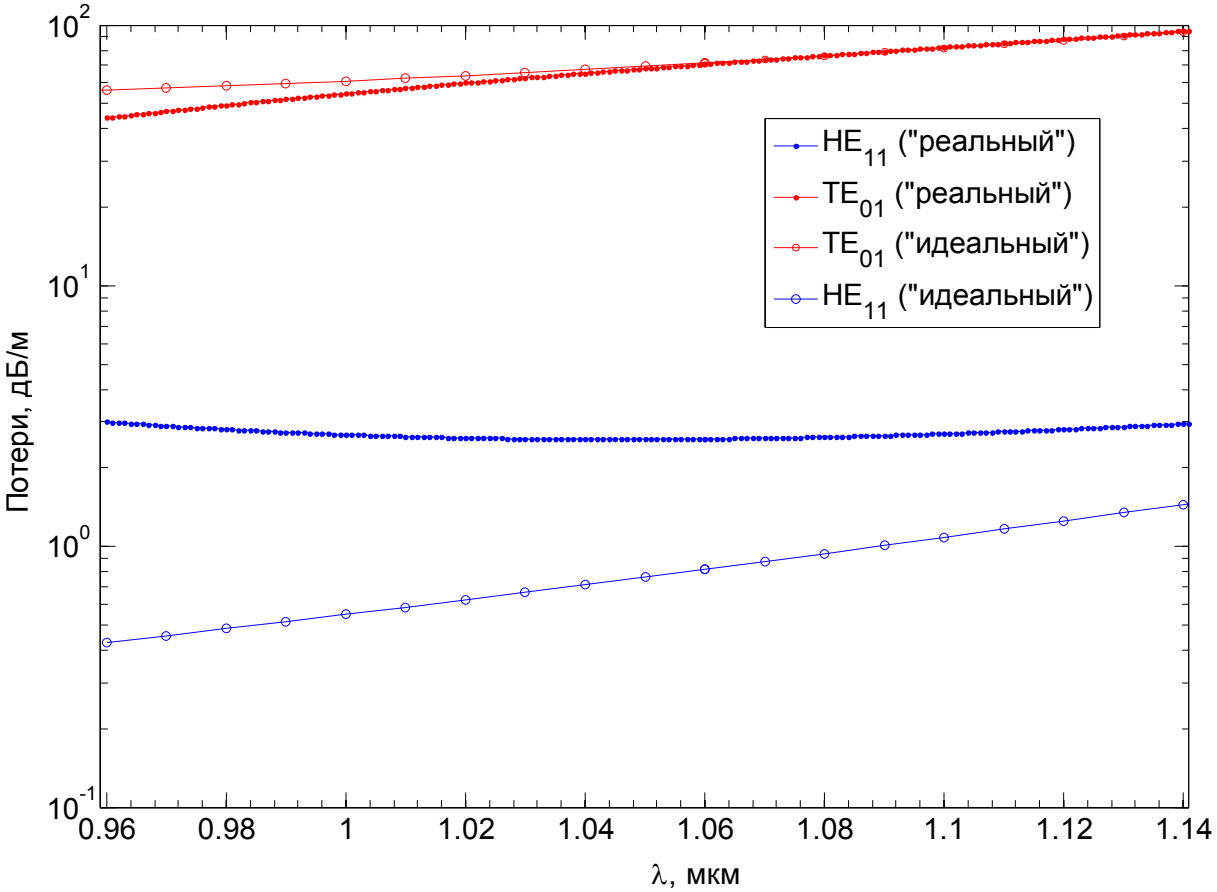

$$\frac{\alpha_{LP01}}{\alpha_{LP11}} \sim \frac{1}{10}$$

("real")
("real")
("ideal")
("ideal")

Results of calculations of overlap integrals of the and second le with the doping region [146] are shown on Fig. 26. By comparing obtained re- s it's possible to make a conclusion that the loss ratio of the fundamental and ond mode equaled to 1/10 is related to 50% of power in the core for second mode 87 % for the fundamental:

$$\frac{\alpha_{LP01}}{\alpha_{LP11}} \sim \frac{1}{10} \Leftrightarrow \begin{matrix} \Gamma_{LP01} = 87\% \\ \Gamma_{LP11} = 50\% \end{matrix}$$

Losses, dB/m

λ (μm)

Therefore even though the signal propagation out from the absorption band of Yb^{3+} will be in slightly multimode regime the assumption was made that in this case it's possible to achieve singlemode lasing due to the selective amplification of the fundamental mode.

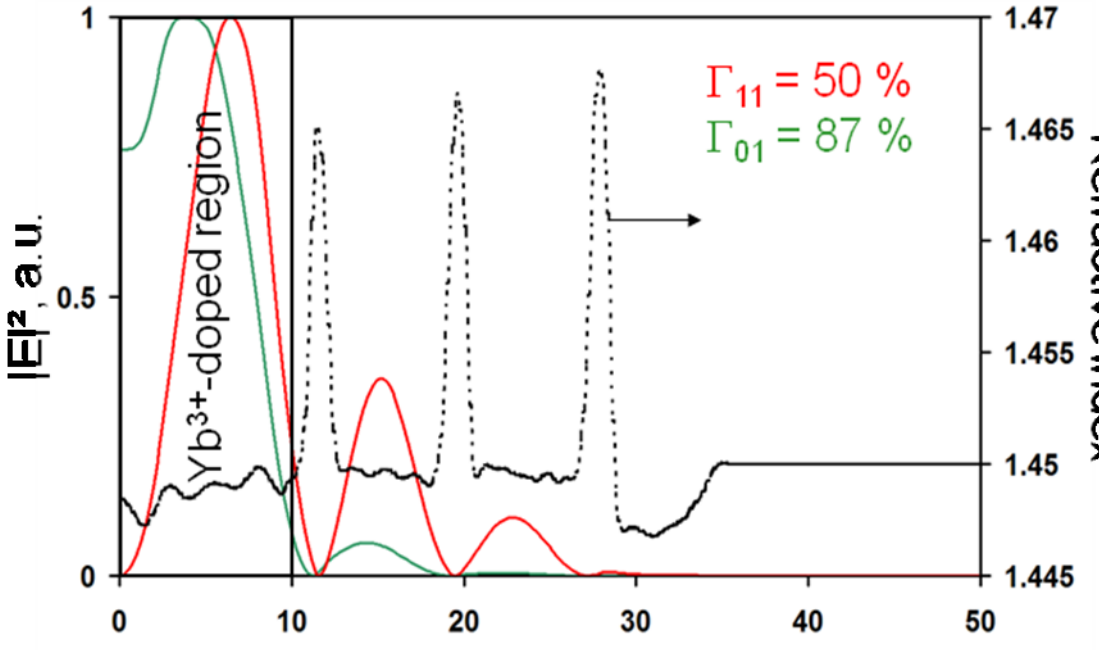

Fig. 26: *To the calculation of overlap integrals of mode's (LP_{01} and LP_{11}) fields intensities distributions with the doping region in BF from Fig.22*

As example, in the work related with realization of the triple-clad LMA waveguide [146] the parts of power in the core 80 % for the fundamental mode and 60 % for second mode were provided the singlemode lasing.

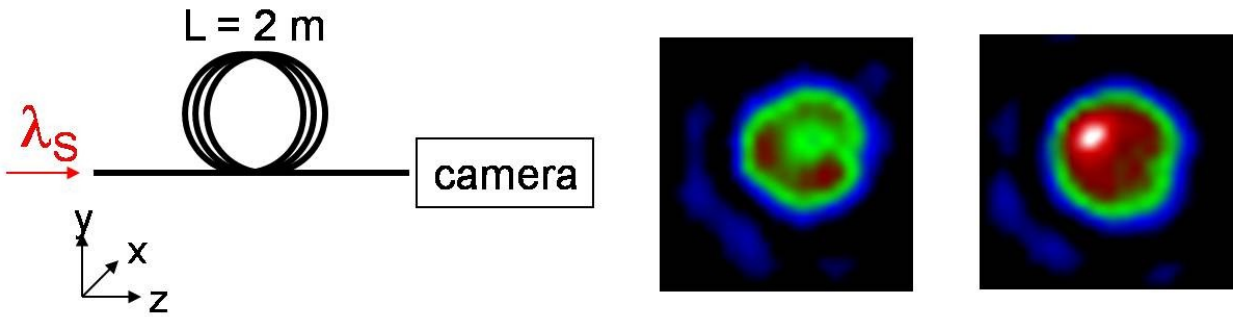

Fig. 27: *Set-up scheme for observation of a mode composition in BF's used in experiment*

Actually, we observed the transverse field intensity distribution at the output of a short (2 m) piece of active BF in absence of pumping. The wavelength of the launched radiation was 1.064 μm. Results are shown in Fig. 27. It is obvious that the unpumped fibre is slightly multimode.

IV.4 Experimental set-up

Scheme of the experimental set-up is shown on Fig. 28. The pump light was delivered by the multimode diode laser emitting at 975 nm with pigtail diameter of 100 μm and NA of 0.22. Launching of pump power was carried out with a couple of 8mm focal-length collimating lenses F1 and F2. Thanks to the high Yb^{3+} ($[Yb^{3+}]$ ~1 % by weight) concentration, the short 2 m-long piece of fiber was used. The cavity mirrors were the dichroic mirror M1 with maximum reflectivity at signal wavelength (R_{max} at λ=1060 nm, T_{max} at λ=975 nm) and the cleaved output end of the fiber with reflectivity ~ 4 %. Laser and remaining pump beams were split at the output by using another dichroic mirror M3 (R_{max} at λ=1060 nm, T_{max} at λ=975 nm).

It should be mentioned that any mechanical stresses on the fiber must be avoided when maintaining it on support plates. Otherwise such stresses disturbs the RIP and can lead to unwanted coupling between core mode and modes of cladding layers distorting the field intensity distribution of the output irradiance.

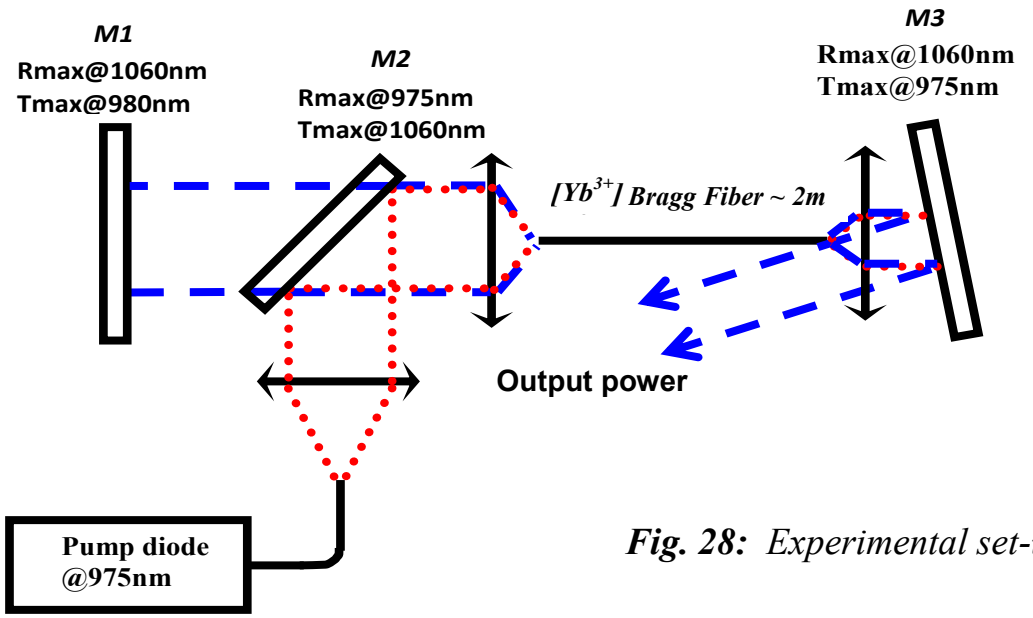

Fig. 28: *Experimental set-up*

IV.5 Experimental results

In the realized scheme the laser generation in active cladding pumped BF was obtained for the first time. A view of working laser is shown on Fig. 29.

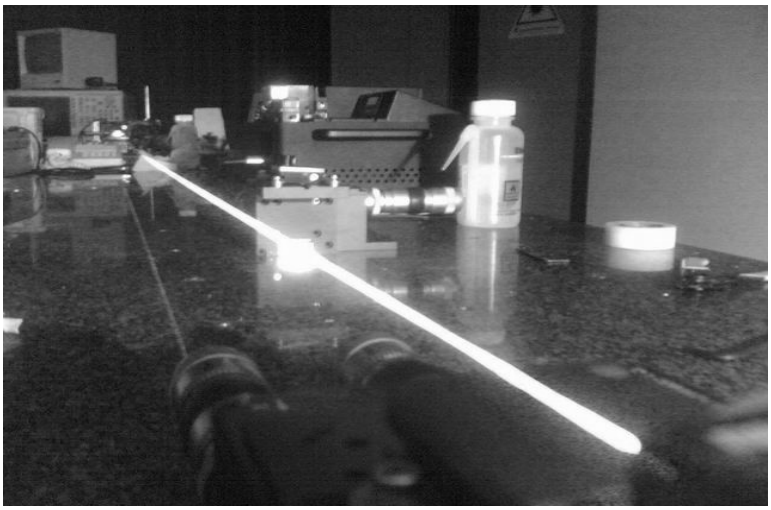

Fig. 29: *Working fiber laser based on 2 m length BF in experimental scheme shown on Fig. 28.*

The transverse distribution of the mode field intensity was observed on CCD-camera. Typical intensity distribution in the lasing regime is shown on in-set to Fig. 30.

Thanks to the three-axis translation stage, the input mirror could be tilted. But mode field intensity pattern was never disturbed (compare for example with Fig. 27) and only decreasing in intensity was observed evidencing that high-order modes were not excited. Hence this was proving the singlemode behavior of the fabricated fiber in the lasing regime. Therefore the assumption about the selective amplification of the fundamental mode was proved experimentally. Launching efficiency reached 67% with respect to the launched power (Fig. 30). A generation spectrum at the output power of 3.3 W is shown on Fig.31.

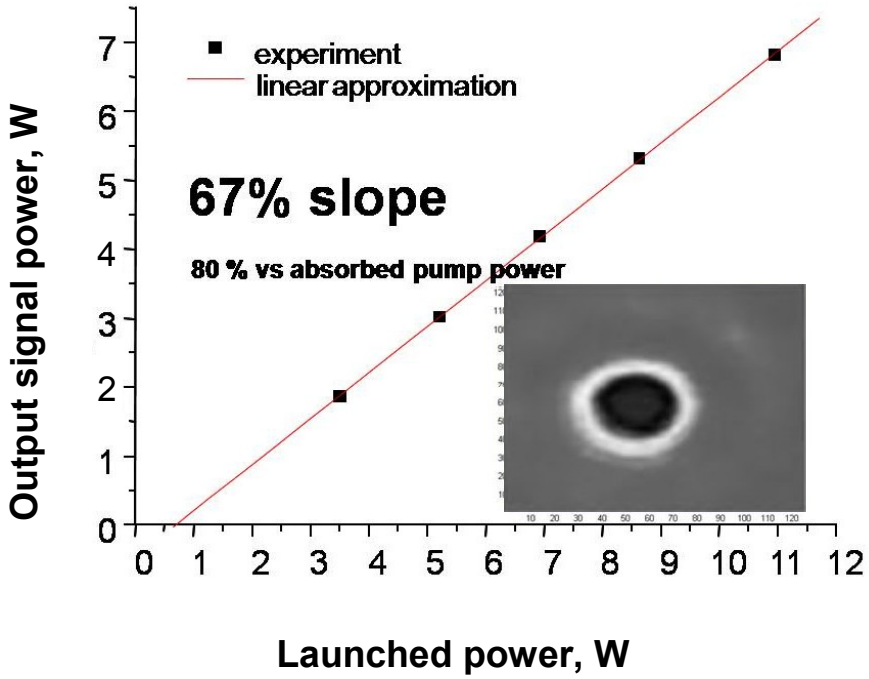

Fig. 30: *Slope efficiency measured with respect to the launched pump power. In-set: observed transverse distribution of the mode field intensity at the output of the 2 m-long straight fiber*

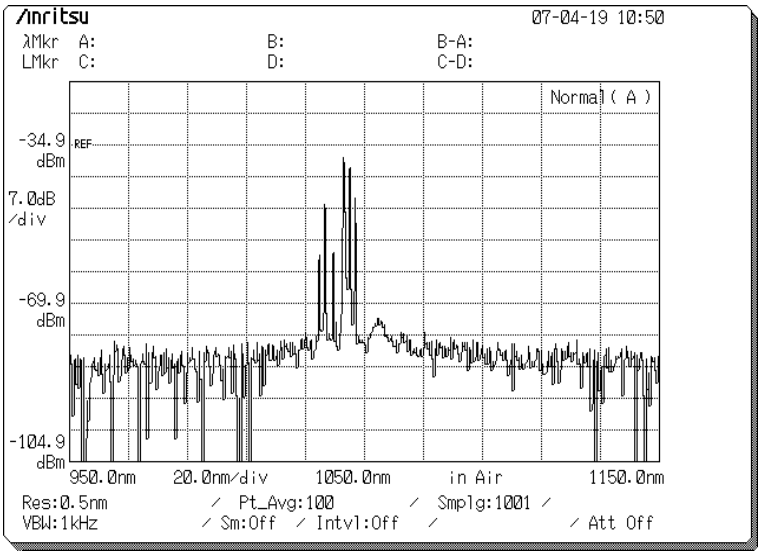

Fig. 31: *The generation spectrum on the output power of 3.3 W*

At least, bend influence on mode shape and lasing efficiency was characterized. It was proved that the lasing efficiency was decreasing no more than 10% down to the bent radius of 7.5 cm. There wasn't observed any distortion of the transverse distribution of the field intensity of output irradiation at the same time (Fig. 32).

For a very tight bend, we do observe the localization of energy towards outer of the bend.

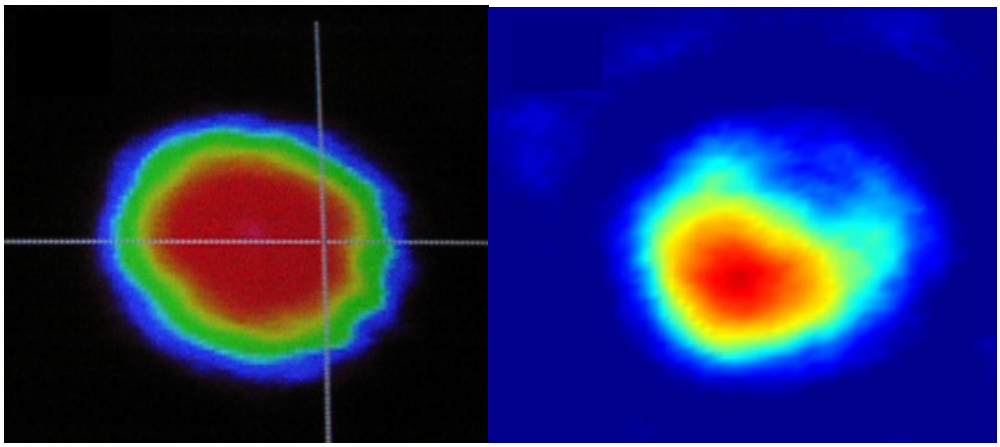

Fig. 32: *The transverse distribution of the mode field intensity*

a) The fundamental mode "unperturbed" by the bend with radius 7.5 cm;

b) The fundamental mode perturbation induced by the bend with small radius 2.5 cm

IV.6 Conclusions

In this chapter the laser generation in the fiber laser based on cladding pumped LMA (200 μm^2 at 1.064 μm) BF was demonstrated for the first time according to our data. It was shown that despite the investigated fiber is working in slightly multimode regime (calculated loss ratio between the second and fundamental modes are ~ 10; second mode was observed experimentally) the singlemode lasing regime is possible due to selective amplification of the fundamental mode. The lasing efficiency of 67% with respect to the launched power was demonstrated. An influence of the fiber bent on lasing efficiency and on shape of transverse distribution of the mode field intensity was investigated. It was shown that the lasing efficiency was decreased no more than 10% down to the bent radius of 7.5 cm. Any distortion of the transverse distribution of the mode field intensity wasn't observed at the same time.

The obtained results allow to consider the using of BF as LMA waveguides very perspective in creation of high power fiber lasers .

Conclusion

In the theoretical part of this dissertation work the optical properties of Bragg and Holey Fibers were analyzed. The most effective calculation methods are in detail presented and realized, which make possible to find the modal composition, optical losses and dispersion in such waveguide structures with the given cladding geometry.

For the Bragg Fibers the method of optimization, which gives the possibility to find the optimum structure of cladding ensuring minimum optical losses at the given wavelength was proposed and realized on the basis of the genetic algorithm. So from the simple considerations the basic criteria are established what mode must be basic in BS with the large and small contrast of the refractive indices of core and shell. Basic properties of ARROW BF are described and it is shown that only by parameters of the nearest to the core, high-index layer all these properties are not determined, but the role of resonances of the cladding as a whole and of its compound resonators proves to be essential.

In case of Holey Fibers the properties of waveguide structures based on tellurite glass were investigated. The influence of geometric parameters on the optical properties of waveguide was calculated, the possibility of zero-dispersion point shift to the required spectral range was shown. The behavior of waveguide losses with a change in the geometry was analyzed. And, finally, the region of geometric parameters, where the realization of single-mode regime is possible, was defined.

In the experimental part of the thesis the active (doped by Yb^{3+} ions with $[Yb^{3+}] \sim 1$ % by weight) LMA (200 μm^2 to 1.064 μm) BF was investigated. The fiber laser based on this BF with pumping into the cladding was realized and the laser generation was obtained for the first time to our knowledge in such type of fibers. It was shown that despite the fact that the investigated in passive regime waveguide works as slightly “multimode” (calculated relation of the losses of the second and fundamental mode is 10; the second mode was observed experimentally) the single-mode

lasing is possible due to the selective amplification of the fundamental mode. The generation efficiency of 67% with respect to the launched power was demonstrated. The influence of bend on shape of the output mode field intensity and effectiveness of lasing was investigated, and it is shown that up to the bending radii 7.5 cm the generation efficiency decreases not more than by 10% and it was not observed distortion in the form of the output mode field intensity.

Refrences

[1] A.S. Biriukov, D.V. Bogdanovich, D.A. Gaponov, A.D. Pryamikov, "*Optical properties of Bragg Fibers*", **38**, N8, pp.620-633, Quant.Electron., (2008).

[2] D. A. Gaponov, A. S. Biryukov, "*Optical properties of microstructure tellurite glass fibres*", Quant. Electron., **36**, N4, pp. 343-348, (2006).

[3] D.A. Gaponov, A.S. Biriukov, "*Effective method of analisys of optical properties of microstructured fibers*", Foton-Express, **6**, pp. 77-104, (2005).

[4] Sebastien Fevrier, Dmitry A. Gaponov, Philippe Roy, Mikhail E. Likhachev, Sergei L. Semjonov, Mikhail M. Bubnov, Evgeny M. Dianov, Mikhail Yu. Yashkov, Vladimir F. Khopin, Mikhail Yu. Salganskii, and Aleksei N. Guryanov, *"High-power photonic bandgap fiber laser",* Opt. Lett., **33**, 7 (2008).

[5] D.A. Gaponov, A.S. Biriukov, *"Numerical modeling of process of light propagation in photonic crystal waveguides by means of cylindrical functions expansion method", scientific* session MEPhI-2005, Section L-1 (2005).

[6] A.S. Biriukov, D.V. Bogdanovich, D.A. Gaponov, A.D. Pryamikov, "*Optical fiber with multilayered dielectrical cladding",* Moscow: Preprint FORC RAS, 2008, 14 (38 p.).

[7] D. Gaponov, P. Roy, S. Février, M. E. Likhachev, S.L. Semjonov, M.M. Bubnov, E. M. Dianov, M.Yu.Yashkov, V. F. Khopin, M. Yu. Salganskii, A. N. Guryanov, *"High-Power Photonic Bandgap Fibre Laser",* Berlin, Germany, ECOC'2007, PD session 3.9 (2007).

[8] Philippe Roy, Laure Lavoute, Sébastien Février, Jean-Louis Auguste, Jean-Marc Blondy, Dmitry Gaponov, Mathieu Devautour, Aude Roy, Philippe Le-proux, Laurent Bigot, Géraud Bouwmans, Vincent Pureur, "Microstructured fibres and applications, *"Microstructured fibres and applications",* CLEO /Europe-IQEC 2007, Topic Area CJ (2007).

[9] Février Sébastien, Gaponov Dmitry, Lecaplain C., Martel G., Roy Philippe, Hideur A, Likhachev Mikhail, Yashkov M.Y., Salganskii M.Y, *"Photonic Bandgap Fibers for High-Power CW and Pulsed Applications",* IEEE/LEOS Winter Topical Meetings, TuD3.1 (2008).

[10] Février Sébastien, Gaponov Dmitry, Roy Philippe, Lecaplain C., Martel G. , Roy Philippe , Hideur A, Likhachev Mikhail , Yashkov M.Y. , Salganskii M.Y, *"Cladding-pumped ytterbium-doped photonic bandgap fibre laser",* Photonics Europe 2008, Paper 6990-21 (2008).

[11] Kapron, F. P., D. B. Keck, R. D. Maurer, *"Radiation losses in glass optical waveguides",* Appl. Phys. Lett., **17**, pp. 423-425 (1970).

[12] P. Yeh, A. Yariv, *"Bragg Reflection Waveguides",* Optics Communications, **19**, 3, pp. 427- 430 (1976).

[13] Yeh P., Yariv A., Marom E, *"Theory of Bragg fiber",* J. Opt. Soc. Am., **68**, pp. 1196-1201 (1978).

[14] E.Yablonovitch, *"Inhibited Spontaneous Emission in Solid State Physics and Electronics",* Phys. Rev. Lett., **58**, pp. 2059 (1987).

[15] John., S, *"Strong Localization of Photons in Certain Disordered Dielectric Superlatticest",* Phys. Rev. Lett., **58**, pp. 2486 (1987).

[16] E.Yablonovitch, T.J.Gmitter, K.M.Leung, *"Photonic Band Structure: The Face Centered Cubic Case Imploying Nonspherical Atoms",* Phys. Rev. Lett., **67**, pp. 2295 (1991).

[17] E.Yablonovitch, *"Photonic band gap structures",* JOSA B, **10**, 2, pp. 283-295 (1993).

[18] K. Ho, C. Chan, C. Soukoulis, R. Biswas, M. Sigalas, *"Photonic band gaps in three dimensions: new layer-by-layer periodic structures",* Solid State Commnun., 89, pp. 413−416 (1994).

[19] V.P.Bykov, *"Spontaneous emission in a periodical medium", JETP*, **62**, 2, pp. 505–513 (1972).

[20] V. P. Bykov, "*Spontaneous emission from a medium with a band spectrum*", Soviet Journal of Quantum Electronics, **4**, 861, pp.861-871 (1975).

[21] P. St.J. Russell, *"NATO Advanced Study Institute on Confined Electrons and Holes",* Erice, Italy (1993).

[22] J. C. Knight, T. A. Birks, P. St. J. Russell, D. M. Atkin, *"All-silica single-mode optical fiber with photonic crystal cladding*", Opt. Lett., **21**, 19, (1996).

[23] T. A. Birks, J. C. Knight, and St. J. Russel, *"Endlessly single-mode photonic crystal fiber",* Optics Letters, **22**, 13, pp. 961–963 (1997).

[24] Knight, J.C.; Birks, T.A.; Cregan, R.F.; Russell, P.S.J.; de Sandro, P.D, *"Large mode area photonic crystal fibre",* Electronics Letters, **34**, 13, pp. 1347-1348 (1998).

[25] R. F. Cregan, B. J. Mangan, J. C. Knight, T. A. Birks, P. St. J. Russell, P. J. Roberts, D. C. Allan, *"Single mode photonic band gap guidance of light in air",* Science, **285**, 5433, pp. 1537−1539 (1999).

[26] Fink Y. Fink, D. J. Ripin, S. Fan, C. Chen, J. D. Joannopoulos, and E. L. Thomas, *"Guiding Optical Light in Air Using an All-Dielectric Structure",* J. Lightwave Technol., **17**, pp. 2039 (1999).

[27] Brechet F., Roy P., Marcou J., Pagnoux D, *"Single-mode propagation into depressed-core-index photonic-bandgapfibre designed for zero-dispersion propagation at short wavelengths",* Electron. Letts., **36**, pp. 514 (2000).

[28] A. Ortigosa-Blanch, J. C. Knight, W. J. Wadsworth, J. Arriaga, B. J. Mangan, T. A Birks, and P. St. J. Russell, *"Highly birefringent photonic crystal fiber",* Opt. Lett., **25**, 18, pp. 1325-1327 (2000).

[29] Jinendra K. Ranka, Robert S. Windeler, and Andrew J. Stentz, *"Visible continuum generation in air–silica microstructure optical fibers with anomalous dispersion at 800 nm",* Optics Letters, **25**, 1 (2000).

[30] W.J. Wadsworth, J.C. Knight, W.H. Reeves and P.St.J. Russell, *"Yb3+-doped photonic crystal fibre laser",* Electron. Lett., **36**, pp. 1452-1453 (2000).

[31] W. Reeves, J. Knight, P. Russell, and P. Roberts, *"Demonstration of ultra-flattened dispersion in photonic crystal fibers",* Opt. Express, **10**, pp. 609-613 (2002).

[32] J. Limpert, T. Schreiber, S. Nolte, H. Zellmer, T. Tunnermann, R. Iliew, F. Lederer, J. Broeng, G. Vienne, A. Petersson, and C. Jakobsen, *"High-power air-clad large-mode-area photonic crystal fiber laser",* Opt. Express, **11**, pp. 818-823 (2003).

[33] F. Luan, A. K. George, T. D. Hedley, G. J. Pearce, D. M. Bird, J. C. Knight, and P. S. J. Russell, *"All-solid photonic bandgap fiber",* Opt. Lett., **29**, pp. 2369-2371 (2004).

[34] P. J. Roberts, F. Couny, H. Sabert, B. J. Mangan, D. P. Willliams, L. Farr, M. W. Mason A. Tomlinson, T. A. Birks, J. C. Knight, and P. St.J. Russell, *"Ultimate low loss of hollow-core photonic crystal fibres",* Optics Express, **13**, 1, pp. 236–244 (2005).

[35] S. Février, R. Jamier and J.-M. Blondy, S. L. Semjonov, M. E. Likhachev, M. M. Bubnov and E. M. Dianov V. F. Khopin, M. Y. Salganskii and A. N. Guryanov, *"Low-loss singlemode large mode area all-silica photonic bandgap fiber",* Optics Express, **14**, 2, pp. 562-569 (2006).

[36] F. Couny, F. Benabid and P. S. Light, *"Large-pitch kagome-structured hollow-core photonic crystal fiber",* Optics Letters, **31**, pp. 3574-3576 (2006).

[37] A. Isomäki and O. G. Okhotnikov, *"Femtosecond soliton mode-locked laser based on ytterbium-doped photonic bandgap fiber",* Opt. Express, **14**, pp. 9238-9243 (2006).

[38] Tanya M. Monro, P. J. Bennett, N. G. R. Broderick, and D. J. Richardson, *"Holey fibers with random cladding distributions",* Optics Letters, **25**, 4 (2000).

[39] Knight, J.C.; Arriaga, J.; Birks, T.A.; Ortigosa-Blanch, A.; Wadsworth, W.J.; Russell, P.St.J, *"Anomalous dispersion in photonic crystal fiber",* Photonics Technology Letters, IEEE, **12**, 7, pp. 807 – 809 (2000).

[40] K. Saitoh, M. Koshiba, N. A. Mortensen, *"Nonlinear photonic crystal fibres: pushing the zero-dispersion towards the visible",* New Journal of Physics, **8**, pp. 207 (2007).

[41] T. Hasegawa, E. Sasaoka, M. Onishi, M. Nishimura, Y. Tsuji, M. Koshiba, *"Hole-assisted lightguide fiber for large anomalous dispersion and low optical loss",* Optics Express, **9**, 13, pp. 681-686 (2001).

[42] K. Saitoh, S. K. Varshney, M. Koshiba, *"Dispersion, birefringence, and amplification characteristics of newly designed dispersion compensating hole-assisted fibers",* Optics Express, **15**, 26, pp. 17724-17735 (2007).

[43] K. Saitoh, M. Koshiba, T. Hasegawa, *"Chromatic dispersion control in photonic crystal fibers: application to ultra-flattened dispersion",* Optics Express, **11**, 8, pp. 843 (2003).

[44] S. M. Abdur Razzak, Y. Namihira, K. Miyagi, F. Begum, S. Kaijage, N. H. Hai, T. Kinjo, N. Zou, *"Dispersion and Confinement Loss Control in Modified Hexagonal Photonic Crystal Fibers",* Optical Review, **14**, 1, pp. 14–16 (2007).

[45] Kim P. Hansen, Jakob Juul Larsen, Jacob Riis Jensen, Søren Keiding, Jes Broeng,Harald R. Simonsen, Anders Bjarklev, *"Super Continuum Generation at 800 nm in Highly Nonlinear Photonic Crystal Fibers with Normal Dispersion",* Lasers and Electro-Optics Society, The 14th Annual Meeting of the IEEE, 2, pp. 703-704 (2001).

[46] Li He, Bojun Yang, Xiaoguang Zhang, and Li Yu, *"Supercontinuum generation from dispersion-flattened photonic crystal f iber using picosecond pulses",* Chinese Optics Letters, **4**, 12, pp. 715 (2006).

[47] J. M. Stone and J. C. Knight, *"Visibly "white" light generation in uniform photonic crystal fiber using a microchip laser",* Opt. Express, **16**, pp. 2670-2675 (2008).

[48] Kazunori Suzuki, Hirokazu Kubota, Satoki Kawanishi, Masatoshi Tanaka, and Moriyuki Fujita, *"Optical properties of a low-loss polarization-maintaining photonic crystal fiber",* Optics Express, **9**, 13, pp. 676-680 (2001).

[49] Yue, Y.; Kai, G.; Wang, Z.; Lu, Y.; Zhang, C.; Sun, T.; Li, Y.; Jin, L.; Liu, J.; Liu, Y.; Yuan, S.; Dong, X, *"Highly Birefringent Elliptical-Hole Photonic Crystal Fiber With Two Big Circular Air Holes Adjacent to the Core",* Photonics Technology Letters, **18**, 24, pp. 2638–2640 (2006).

[50] Do-Hyun Kim and Jin U. Kang, *"Sagnac loop interferometer based on polarization maintaining photonic crystal fiber with reduced temperature sensitivity",* Optics Express, **12**, 12, pp. 4490 (2004).

[51] Andrew Michie, John Canning, Katja Lyytikäinen, Mattias Åslund, and Justin Digweed, *"Temperature independent highly birefringent photonic crystal fibre",* Optics Express, **12**, 21, pp. 5160 (2004).

[52] D. R. Scifres, *"Multiple core fiber lasers and optical amplifiers",* US Patent #5,566,196 (1996).

[53] G. Bouwmans, R. M. Percival, W. J. Wadsworth, J. C. Knight, and P. St. J. Russell, *"High-power Er:Yb fiber laser with very high numerical aperture pump-cladding waveguide",* Appl. Phys. Lett., **83**, pp. 817 (2003).

[54] X. Zhu, A. Schülzgen, L. Li, H. Li, V. L. Temyanko, J. V. Moloney, and N. Peyghambarian, *"Birefringent in-phase supermode operation of a multicore microstructured fiber laser",* Optics Express, **15**, 16, pp. 10340 (2007).

[55] Blanchard P.M., Burnett J.G., Erry G.R.G., Greenaway A.H., Harrison P., Mangan B., Knight J.C., Russell P.S.J., Gander M.J., McBride R., Jones J.D.C, *"Two-dimensional bend sensing with a single, multi-core optical fibre",* Smart Materials and Structures, **9**, 2, pp. 132-140 (2000).

[56] Joannopoulos. *Photonic Crystals. Molding the Flow of Light.*

[57] B. Temelkuran et al, *"Wavelength-scalable hollow optical fibres with large photonic bandgaps for CO2 laser transmission",* Nature, 420, pp. 650 (2002).

[58] G. Ouyang, Y. Xu, and A. Yariv, *"Theoretical study on dispersion compensation in air-core Bragg fibers",* **10**, 17, pp. 899–908 (2002).

[59] Frédéric Gérôme, Sébastien Février, Andrey D. Pryamikov, Jean-Louis Auguste, Raphaël Jamier, Jean-Marc Blondy, Mikhail E. Likhachev, Mikhail M. Bubnov, Sergei L. Semjonov, and Evgeny M. Dianov, *"Highly dispersive large mode area photonic bandgap fiber",* Optics Letters, **32**, 10, pp. 1208-1210 (2007).

[60] A.Yariv and P.Yeh. *OpticalWaves in Crystals: Propagation and Control of Laser Radiation.* New York : Wiley, 1984.

[61] J. A. West, C. M. Smith, N. E Borrelli. D. C. Allan, and K. W. Koch, *"Surface modes in air-core photonic band-gap fibers",* Optics Express, **12**, 8, pp. 1485-1 496 (2004).

[62] G. J. Pearce, J. M. Pottage, D. M. Bird, P. J. Roberts, J. C. Knight, P. St.J. Russell, *"Hollow-core PCF for guidance in the mid to far infra-red",* Optics Express, **13**, 185, pp. 6937 (2005).

[63] T. Ritari, J. Tuominen, H. Ludvigsen, J. Petersen, T. Sørensen, T. Hansen, and H. Simonsen, *"Gas sensing using air-guiding photonic bandgap fibers",* Optics Express, **12**, 17, pp. 4080-4087 (2004).

[64] S. Fevrier, P. Viale, M. Lelek, F. Louradour, J. L. Auguste, P. Roy, J. M. Blondy, *"Singlemode low-index liquid core holey fibre",* in Proc. ECOC' 2005 (Glasgow), paper Tu1.4.3. (2005).

[65] C. de Matos and J. Taylor, *"Chirped pulse Raman amplification with compression in air-core photonic bandgap fiber",* Optics Express, **13**, 8, pp. 2828-2834 (2005).

[66] T. P. White, R. C. McPhedran, C. M. de Sterke, N. M. Litchinitser, B. J. Eggleton, *"Resonance and scattering in microstructured optical fibers",* Opt. Lett., **27**, pp. 1977-1979 (2002).

[67] N. M. Litchinitser, S. C. Dunn, B. Usner, B. J. Eggleton, T. P. White, R. C. McPhedran, and C. M. de Sterke, *"Resonances in microstructured optical waveguides",* Optics Express, **11**, 10, pp. 1243-1251 (2003).

[68] P. Steinvurzel, B. T. Kuhmley, T. P. White, M. J. Steel, C. M. de Sterke, andd B. J. Eggleton, *"Longwavelength anti-resonant guidance in high index inclusion microstructured fibers",* Optics Express, **12**, 22, pp. 5424-5433 (2004).

[69] Guobin Ren, Ping Shum, Liren Zhang, and Xia Yu, Weijun Tong, Jie Luo, *"Low-loss all-solid photonic bandgap fiber",* Optics Letters, **32**, 9, pp. 1023 (2007).

[70] T. D. Hedley, D. M. Bird, F. Benabid, J. C. Knight, P. St. J. Russell, *"Modelling of a novel hollow-core photonic crystal fibre",* in Proc. QELS, Baltimore MA, paper QTuL4 (2003).

[71] G. J. Pearce, G. S. Wiederhecker, C. G. Poulton, S. Burger, and P. St. J. Russell, *"Models for guidance in kagome-structured hollow-core photonic crystal fibres",* Opt. Express, **15**, 20, pp. 12680-12685 (2007).

[72] A. Argyros and J. Pla, *"Hollow-core polymer fibres with a kagome lattice: potential for transmission in the infrared",* Opt. Express, **15**, 22, pp. 7713-7719 (2007).

[73] N.J.Doran and K.J.Blow, *"Cylindrical Bragg Fibres: A Design and Feasibility Study for Optical Communications",* J. Lightwave Tech., **4** , pp. 588-590 (1983).

[74] A.N., Lazarchik, *"Bragg waveguides",* Radiotekh. Radioelektron., **33**, pp. 36-43 (1988).

[75] C. M. de Sterke, I. M. Bassett and A. G. Street, *"Differential losses in Bragg fibres",* J. Appl. Phys., **76**, 680 (1994).

[76] Y. Xu, R. K. Lee, and A. Yariv, *"Asymptotic analysis of Bragg fibers",* Opt. Lett., **25**, pp. 1756-1758 (2000).

[77] Melehin V.N., Manenkov A.B., Zh. Teh. Fiz., **38**, 2113 (1968).

[78] Melehin V.N., Manenkov A.B., in Elektronika bol'shikh moshchnostei (High-power Electronics). (Moscow: Nauka, 1969). N**6**, p.161.

[79] Manenkov A.B., Izv. Vysh. Uchebn. Zaved., Ser. Radiofiz., **14**, p. 606 (1971).

[80] Manenkov A.B., Radiotekh. Radioelektron., **22**, 2043 (1977).

[81] Manenkov A.B., Melehin V.N., Radiotekh. Radioelektron., **24**, p. 1282 (1979).

[82] Nikolaev V.V., Sokolovskii G.S., Kalitievskii M.A., "*Bragg reflectros for cylindrical waves",* Fiz. Tekh. Poluprovodn*,* **33**, 2, pp. 174-179 (1999).

[83] Born M., Wolf E., *Principles of Optics* (Oxford: Pergamon Press 1969; Moscow: Nauka, 1973).

[84] F. Brechet, P. Leproux, P. Roy, J. Marcou, and D. Pagnoux, *"Analysis of bandpass filtering behavior of singlemode depressed-core-index photonic bandgap fibre",* Elec. Lett., **36**, pp. 870-872 (2000).

[85] T. Kawanishi and M. Izutsu, *"Coaxial periodic optical waveguide",* Opt. Express, **7**, pp. 10-22 (2000).

[86] Ibanescu M., Fink Y., Fan S., Thomas E.L., Joannopoulos J.D, *"An All-Dielectric Coaxial Waveguide",* Science, **289** , 21 , pp. 415-419 (2000).

[87] Marcou J.; Brechet F.; Roy P, *"Design of weakly guiding Bragg fibres for chromatic dispersion shifting towards short wavelengths",* J. Opt. A: Pure and App. Opt., **3**, 6, pp. 144-153 (2001).

[88] G. Ouyang, Y. Xu, and A. Yariv, *"Comparative study of air-core and coaxial Bragg fibers: single-mode transmission and dispersion characteristics",* Opt. Express, **9**, pp. 733-747 (2001).

[89] S. Johnson, M. Ibanescu, M. Skorobogatiy, O. Weisberg, T. Engeness, M. Soljacic, S. Jacobs, J. Joannopoulos, and Y. Fink, *"Low-loss asymptotically single-mode propagation in large-core OmniGuide fibers",* Opt. Express, **9**, pp. 748-779 (2001).

[90] Hart S. D., Maskaly G. R., Temelkuran B., Prideaux P. H., Joannopoulos J. D., Fink Y., *"External Reflection from Omnidirectional Dielectric Mirror Fibers",* Science, **296**, pp. 511-513 (2002).

[91] Xu Y., Ouyang G.X., Lee R.K., Yariv A, *"Asymptotic matrix theory of Bragg fibers",* J. Lightwave Technol., **20**, pp. 428-440 (2002).

[92] G. Ouyang, Y. Xu, and A. Yariv, *"Theoretical study on dispersion compensation in air-core Bragg fibers",* Optics Express, **10**, 17, pp. 899–908 (2002).

[93] N. M. Litchinitser, A. K. Abeeluck, C. Headley, and B. J. Eggleton, *"Antiresonant reflecting photonic crystal optical waveguides",* Opt. Lett., **27**, pp. 1592-1594 (2002).

[94] A. Abeeluck, N. Litchinitser, C. Headley, and B. Eggleton, *"Analysis of spectral characteristics of photonic bandgap waveguides",* Opt. Express, **10**, pp. 1320-1333 (2002).

[95] Bassett and A. Argyros, *"Elimination of polarization degeneracy in round waveguides",* Opt. Express, **10**, pp. 1342-1346 (2002).

[96] A. Argyros, *"Guided modes and loss in Bragg fibres",* Opt. Express, **10**, pp. 1411-1417 (2002).

[97] Ibanescu M., Johnson S.G., Soljacic, M., Joannopoulos J. D., Fink Y, *"Analysis of mode structure in hollow dielectric waveguide fibers",* Phys. Rev. E, **67**, 046608 (2003).

[98] Xu Y., Yariv A., Fleming J.G., Lin S.Y, *"Asymptotic analysis of silicon based Bragg fibers 2003",* Opt. Express, **11**, pp. 1039-1049 (2003).

[99] T. Engeness, M. Ibanescu, S. Johnson, O. Weisberg, M. Skorobogatiy, S. Jacobs, and Y. Fink, *"Dispersion tailoring and compensation by modal interactions in OmniGuide fibers",* Opt. Express , **11**, pp. 1175-1196 (2003).

[100] S. Février, P. Viale, F. Gérôme, P. Leproux, P. Roy, J.-M. Blondy, B. Dussardier, and G. Monnom, *"Very large effective area singlemode photonic bandgap fibre",* Electron. Lett., **39**, 17, pp. 1240-1242 (2003).

[101] S. Guo, S. Albin, and R. Rogowski, *"Comparative analysis of Bragg fibers",* Opt. Express, **12**, 1, pp. 198-207 (2004).

[102] Kuriki K., Shapira O., Hart S.D., Benoit G., Kuriki Y., Viens J.F, Bayindir M., Joannopoulos J.D., Fink J.D, *"Hollow multilayer photonic bandgap fibers for NIR applications",* Opt. Express, **12**, 8, pp. 1510-1517 (2004).

[103] Ni Yi, Zhang Lei, Gu Chong, Jia Shu, Peng Jiangde, *"A novel design for all-solid silica Bragg fiber with zero-dispersion wavelength at 1550 nm",* Opt. Express, **12**, 19, pp. 4602 (2004).

[104] Alam I., Sakai Jun-ichi, *"Classification and properties of radiation and guided modes in Bragg fiber",* Opt. Comm., **250**, pp. 84-94 (2005).

[105] Abdel-Baset M.A. Ibrahim, P.K. Choudhury, M.S. Alias, *"On the analytical investigation of fields and power patterns in coaxial omniguiding Bragg fibers",* Optik, **117**, 1 (2006).

[106] M.E. Likhachev, Yu.A. Uspenskii, S.L. Semjonov, M.M. Bubnov, E.M. Dianov, E.E. Uzorin, O.S. Simokhin, A.V. Vinogradov, R. Jamier, S. Février, and J.-M. Blondy, *"Fabrication of Solid Bandgap Fibres with Increased Bandwidth by Modification of Outer Cladding",* ECOC'2006, Th4.2.5 (2006).

[107] M.E. Likhachev, S.L. Semjonov, M. M. Bubnov, E. M. Dianov, V. F. Khopin, M. Yu. Salganskii, M. A. Gurjanov, A. N. Gurjanov, R. Jamier, P. Viale, S. Février,

J-M Blondy "*Development and study of Bragg fibres with a large mode field and low optical losses ",* Quant. Electron. **36**, 7, pp. 581-586 (2006).

[108] Jun-ichi, Sakai, *"Hybrid modes in a Bragg fiber: general properties and formulas under the quarter-wave stack condition",* J. Opt. Soc. Am. B, **22**, 11, pp. 2319-2330 (2005).

[109] Sakai, Jun-ichi, *"Optical power confinement factor in a Bragg fiber: 1. Formulation and general properties",* J. Opt. Soc. Am. B, **24**, 1, pp. 9-19 (2007).

[110] Y. A. Uspenskii, E. E. Uzorin, A. V. Vinogradov, M. E. Likhachev, S. L. Semjonov, M. M. Bubnov, E. M. Dianov, R. Jamier, and S. Février, *"Effect of polymer coating on leakage losses in Bragg fibers",* Opt. Lett., **32**, 10, pp. 1202-1204 (2007).

[111] A.Snyder, J. Love. *Optical Waveguide Theory* (London: Kluwer 1983; Moscow: Radio i svyaz' 1987).

[112] W.C, Chew. *Waves and Fields in Inhomogeneous Media.* NY : Van Nostrand, 1990.

[113] D.E., Goldberg. *Genetic Algorithms in Search, Optimization and Machine Learning.* Boston : Kluwer, Acad. Publishers, 1989.

[114] M. Abramowitz, I.A. Stegun, *Handbook of Mathematical Functions (New York: Dover, 1965; Moscow: Nauka*, 1979).

[115] L. Poladian, N. Issa, and T. Monro, *"Fourier decomposition algorithm for leaky modes of fibres with arbitrary geometry",* Opt. Express, **10**, pp. 449-454 (2002).

[116] Y. Kokubun, T. Baba, T. Sakaki and K. Iga,, *"Low loss antiresonant reflecting optical waveguide on Si substrate in visible-wavelength region",* Electron. Lett., **22**, 22, pp. 892-893 (1986).

[117] T. Baba, Y. Kokubun, T. Sakaki and K. Iga, *"Loss reduction of an ARROW waveguide in shorter wavelength and its stack configuration",* J. Lightwave Technol., **6**, 9, pp. 1440-1445 (1988).

[118] Laegsgaard, J, *"Gap formation and guided modes in photonic bandgap fibres awith high-index rods",* J. Opt. A: Pure and Appl. Opt., **6**, pp. 798-804 (2004).

[119] A. Argyros, T. Birks, S. Leon-Saval, C. M. Cordeiro, F. Luan, and P. S. J. Russell, *"Photonic bandgap with an index step of one percent",* Opt. Express, **13**, 1, pp. 309-314 (2005).

[120] G. Bouwmans, L. Bigot, Y. Quiquempois, F. Lopez, L. Provino, and M. Douay, *"Fabrication and characterization of an all-solid 2D photonic bandgap fiber with a low-loss region (< 20 dB/km). around 1550 nm",* Opt. Express, **13**, 21, pp. 8452-8459 (2005).

[121] G. Renversez, P. Boyer, and A. Sagrini, *"Antiresonant reflecting optical waveguide microstructured fibers revisited: a new analysis based on leaky mode coupling",* Opt. Express, **14**, 12, pp. 5682-5687 (2006).

[122] J. Broeng, S. Barkou, T. Sondergaard, A. Bjarklev, *"Analysis of air-guiding photonic bandgap fibers",* Opt. Let., **25**, 2, (2000).

[123] W. Zhi, R. Guobin, L. Shuqin, J. Shuisheng, *"Supercell lattice method for photonic crystal fibers",* Optics Express, **11**, 9, (2003).

[124] W.Wijngaard, *"Guided normal modes of two parallel circular dielectric rods",* J. Opt. Soc. Am, **63**, 8, (1973).

[125] W.Wijngaard, *"Some normal modes of an infinite hexagonal array of identical circular dielectric rods",* J. Opt. Soc. Am, **64**, 8, (1974).

[126] H. S. Huang, H.-C. Chang, *"Analysis of Equilateral Three-Core Fibers by CHEM",* J. Lightwave Technol., **8**, 6, (1990).

[127] C.-Sh. Chang, H.-Ch. Chang, *"Theory of the Circular Harmonics Expansion for Multipole-Optical-Fiber System",* J. Lightwave Technol., 12, 3, (1994).

[128] K.M.Lo, R.C. McPhedran, I.M. Basset, G.W. Milton, *"An electromagnetic theory of dielectric waveguides with multiple embedded cylinders",* J. Lightwave Technol., **12**, 3, (1994).

[129] T.P. White, B.T.Kuhlmey, R.C.McPhedran, *"Multipole method for microstructured optical fibers. I. Formulation",* J.Opt.Soc.Am. B, **19**, 10, (2002).

[130] T.P. White, B.T.Kuhlmey, R.C.McPhedran, *"Multipole method for microstructured optical fibers. II. Implementation and results",* J. Opt. Soc. Am. B, **19**, 10, (2002).

[131] S. Campbell, R. C. McPhedran, C. Martijn de Sterke, L. C. Botten, *"Differential multipole method for microstructured optical fibers",* J. Opt. Soc. Am. B, **21**, 11, (2004).

[132] Boris T. Kuhlmey, Karrnan Pathmanandavel and Ross C. McPhedran, *"Multipole analysis of photonic crystal fibers with coated inclusions",* Opt. Express, **14**, 22, , pp. 10851-10864 (2006).

[133] I.S. Gradstein, I.M. Ryzik, *Tables of integrals, sums, series and products, Moscow* : Nauka, 1971.

[134] Wang J.S., Vogel E.M., Snitzer E, *"Tellurite Glass: a New Candidate for Fiber Devices",* Opt. Mater., **3**, 3 (1994).

[135] H. Nasu, O. Matsushita, K. Kamiya, H. Kobayashi, and K. Kubodera, *"Third harmonic generation from Li2O-TiO2-TeO2 glasses",* J. Non-Cryst. Solids., **124**, pp. 275-277 (1990).

[136] Ghosh, G, *"Sellmeier coefficients and chromatic dispersions for some tellurite glasses",* J. Am. Ceram. Soc., **78**, pp. 2828 - 2830 (1995).

[137] Bjarklev A., Broeng J., Bjarklev A.S. *Photonic Crystal Fibres.* Boston/Dordrecht/London : Kluwer Acad. Publ., 2003.

[138] D. Gaponov, P. Roy, S. Février, M. E. Likhachev, S.L. Semjonov, M.M. Bubnov, E. M. Dianov, M.Yu.Yashkov, V. F. Khopin, M. Yu. Salganskii, A. N. Guryanov, *"High-Power Photonic Bandgap Fibre Laser",* ECOC'2007, Pds3.9 (2007).

[139] Agrawal G., *Nonlinear Fiber Optics (*New York: Academic Press 1995, Moscow: Mir, 1996).

[140] P. Koplow, D. Kliner, L. Goldberg, *"Single-mode operation of a coiled multimode fiber amplifier",* Opt. Lett., **25** , pp. 442–444 (2000).

[141] P. Wang, L. J. Cooper, J. K. Sahu, and W. A. Clarkson, *"Efficient single-mode operation of a cladding-pumped ytterbium-doped helical-core fiber laser",* Opt. Lett., **31**, pp. 226-228 (2006).

[142] Marcuse, D, *"Radiation loss of a helically deformed optical fiber",* J. Opt. Soc. Am., **66**, 10, , pp. 1025-1031 (1976).

[143] C-H Liu, G. Chang, N. Litchinitser, D. Guertin, N. Jacobsen, K. Tankala, A. Galvanauskas, *"Chirally Coupled Core Fibers at 1550-nm and 1064-nm for Effectively Single-Mode Core Size Scaling",* CLEO'2007, CTuBB3 (2007).

[144] Y. Chen, T. McComb, V. Sudesh, M. Richardson, M. Bass, *"Very large-core, single-mode, gain-guided, index-antiguided fiber lasers",* Opt. Lett., **32**, pp. 2505-2507 (2007).

[145] S. Février, R. Jamier, J.-M. Blondy, S. L. Semjonov, M. E. Likhachev, M. M. Bubnov, E. M. Dianov, V. F. Khopin, M. Y. Salganskii, A. N. Guryanov, *"Low Loss Large Mode Area Bragg Fibre",* ECOC'2005, PD Th4.4.3 (2005).

[146] P. C. Becker, N. A. Olsson, J. R. Simpson, *Erbium-Doped Fiber Amplifiers* Academic Press, 1999, chapter 5, pp. 140-144

[147] Pierre Laperle, Claude Paré, Huimin Zheng, André Croteau, and Yves Taillon, *"Yb-doped LMA triple-clad fiber laser",* Photonics North 2006, 6343, 2, pp. 63430X.1-63430X.9 (2006).

[148] Marcuse, D. *Theory of dielectric optical waveguides*. Second edition. Academic Press.

[149] Drexhage, Martin G, *"Infrared Optical Fibers",* Scientific American, **259**, 5, pp. 110 (1988).

[150] A.P. Prudnikov, Yu.A. Brychkov, O.I. Marichev, *Integrals and Series. Special Functions*, Moscow: Nauka, 1983

[151] McIsasc, P.R, *"Symmetry-induced modal characteristics of uniform waveguides. I.Summary of results",* IEEE Trans. Microwave Theory Tech., MTT-23 (1975).

[152] Russell, M. [online] http://www.ecse.rpi.edu/~qji/CV/svd_review.pdf.

[153] Broyden, C.G, *"A Class of Methods for Solving Nonlinear Simultaneous Equations",* Math. Comp., **19**, 92, , pp. 577-593 (1965).

[154] Broyden, C. G, *"Quasi-Newton Methods and their Application to Function Minimisation",* Math. Comp., **21**, 99 (1967).

[155] Knight, J. C, *"Photonic crystal fibres",* Nature, **424**, pp. 847-851 (2003).

[156] Geraud Bouwmans, Vincent Pureur, Aurelie Betourne, Yves Quiquempois, Mathias Perrin, Laurent Bigot, Marc Douay, *"Opt. Quant. Electron",* Progress in solid core photonic bandgap fibers [Online]. Available: http://dx.doi.org/10.1007%2Fs11082-007-9164-7 (2007).

[157] E. Yamashita, S. Ozeki, K. Atsuki, *"Modal analysis method for optical fibers with distributed multiple cores",* J. Light. Tech., **LT-3**, 2, pp. 341 – 346 (1985).

Propriétés optiques de fibres optiques microstructurées et laser à fibre de Bragg à grande aire modale

De nos jours, nous observons une augmentation constante de la quantité de publications liées aux fibres microstructurées (MOFs). Bien que les aspects fondamentaux de leurs propriétés soient souvent éludés, leurs applications sont attrayantes pour de nombreux domaines de la science et la technologie en raison de leurs propriétés optiques uniques. Mon travail est consacré, d'une part à l'analyse comparative de certaines MOF bien connues à l'aide de différentes méthodes numériques et d'autre part, à la création expérimentale d'un laser à fibre monomode à grande aire modale (LMA) basé sur une fibre à bande photonique 1-D (fibre de Bragg, BF). Au cours de l'étude théorique, nous avons porté une attention particulière à l'étude de la structure de gaine. Nous avons en particulier montré le rôle de la réflexion radiale du champ sur l'interface silice polymère dans la hiérarchie des modes pour des fibres à cœur creux ou plein. Nous avons analysé en détail le cas des fibres, dites, Arrow (Antiresonant Reflection Optical Waveguides). Cette étude révèle comment décrire correctement les pertes de confinement d'un éventail arbitraire de fibres ARROW. Nous avons constaté quelques inexactitudes dans des travaux antérieurs bien connus et nous avons alors mis en œuvre et appliqué la méthode multipôle à l'analyse de ce type de fibres. Nous avons étudié de plus, les propriétés optiques de fibres microstructurées en verre de tellure au moyen de cette méthode. Finalement, dans la partie expérimentale, nous avons étudié des fibres de Bragg dopées à l'ytterbium. Nous avons développé un laser basé sur cette fibre mis en œuvre un système de pompage par la gaine. Nous avons obtenu, pour la première fois, l'émission d'un faisceau monomode et démontré l'excellente résistance aux pertes par courbure de ce type de fibre en régime d'oscillation laser.

Mots clefs

Fibre optique microstructurée, fibre de Bragg, fibre microstructurée en verre de tellure, grande aire modale, laser à fibre

Optical properties of Microstructured Optical Fibers and fiber laser based on Large Mode Area Bragg Fiber

Nowadays we observe a constant increasing of the amount of publications connected with **Microstructured Optical Fibers** (MOFs). Nevertheless the unclear physical questions are still remaining in this field. From the other hand, applying of such structures is attractive in different fields of science and technology due to their unique optical properties. Our work is devoted to the theoretical analysis of some of the basic MOF types and to the experimental creation of **fiber laser** based on **large mode area** (LMA) 1-D photonic bandgap fiber (i.e. **Bragg Fiber**, BF). In theoretical part we developed the original method which allows to obtain the optimal cladding structures of Bragg Fibers at the given wavelength. We showed how Fresnel reflection plays a role in the modes hierarchy in BF with the hollow and solid cores. We analyzed the case of, so called, ARROW (Antiresonant Reflection Optical Waveguides) BF in quite detail. The analysis showed how ones can properly describe the loss spectrum of an arbitrary ARROW BF. We found some inaccuracies in well-known original works and then realized the multipole method for analysis of 2-D MOFs. We investigated the optical properties of **Holey Fibers** based on perspective for fiber optics **tellurite glass** of concrete type by means of this method. In the experimental part we investigated the Yb-doped LMA BF. We created a fiber laser based on this fiber with pumping into the cladding. We obtained the efficient singlemode lasing with low bend sensitivity, to the best of our knowledge, for the first time in such type of fibers.